

การเตรียมและการเพิ่มความคงตัวของโครงสร้างของแข็งรูปอสัณฐานเอกซเรย์ของซิลลูทามอลซิลเฟต
ที่ถูกดูดซับบนเมโซพอร์ซิลิกา



บทคัดย่อและแฟ้มข้อมูลฉบับเต็มของวิทยานิพนธ์ตั้งแต่ปีการศึกษา 2554 ที่ให้บริการในคลังปัญญาจุฬาฯ (CUIR)
เป็นแฟ้มข้อมูลของนิสิตเจ้าของวิทยานิพนธ์ ที่ส่งผ่านทางบัณฑิตวิทยาลัย

The abstract and full text of theses from the academic year 2011 in Chulalongkorn University Intellectual Repository (CUIR)
are the thesis authors' files submitted through the University Graduate School.

วิทยานิพนธ์นี้เป็นส่วนหนึ่งของการศึกษาตามหลักสูตรปริญญาเภสัชศาสตรมหาบัณฑิต

สาขาวิชาเภสัชอุตสาหกรรม ภาควิชาวิทยาการเภสัชกรรมและเภสัชอุตสาหกรรม

คณะเภสัชศาสตร์ จุฬาลงกรณ์มหาวิทยาลัย

ปีการศึกษา 2560

ลิขสิทธิ์ของจุฬาลงกรณ์มหาวิทยาลัย

PREPARATION AND STABILIZATION OF X-RAY AMORPHOUS SOLID STATE STRUCTURE
OF SALBUTAMOL SULFATE ADSORBED ON MESOPOROUS SILICA



A Thesis Submitted in Partial Fulfillment of the Requirements
for the Degree of Master of Science in Pharmacy Program in Industrial Pharmacy
Department of Pharmaceutics and Industrial Pharmacy
Faculty of Pharmaceutical Sciences
Chulalongkorn University
Academic Year 2017
Copyright of Chulalongkorn University

ตรีรัก ประเสริฐศรี : การเตรียมและการเพิ่มความคงตัวของโครงสร้างของแข็งรูปอสัณฐานเอกซเรย์ของซัลบูทามอลซัลเฟตที่ถูกดูดซับบนเมโซพอร์รัสซิลิกา (PREPARATION AND STABILIZATION OF X-RAY AMORPHOUS SOLID STATE STRUCTURE OF SALBUTAMOL SULFATE ADSORBED ON MESOPOROUS SILICA) อ.ที่ปรึกษา
วิทยานิพนธ์หลัก: อ. ภก. ดร.วันชัย จงเจริญ, อ.ที่ปรึกษาวิทยานิพนธ์ร่วม: อ. ภญ. ดร. นฤพร สุตันทวีบูลย์, 86 หน้า.

วัตถุประสงค์ของการศึกษานี้มุ่งเป้าถึงการเตรียมซัลบูทามอลซัลเฟต ในรูปอสัณฐานเอกซเรย์ด้วยตัวพามาโซพอร์รัสซิลิกา (เอส 244 ซิลิกา) โดยวิธีอินซิเปียน เวตเนส อิมเพรกเนชัน และศึกษาเพิ่มเติมถึงผลของพอลิไวนิลไพโรลิโดน (พีวีพี) เค 12 สำหรับการเพิ่มความคงสภาพโครงสร้างทางของแข็งรูปอสัณฐาน เริ่มต้นโดยเตรียมสารละลายของซัลบูทามอลซัลเฟตและบรรจุลงบนเอส 244 ซิลิกา ผลิตภัณฑ์ที่ได้มาแสดงการเรียงตัวแบบไม่เป็นระเบียบของซัลบูทามอลซัลเฟตซึ่งมีระยะเวลาการเปลี่ยนรูปโครงสร้างไปสู่รูปผลึกนานกว่าเมื่อเทียบกับรูปอสัณฐานที่ได้จากการบด ซึ่งอธิบายได้ว่าซัลบูทามอลซัลเฟตวางตัวอยู่อย่างกระจุกกระจายบนพื้นผิวของซิลิกาโดยไม่มีการเกาะรวมตัวของโมเลกุลเนื่องจากพันธะไฮโดรเจนและแรงดึงดูดอย่างอ่อนจึงทำให้การเคลื่อนที่ของโมเลกุลช้ากว่ารูปอสัณฐานที่ได้จากการบดที่มีการเรียงตัวแบบไม่เป็นระเบียบ นั่นคืออสัณฐานเอกซเรย์ซัลบูทามอลซัลเฟตที่เตรียมขึ้นมีความคงตัวดีกว่า พีวีพี เค 12 ซึ่งเป็นพอลิเมอร์ไวนิลสายสั้นถูกใช้เป็นต้นแบบสำหรับการเพิ่มความคงสภาพรูปอสัณฐาน พีวีพี เค 12 ให้ผลอันไม่พึงประสงค์ต่อรูปอสัณฐานเอกซเรย์ซัลบูทามอลซัลเฟตที่ถูกดูดซับบนเอส 244 ซิลิกา พีวีพี เค 12 ที่ความเข้มข้นร้อยละ 5 ถึง 30 โดยน้ำหนักของยา สามารถเร่งการก่อรูปผลึกบนพื้นผิวเอส 244 ซิลิกาได้อย่างชัดเจน ในขณะที่ความเข้มข้นที่ต่ำกว่าร้อยละ 0.1 ถึง 1 โดยน้ำหนัก ให้ผลต่ออัตราการเปลี่ยนรูปโครงสร้างอสัณฐานเทียบเคียงกับกลุ่มควบคุม (ผลิตภัณฑ์ที่ไม่มีพีวีพี เค 12) การค้นพบนี้ขัดแย้งกับงานวิจัยหลายชิ้นก่อนหน้านี้ที่แสดงผลเชิงบวกของพอลิเมอร์ความเข้มข้นสูงที่มีต่อการชะลอระยะเวลาการเปลี่ยนรูปโครงสร้างของอสัณฐานซึ่งอาจเกี่ยวเนื่องจากระดับของการแย่งจับบนพื้นผิวซิลิกาของพีวีพี เค 12 หรือโมเลกุลของซัลบูทามอลซัลเฟต

ภาควิชา	วิทยาการเภสัชกรรมและเภสัช	ลายมือชื่อนิสิต
	อุตสาหกรรม	ลายมือชื่อ อ.ที่ปรึกษาหลัก
สาขาวิชา	เภสัชอุตสาหกรรม	ลายมือชื่อ อ.ที่ปรึกษาร่วม
ปีการศึกษา	2560	

5776109433 : MAJOR INDUSTRIAL PHARMACY

KEYWORDS: MESOPOROUS SILICA / AMORPHOUS / CRYSTALLIZATION / X-RAY POWDER
DIFFRACTOMETRY / POLYMER

TREERUK PRASERTSRI: PREPARATION AND STABILIZATION OF X-RAY
AMORPHOUS SOLID STATE STRUCTURE OF SALBUTAMOL SULFATE ADSORBED
ON MESOPOROUS SILICA. ADVISOR: WANCHAI CHONGCHAROEN, Ph.D., CO-
ADVISOR: NARUEPORN SUTANTHAVIBUL, Ph.D., 86 pp.

The main objective of this study was to focus on the preparation of X-ray amorphous salbutamol sulfate (SS) with mesoporous silica (S244 silica) carrier by using incipient wetness impregnation approach and further investigated on the utilization of poly (vinylpyrrolidone) (PVP) K12 for the stabilization of amorphous produced. Initially, SS was prepared in solution state and later loaded on S244 silica. The output product showed the non-ordered arrangement of SS with the longer interconversion time to crystalline when comparing with ground amorphous SS. It should be explained that SS was located on the silica surface randomly with no molecular packing according to hydrogen-bonding and weak attractive forces. The molecular mobility was then slower than non-ordered amorphous ground SS. Therefore, the more stable X-ray amorphous SS was gained. PVP K12, short chain vinyl polymer, was utilized as a model polymer for amorphous stabilization. It provided an adverse effect for X-ray amorphous SS adsorbed on S244 silica. The PVP K12 concentration 5 to 30% w/w of drug obviously accelerated the crystalline form formation on the S244 silica surface. Meanwhile, the lower concentration 0.1-1% w/w showed comparable result on the amorphous interconversion rate to that of the control (product not contain PVP K12). This finding contradicted to several previous reported that showed the positive effect of higher concentration of polymer on the retardation of amorphous interconversion. It might be due to the degree of competitiveness on the surface adsorption of silica surface and PVP K12 or SS molecule.

Department: Pharmaceutics and Student's Signature

 Industrial Pharmacy Advisor's Signature

Field of Study: Industrial Pharmacy Co-Advisor's Signature

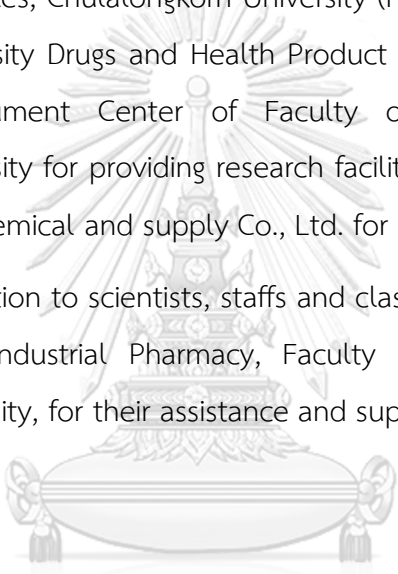
Academic Year: 2017

ACKNOWLEDGEMENTS

I would like to express my sincere gratitude to my advisor, Wanchai Chongchareon, Ph.D., for invaluable advice, attention and encouragement throughout my study. In addition, I wish to express appreciation to my thesis co-advisor, Narueporn Sutanthavibul, Ph.D., for helpful suggestion and encouragement.

This work was supported by the Annual Research Found of the Faculty of Pharmaceutical Sciences, Chulalongkorn University (Phar2557-RG02). We thank the Chulalongkorn University Drugs and Health Product Innovation Promotion Center and Research Instrument Center of Faculty of Pharmaceutical Sciences, Chulalongkorn University for providing research facilities. We thank Grace GmbH & Co. and Tinnakorn Chemical and supply Co., Ltd. for SYLOID® 244 FP silica.

My appreciation to scientists, staffs and classmates in the Department of Pharmaceutics and Industrial Pharmacy, Faculty of Pharmaceutical Sciences, Chulalongkorn University, for their assistance and support on this research project.



จุฬาลงกรณ์มหาวิทยาลัย
CHULALONGKORN UNIVERSITY

CONTENTS

	Page
THAI ABSTRACT	iv
ENGLISH ABSTRACT	v
ACKNOWLEDGEMENTS	vi
CONTENTS	vii
LIST OF TABLES	1
LIST OF FIGURES	1
LIST OF ABBREVIATIONS	1
CHAPTER I INTRODUCTION	1
CHAPTER II LITERATURE REVIEW.....	1
2.1 Amorphous.....	1
2.2 Characterization of amorphous	2
2.3 Preparation method of amorphous phase	3
2.4 Stabilization an amorphous drug	4
2.4.1 Polymeric solid dispersion	4
2.4.2 Porous media system.....	6
2.5 Model drug	9
2.6 Mesoporous silica.....	12
2.7 Polymer	13
CHAPTER III MATERIALS AND METHODS.....	19
3.1. Preparation of X-ray amorphous SS powder.....	22
3.2. Preparation of SS adsorbed on mesoporous silica	22
3.3. Preparation of SS adsorbed on mesoporous silica with polymer	23

	Page
3.4. Solid state characterization	23
3.4.1 Crystal morphology.....	23
3.4.2 Solid state molecular arrangement	24
3.4.3 Thermal analysis.....	24
3.4.3.1 Differential scanning calorimetry (DSC):.....	24
3.4.3.2 Thermogravimetric analysis (TGA):	24
3.4.4 Molecular interaction	24
3.5. Quantitative determination of the degree of crystallinity of SS.....	25
3.6. Determination of SS quantity adsorbed on mesoporous silica	26
3.7. Stability investigation	26
CHAPTER IV RESULTS AND DISCUSSION	27
4.1. Characterization of SS raw material and milled SS.....	27
4.1.1 Characterization of SS raw material.....	27
4.1.2 Characterization of milled SS produced	33
4.2. Stability of X-ray amorphous milled SS.....	42
4.3. Preparation and solid state characterization of SS adsorbed on mesoporous silica.....	45
4.4. Stability of SS adsorbed on mesoporous silica.....	55
4.5. Preparation and solid state characterization of SS adsorbed on mesoporous silica with polymer.....	57
4.6. Stability of SS adsorbed on mesoporous silica with polymer	61
CHAPTER V CONCLUSIONS	65
REFERENCES	67
VITA.....	86

LIST OF TABLES

Table 1 Pharmaceutical features of a crystalline and its amorphous counterpart. .1	
Table 2 International Union of Pure and Applied Chemistry classification of porous media.6	6
Table 3 DSC of crystalline SS form I and form II..... 11	11
Table 4 Physical characterization of the S244 silica and SAL-1 silica. 13	13
Table 5 Average molecular weight of PVP at different K-value. 14	14
Table 6 Loaded quantity of SS and time of milling of the preparation of amorphous SS. 22	22
Table 7 Master formula of SS with PVP K12 in hydroalcoholic solution. 23	23
Table 8 FTIR band assignments, positions, and intensities of SS and X-ray amorphous milled SS. 41	41
Table 9 FTIR band assignments, positions, and intensities of SS adsorbed on S244 silica, the physical mixture of SS with S244 silica at 40% w/w. 55	55
Table 10 Quantity of SS in sample of SS adsorbed on S244 silica at different time of impregnation..... 80	80
Table 11 Quantity of SS in sample of SS adsorbed on S244 silica with PVP K12 at different concentration of PVP K12..... 80	80
Table 12 HPLC; linearity and range of SS. 81	81
Table 13 HPLC; repeatability and intermediate precision. 84	84
Table 14 HPLC; percent recovery of SS. 84	84

LIST OF FIGURES

Figure 1 Approach for preparing of amorphous phase.....	3
Figure 2 Chemical structure of SS.	9
Figure 3 XRPD of ground SS.	9
Figure 4 XRPD of crystalline SS form I.	10
Figure 5 XRPD of crystalline SS form II.	10
Figure 6 XRPD of crystalline SS form III.	10
Figure 7 Rate of recrystallization of amorphous SS at 25°C and 70, 80 and 90 %RH.	11
Figure 8 Simulate figure of SYLOID® FP silica.....	12
Figure 9 XRPD patterns of itraconazole loaded on mesoporous silica	13
Figure 10 Chemical structure of PVP.....	14
Figure 11 Viscosity curves for the soluble Kollidon® grades in water.....	14
Figure 12 Nucleation rate as a function of PVP K29/32 concentration.	15
Figure 13 T _g of amorphous felodipine as a function of weight fraction of PVP.....	15
Figure 14 FTIR of felodipine/PVP solid dispersion at different weight ratio.	16
Figure 15 Comparative XRPD of 50% w/w paracetamol dispersions spray dried with various PVP freshly prepared.....	16
Figure 16 XRPD patterns of co-milled SS: PVP and physical mixture of milled SS: PVP after stored at 22°C and 15/75% RH for 7 days.....	17
Figure 17 FTIR spectra of SS, milled SS, PVP, physical mixture of milled SS: PVP 1:1, co-milled mixtures of SS: PVP (1:1, 3:1 and 5:1).	17
Figure 18 Comparative FTIR spectra of SS reference standard referred to BP 2015 (A) and SS raw material used (B).....	28

Figure 19 Comparative XRPD of SS crystalline form I (A) and SS raw material used (B).	29
Figure 20 Photomicrograph of SS under bright field (A) and polarized light (B) (at magnification of 400).	30
Figure 21 DSC and TGA thermograms of SS raw material.....	32
Figure 22 Physical appearance of the SS raw material under different heating temperatures.	32
Figure 23 Comparative XRPD of milled SS at time of milling of 2 hours with different of loaded quantities.	34
Figure 24 Comparative XRPD of milled SS at loaded quantity of 0.5 g with different times of milling.	34
Figure 25 Photomicrograph of X-ray amorphous milled SS under bright field (A) and polarized light (B) (at magnification of 400).	35
Figure 26 DSC and TGA thermograms of X-ray amorphous milled SS.....	37
Figure 27 Physical appearance of X-ray amorphous milled SS under different heating temperature.	38
Figure 28 Chemical structure of SS.	39
Figure 29 Comparative FTIR spectra of X-ray amorphous milled SS and SS raw material.....	40
Figure 30 Comparative XRPD of X-ray amorphous SS powder stored for 75 ± 5% RH, room temperature for 2, 2.25 and 2.5 hours, respectively.	43
Figure 31 Photomicrograph of X-ray amorphous SS powder stored at 75 ± 5% RH, room temperature for 1 day under bright field (A) and polarized light (B) (at magnification of 400).	44
Figure 32 Comparative XRPD of crystalline SS form I (A), S244 silica (B) and SS adsorbed on S244 silica three times (C).	46

Figure 33 Comparative XRPD of SS adsorbed on S244 silica at three, six and nine times of impregnation, respectively.....	46
Figure 34 Comparative XRPD of SS adsorbed on S244 silica at three, four and five times of impregnation, respectively.....	47
Figure 35 Photomicrograph of S244 silica under bright field (A) polarized light (B) (at magnification of 400).	48
Figure 36 Photomicrograph of SS adsorbed on S244 silica under bright field (A) polarized light (B) (at magnification of 400).	49
Figure 37 DSC and TGA thermograms of SS adsorbed on S244 silica.....	50
Figure 38 Physical appearance of the SS adsorbed on S244 silica under difference heating temperature.	51
Figure 39 Comparative DSC thermograms of S244 silica (A), SS adsorbed on S244 silica (B) the physical mixture of SS with S244 at 40% w/w (C) and SS (D).	52
Figure 40 Comparative DSC thermograms of SS adsorbed on S244 silica (A) and the physical mixture of X-ray amorphous milled SS with S244 silica at 40% w/w (B).	53
Figure 41 Comparative FTIR spectra of SS adsorbed on S244 silica, the physical mixture of SS with S244 silica at 40% w/w, SS and S244 silica.....	54
Figure 42 Comparative XRPD of SS adsorbed on S244 stored at 75 ± 5% RH, room temperature at different storage times of 2.5, 24, 44 and 64 hours, respectively.	56
Figure 43 Comparative XRPD of SS adsorbed on S244 stored at 75 ± 5% RH, room temperature at different storage times of 26, 64 and 117 days, respectively.....	56
Figure 44 Comparative XRPD of SS adsorbed on S244 silica with and without PVP K12 30% w/w of SS at five times of impregnation.	58
Figure 45 Comparative XRPD of SS adsorbed on S244 silica with PVP K12 30% w/w of SS between four and haft times and five times of impregnation.	58

Figure 46 Comparative FTIR spectra of SS adsorbed on S244 silica with PVP K12 at 30% w/w of SS, SS adsorbed on S244 silica and PVP K12.	59
Figure 47 Comparative XRPD of SS adsorbed on S244 silica with PVP K12 at different concentration freshly prepared.	60
Figure 48 Comparative XRPD of SS adsorbed on S244 silica with PVP K12 at 10, 20 and 30% w/w of SS stored at $75 \pm 5\%$ RH, room temperature for 6 days.	61
Figure 49 Comparative XRPD of SS adsorbed on S244 silica with PVP K12 at 1, 5 and 10% w/w stored at $75 \pm 5\%$ RH, room temperature for 12 days.	62
Figure 50 Comparative XRPD of SS adsorbed on S244 silica with PVP K12 at 0.1, 0.5 and 1% w/w of SS stored at $75 \pm 5\%$ RH, room temperature for 20 days.	63
Figure 51 % Weight loss of freshly prepared SS adsorbed on S244 silica after subjected into hot air oven at 40°C for different drying time.	76
Figure 52 the flow chart of incipient wetness impregnation process with different impregnation times.	77
Figure 53 XRPD of the physical mixture between moisture equilibrated milled SS (crystalline form I small particle size) and S244 silica (as the placebo) at different spike concentrations.	78
Figure 54 XRPD calibration curve of peak height at $10.6^{\circ}2\theta$ and % crystallinity of SS form I.	79
Figure 55 XRPD calibration curve of signal to noise ratio and % crystallinity of SS.	79
Figure 56 HPLC; calibration curve of SS.	82
Figure 57 HPLC chromatogram of SS.	82
Figure 58 HPLC chromatogram of S244 silica.	82
Figure 59 HPLC chromatogram of PVP K12.	83
Figure 60 HPLC chromatogram of SS adsorbed on S244 silica.	83

Figure 61 HPLC chromatogram of SS adsorbed on S244 silica with PVP K12 30%
w/w of SS. 83

Figure 62 HPLC chromatogram of SS solution incubated at 80°C for 42 hours. 85



LIST OF ABBREVIATIONS

ATR-IR	attenuated total reflectance infrared spectroscopy
BP	british Pharmacopoeia
CPP	critical process parameter
DSC	differential scanning calorimetry
FTIR	fourier transform infrared spectroscopy
g	gram
h	hour
HCl	hydrochloric acid
HPLC	high performance liquid chromatography
HPMC	hydroxypropyl methylcellulose
HPMCAS	hydroxypropyl methylcellulose acetate succinate
LOD	limit of detection
LOQ	limit of quantification
nm	nanometer
PLM	polarized light microscopy
PLS	partial least squares
PSD	polymeric solid dispersion
PVP	poly (vinylpyrrolidone)
r^2	coefficient of determination
RH	relative humidity
SS	salbutamol sulfate
S244 silica	SYLOID [®] 244 silica
SAL-1 silica	SYLOID [®] AL-1 silica
S/N	signal to noise
T_g	glass transition temperature
T_m	melting temperature
TGA	thermogravimetric analysis
XRPD	X-ray powder diffraction

CHAPTER I

INTRODUCTION

Amorphous structure is one of the most promising solid state structure for generic drug product development due to the less possibility on the patent infringement. Original drug product commonly is comprised of the solid state structure of active ingredient that developed by their own rights. Most of that goes to crystalline structure. Meanwhile, amorphous is not favorable to develop due to its thermodynamic instability. In addition, amorphous structure is not precisely determined on the ordering of molecule arrangement in solid state. Therefore, the patent rights on amorphous is less possible. Amorphous state can be prepared by various approaches. However, some approaches provide the less stable amorphous due to the faster rate of interconversion to crystalline. One of the most interesting alternative approach is the utilization of mesoporous substrate which facilitates the deposition of interested drug molecule as amorphous (49). Mesoporous silica has been widely studied in term of the potential of drug adsorption for improving water solubility. It showed the positive result of amorphous phase formation of adsorbed drug on silica particle with more favorable stability (32). However, there are several reports found the ability of amorphous stabilization with specified polymer (35). The main mechanism of polymeric stabilization dealt with the inhibition of recrystallization. The polymer chain influenced on the molecular mobility of non-order arrangement of drug molecule which eventually resulted in the slower recrystallization. Reactive group and chain length of polymer are an important characteristic on the ability of amorphous stabilization. Thus, combination between the adsorption of interested drug molecule on silica particles in conjunction with polymer might provide a better solid state stability of amorphous nature (34).

Objectives of the study

1. To prepare X-ray amorphous salbutamol sulfate (SS) adsorbed on mesoporous silica (SYLOID S244[®] FP silica).
2. To investigate the effect of SYLOID S244[®] FP silica and poly (vinylpyrrolidone) (PVP) K12 on the deceleration of X-ray amorphous SS to crystalline solid state structure.



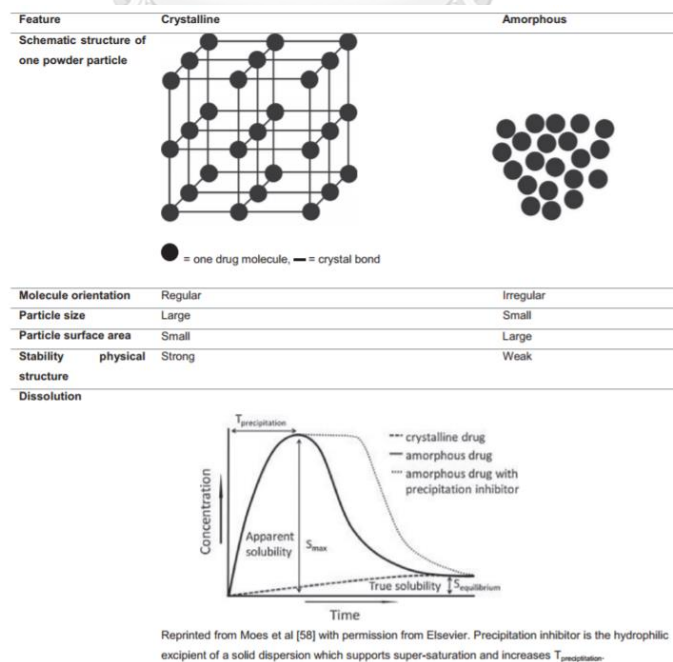
CHAPTER II

LITERATURE REVIEW

2.1 Amorphous

The amorphous state is high energy form of substance that contains no long - range order of molecular arrangement. Amorphous materials generally have more molecular motion and provide the high thermodynamic properties that eventually resulting in higher apparent solubility, dissolution rate and bioavailability, respectively. Pharmaceutical features of crystalline and amorphous of drug are summarized and shown in Table 1 (54). There are several main advantages of amorphous material over its crystalline counterpart such as the high solubility. However, most of amorphous materials typically have a high internal energy leading to high chemical reactivity and finally tend to crystallize at the end. Thus, the production of stabilized amorphous drugs is a challenging and more promising approach in order to maintain its non-order structure (15,38).

Table 1 Pharmaceutical features of a crystalline and its amorphous counterpart.



S_{max} : highest apparent solubility.
 $T_{precipitation}$: time at which drug starts to precipitate after having reached its highest apparent solubility.
 $S_{equilibrium}$: intrinsic solubility of the drug.

2.2 Characterization of amorphous

The characterization of pharmaceutical solids can be performed by using several techniques. Solid-state analytical techniques are divided into four categories based on the type of solid-state phenomena involving with the particular studies (10).

1. Studies involving crystal polymorphism and polymorphic transformations
2. Studies involving amorphization and recrystallization
3. Studies involving solvate systems
4. Studies involving cocrystals

Amorphization and recrystallization of drug may be occurred during common pharmaceutical processes such as spray drying, freeze drying or milling. This phenomena can be detected by several techniques. Polarized light microscopy (PLM) and X-ray powder diffraction (XRPD) are primary method of used for the investigation of amorphous due to simple and precise technique (10). Moreover, the determination of degree of amorphization is an important issue in order to monitor the progress of such phenomena. Example of quantification technique of particular amorphous or crystalline counterpart is XRPD including calorimetry, microscopy and spectroscopy. The combination of multiple methods mentioned earlier provides the comprehensive of solid-state structure evaluation. XRPD is one of the most favorable technique that has been used in the pharmaceutical field (62). The experiments using XRPD technique related to the quantification of amorphous or crystalline content are as following. Zellnitz et al. determined the level of amorphous/crystalline ratio by using chemometric approaches with the using of partial least squares (PLS) method implemented in the PANalytical HighScore (71). On the same hand, Zidan et al. calculated the percent of crystallinity by using PLS models constructed with Unscrambler software (73). However, above method are quite complicated because the specified software needed to be used for calculation. Anyhow, it has an alternative technique dealing with the utilization of the relationship between amorphous content and Bragg's characteristic peak responses of specified crystalline form from XRPD. Curtin et al. used the calibration curve of peak intensity versus crystalline SS weight fraction to quantify the degree of crystallinity (13).

2.3 Preparation method of amorphous phase

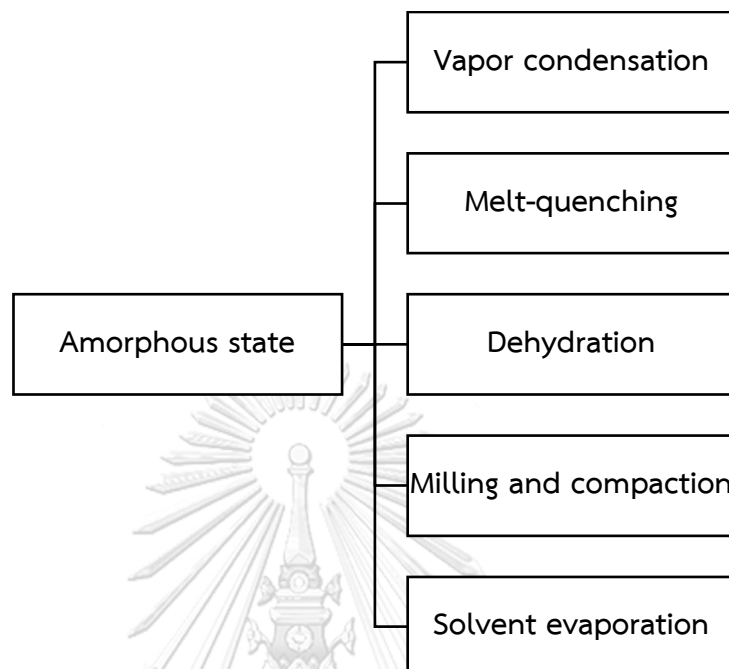


Figure 1 Approach for preparing of amorphous phase.

Amorphous material can be prepared by various approaches as shown in Figure 1 (22,38,40,49,70). Milling is the unit operation that is commonly used for reducing the particle size of material. However, it is the destructive method contains high mechanical activation energy. The impactation and attrition energy found in milling process lead to induce the polymorphic transformation or the disordering of drug structure (amorphous formation) (14,42,68). There are many milling techniques can cause the amorphization such as jet milling (56), ball milling (5,13,19), cryogenic milling (12). Ball milling is the most common technique for size reduction of particles used in pharmaceutical industry. This simple milling technique can produce amorphous phase. The examples of amorphous prepared by ball milling are as follows. X-ray amorphous state of salbutamol sulfate was generated by planetary ball milling (5). X-ray amorphous lactose was also produced by planetary ball milling (68). In addition, fananserine was amorphized when ground by planetary ball milling (14).

2.4 Stabilization an amorphous drug

The principal advantage of amorphous drug is a high solubility and bioavailability. However, the amorphous drug is thermodynamically unstable due to high internal energy level and high entropy. Freshly prepared amorphous usually converts to its stable crystalline counterpart upon certain specific environment. Amorphous salbutamol sulfate started to crystallize and yielded stable crystalline form I within 1.5 hours after kept at 25°C and 70% relative humidity (RH) (71). Amorphous ketoconazole turn to be crystalline form at 85°C within 20 minutes (45). The temperature of 49°C and water vapor pressure of 23 Torr of storage could induce the transformation of amorphous carbamazepine to crystalline within less than 50 minutes (40). Thus, there are many development of effective approaches in order to maintain the existing of amorphous content (38). Polymeric solid dispersions (PSD) and mesoporous media are the interesting alternative approaches for amorphous stabilization since they are practical and flexible to be used in pharmaceutical industry.

2.4.1 Polymeric solid dispersion

The concept of PSD is the distribution of drug molecules throughout the matrix of polymer network molecularly. Each individual drug molecule is embedded in the network of polymer via physical interaction (the appropriateness between molecular volume of drug and the free space between polymer chains) and/or chemical interaction through the active functional group of both polymer and drug. Polymer directly influenced on the stabilization of amorphous drug by several mechanisms such as crystallization inhibition, anti-plasticization (increase glass transition temperature (T_g)), reduction of molecular mobility of drug molecule (4), intermolecular interactions and reduction of the chemical potential of drug (60).

There are several approaches for the preparation of PSD based on the aid of solvent.

2.4.1.1 Non-solvent method

Fusion method, non-solvent used method, are performed by heating the physical mixture of drug and polymer until molten homogeneous mixture

is gained and then allowed to cool down. The final output is presented in the form of solid mass contained molecular dispersed drug. It has been sieved, pulverized or crushed to obtain the optimal particles of PSD before using. This method shows disadvantages particularly for thermo labile drug. In particular, high melting point drug is not suitable for using with this method of preparation due to the requirement of high melting temperature that can cause degradation.

2.4.1.2 Solvent method

This method comprising of freeze drying, spray drying and solvent evaporation. It has the benefit for heat degraded drug according to no need of the excessive heat for preparation. Generally, this method is involving the dissolving of drug and polymer in selected solvent. The polymeric solution containing drug is then subjected into appropriated instrument for removing the excess solvent (4). The final product yield the molecular drug dispersed in polymer.

The examples of polymer used in PSD are hydroxypropyl methylcellulose acetate succinate (HPMCAS), hydroxypropyl methylcellulose (HPMC) and poly (vinylpyrrolidone) (PVP). They were the effective polymer that could decrease the nucleation rate of amorphous felodipine in spin-coated film form at low concentration (3-25% w/w). The T_g of solid dispersion containing HPMC and HPMCAS was not significantly different from pure felodipine whereas T_g of solid dispersion containing PVP was increased significantly. It might be due to the fact that HPMC and HPMCAS stabilized the amorphous felodipine through steric stabilization. Meanwhile, PVP stabilized amorphous felodipine via anti-plasticization. However, hydrogen bonding interactions were formed between felodipine and all of polymers (34). Higher level of PVP (70-90% w/w) was used with resveratrol or griseofulvin in the preparation of solid dispersion, the amorphous solid dispersions nature was found. PVP and resveratrol form the hydrogen bonding while PVP had not shown any interaction with griseofulvin. Therefore, PVP-resveratrol dispersion showed the more stable amorphous than PVP-griseofulvin under the accelerated testing condition (66).

However, the matching of appropriated polymer to interested drug molecule in order to gain stable PSD was complicate. It is very important that drug and polymer

must correlated in term of chemical structure, functional groups, molecular weight, structural flexibility, complexity, melting temperature (T_m) or T_g including the viscosity of drug and polymer (4).

2.4.2 Porous media system

Porous media is a solid material which contains cavities, channels or interstices. It may be regarded as porous (28). It demonstrated the ability of amorphous formation and stabilization synchronously. The mechanism involving amorphous stabilization of porous media was proposed through both physical and chemical interaction. Physical interaction related to the pore size and surface area. Chemical interaction involved the interaction between drug molecule and surface functional group of porous media. Regarding to the appropriateness of both physical and chemical interaction of drug and porous media, drug molecule was adsorbed and fix on the surface of porous media. Therefore, drug molecules were become low free energy and existed in an amorphous state (49,51).

In term of physisorption, International Union of Pure and Applied Chemistry classification of porous media has classified porous media by their pore size (Table 2) (27).

Table 2 International Union of Pure and Applied Chemistry classification of porous media.

Type of Pores	Mean Pore Diameter (nm)
Micropore	Less than 2
Mesopore	Between 2 and 50
Macropore	Greater than 50

Different size of porous media provides the different physisorption isotherm and adsorption behavior. Macroporous media has a large pore with the behavior like flat surface whereas microporous media has too small pore dominated the interaction between wall to wall. On the other hand, mesoporous media has the mean pore

diameter around 2-50 nm. It has the adsorption behavior depend not only on adsorbate-pore wall interaction but also adsorbate-adsorbate interaction. They will lead to capillary condensation which affected the equilibrium of adsorbate molecules (43,49,58). Itraconazole loaded on mesoporous media such as Syloid[®] AL-1 silica (SAL-1 silica), Syloid[®] 244 silica (S244 silica), thermally oxidized Psi and thermally carbonized Psi particles had not shown the characteristic diffraction peaks of crystalline form itraconazole. In addition, there were no extra bands found in Fourier Transform Infrared (FTIR) spectra when compared with physical mixture. Therefore, non-crystalline itraconazole was possibly formed due to physical interaction between itraconazole molecule and surface of mesoporous media (32). Another amorphous system prepared from adsorption with mesoporous silica was ezetimibe. It was loaded on Sylysia[®] 740 and yield amorphous state of ezetimibe due to the disappearing of diffraction peaks of crystalline form including broad diffusive X-ray scattering pattern. Solid-state nuclear magnetic resonance results also confirmed and indicated the strong hydrogen bonding between ezetimibe and Sylysia[®] 740 (65).

Mesoporous silica had been used to stabilize amorphous drug for a period of time. It can be classified into two main groups as ordered and non-ordered mesoporous silica. Ordered mesoporous silica means porous materials that exhibit uniform mesopore (for example SBA-15 and MCM-41) (9). Whereas non-ordered mesoporous silica are referred to the disordered of pore structure material (for example SYLOID[®], SYLYSIA[®], AEROPERL[®] and NEUSILIN[®]) (9,37). The advantage of non-ordered mesoporous silica is the availability in manufacturing scale and inexpensive while ordered mesoporous silica is available only in lab scale and so more expensive. Hence, non-ordered mesoporous silica is now prompt to be used by several research particularly in the manufacturing scale of amorphization.

Preparation of drug adsorbed on porous media mainly used organic solvent. The common process is relating to the dissolving of drug in organic solvent and loaded on the mesoporous media to allow drug adsorption. Then, the residual solvent was removed at elevated temperature or vacuum (49,69). The mixing process between drug solution and mesoporous media could be distinguished as two type. The first one, solvent evaporation, the porous media was added to drug solution with excess

amount of solvent. Whilst, the second was incipient wetness impregnation, a sufficient quantity of solvent was indicated and brought to make the drug solution. It was then added to mesoporous media in order to provide the wet state of mesoporous powder. This method was proved to be the more efficient of drug loading.

The polarity of solvent used for incipient wetness impregnation is an important factor for providing the high drug loading. The competition between solvent and drug molecules to be adsorbed on mesoporous surface should be considered. High polarity solvent more frequent effected on the lower drug loading. Ibuprofen solution prepared with different organic solvent showed the different drug loading on silicon dioxide. The higher the polarity of solvent the lower the amount of ibuprofen loaded. It was due to the competitive interaction between ibuprofen and solvent molecules on functional surface of silicon dioxide (8). The optimization of polarity of solvent system used for incipient wetness impregnation was critically concerned. The blending of solvents of different polarity was able to achieve the optimum polarity and would be used for amorphous preparation by surface adsorption.

According to the argument of the utilization of fume silica in pharmaceutical industry, safety concerned was recognized. Safety of mesoporous silica depended on the size, morphology, surface functionalization and concentration of use (57,69). Smaller particles and lower concentration had negligible effect when compared with larger particles and higher concentration in terms of uptake, viability and immune regulatory markers (23,64). The morphology of mesoporous silica play an important role on cellular toxicity. Long rod-like silica nanoparticles were more susceptible than spherical nanoparticle on the apoptosis of A375 human melanoma cell (24). Surface functionalization was also a key role on safety. MCM-41 grafted aminopropyl groups and grafted mercaptopropyl groups that had been known as surface functionalization ordered-mesoporous silica showed the less cytotoxicity than MCM-41 (17). The most significant factor was concentration of mesoporous silica used. It was found that the lower the concentration the less the toxicity (69).

2.5 Model drug

Salbutamol sulfate (SS) or bis [(1 RS)-2-[1, 1-dimethylethyl) amino]-1-[4-hydroxy-3-(hydroxymethyl) phenyl] ethanol] sulfate showed the chemical structure as seen in Figure 2 (46). It is β_2 -adrenoceptor agonist used for the treatment of bronchial asthma. It is freely soluble in water and less soluble in ethanol.

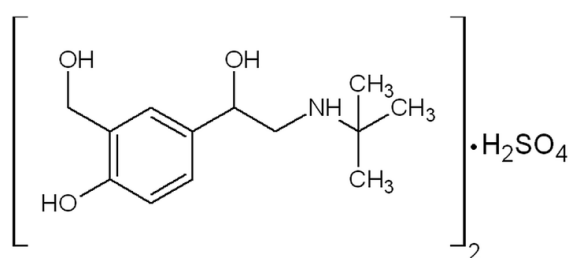


Figure 2 Chemical structure of SS.

In term of the solid state structure of SS, it shows polymorphism. Solid state structure of SS consisted of three crystalline forms (50,53) (form I, II and III) including an amorphous counterpart (5,11,13,71). Crystalline form I is the most stable form. The characteristic of amorphous SS was investigated with XRPD. Amorphous halo pattern was found when SS had been ground (Figure 3) (5). Meanwhile, three of crystalline polymorphs provide the specific X-ray diffraction patterns as seen in Figure 4-6 (50). Crystalline SS form I is characterized with the distinct peaks at 10.6, 18.4, 21.3 and 23.0 $^{\circ}2\theta$ while form II is characterized with the distinct peaks at 8.7, 15.2, 19.1 and 27.2 $^{\circ}2\theta$. For form III, the major peak response is 5.5, 6.9, 7.3 and 18 $^{\circ}2\theta$.

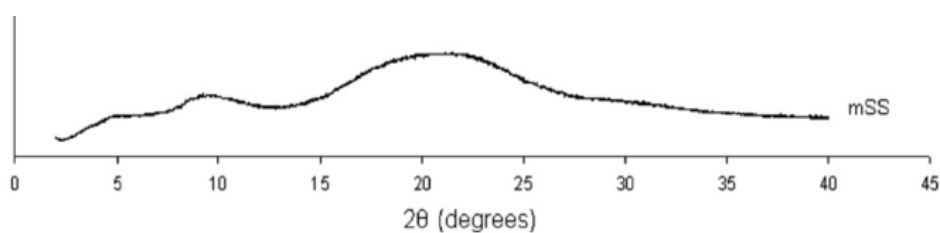


Figure 3 XRPD of ground SS.

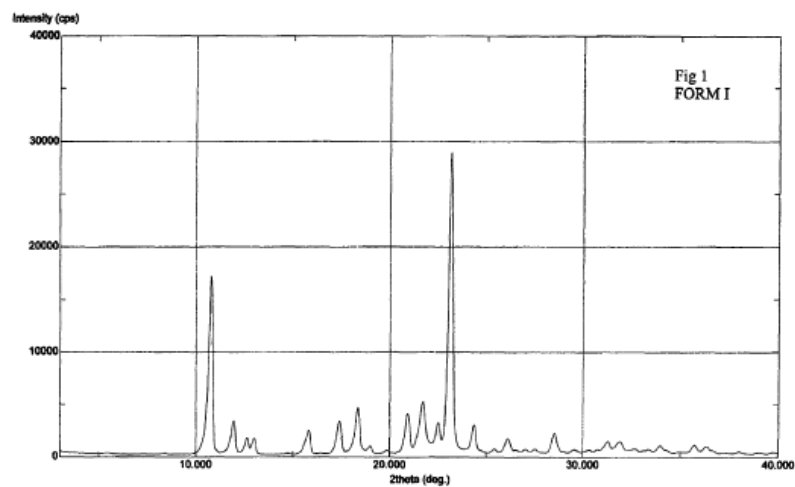


Figure 4 XRPD of crystalline SS form I.

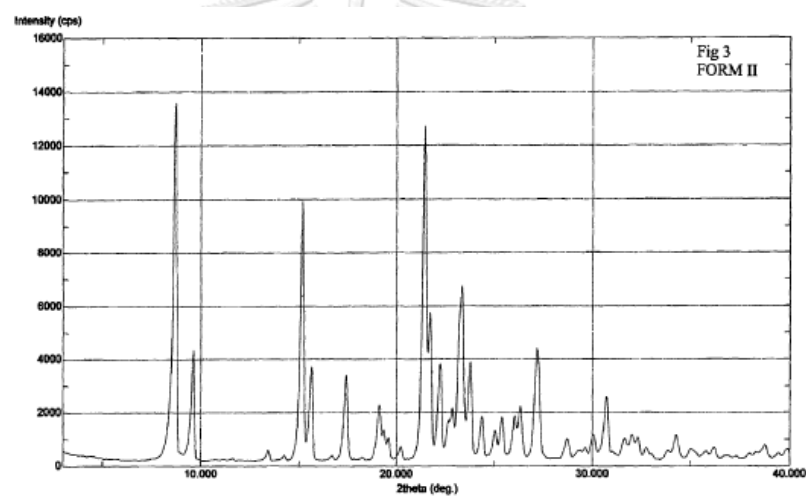


Figure 5 XRPD of crystalline SS form II.

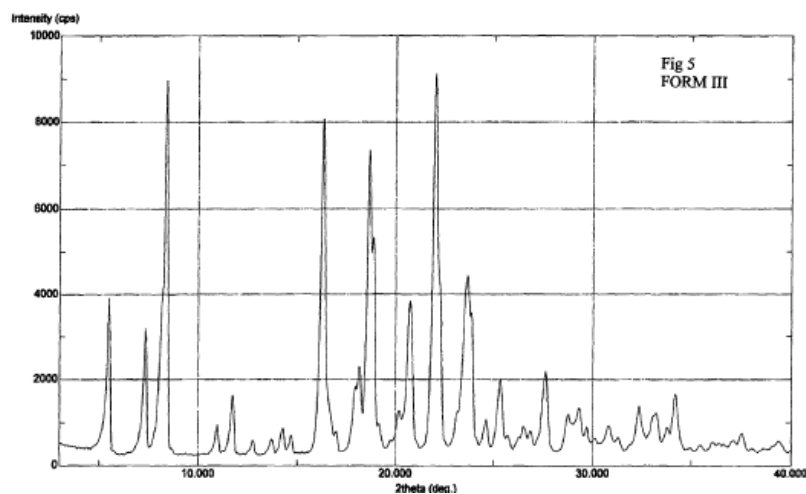


Figure 6 XRPD of crystalline SS form III.

Among crystalline forms of SS, the thermal history of form I and form II was available. DSC thermogram of crystalline form I showed the first endothermic peak around 205-210°C that referred to melting with decomposition (13,16,39,56). Meanwhile, form II showed 7°C higher melting temperature than that of form I (Table 3) (47).

Table 3 DSC of crystalline SS form I and form II

Thermal events	RSS Form I		RSS Form II	
	Endotherm (°C)	Heat (J/g)	Endotherm (°C)	Heat (J/g)
Decomposition 1	210	14	217	19
Decomposition 2	288	15	283	15
Decomposition 3	328	11	328	9

The interconversion pathway of amorphous and crystalline SS was discovered. Amorphous SS was possibly prepared by several approaches such as spray drying (71), milling (13). Unfortunately, freshly prepared amorphous SS was not stable and turn to be more stable crystalline after storage. The rate of interconversion of amorphous SS to stable crystalline was rapid after exposure under high humidity and/or high temperature. Pure crystalline SS was gained after amorphous SS was stored at 70% and 90% RH within 4 and 1 hour, respectively (Figure 7). The higher temperature of 35°C led to induced the faster recrystallization of amorphous SS when compared with lower temperature of 25°C (71).

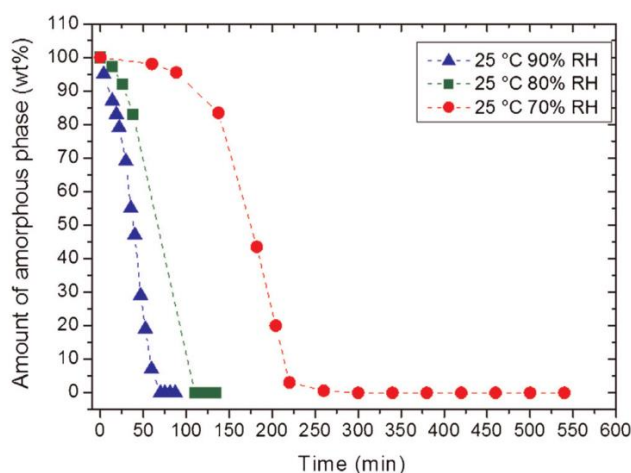


Figure 7 Rate of recrystallization of amorphous SS at 25°C and 70, 80 and 90 %RH.

As described earlier, SS existing in both three crystallines and amorphous state. Amorphous state of SS could recrystallize within short time after exposure to severe condition of humidity and/or temperature. Thus, SS was suitable to use as a model drug because the investigation of recrystallization of amorphous phase was possibly determined in the short term period.

2.6 Mesoporous silica

SYLOID[®] FP silica was in the class of non-ordered mesoporous silica (disordered pore structure) which has high internal porosity, high surface area and high adsorptive capacity as seen in simulate figure (Figure 8) (18).

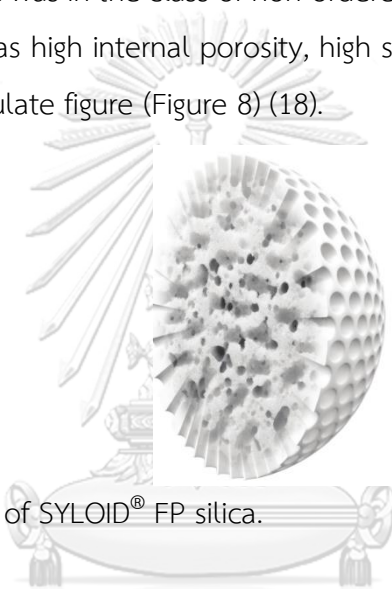


Figure 8 Simulate figure of SYLOID[®] FP silica.

It can be applied to use as multifunctional ingredient such as glidant, adsorbents (18,32). Moreover, it can act as carrier to produce an amorphous drug in order to improve drug solubility (38). S244 silica and SAL-1 silica were used in the study of enhancing dissolution of poorly soluble drug (32,41,48). Low and high concentration of itraconazole solution were possibly loaded on S244 and SAL-1 silica by using immersion method. They were appeared as amorphous phase in which resulted higher dissolution (Figure 9) (32). The amount of itraconazole loaded into S244 silica was higher than that of SAL-1 silica as a result of the high pore volume of S244 (32). Comparison of physical characterization of the S244 silica and SAL-1 silica shown in Table 4 (32).

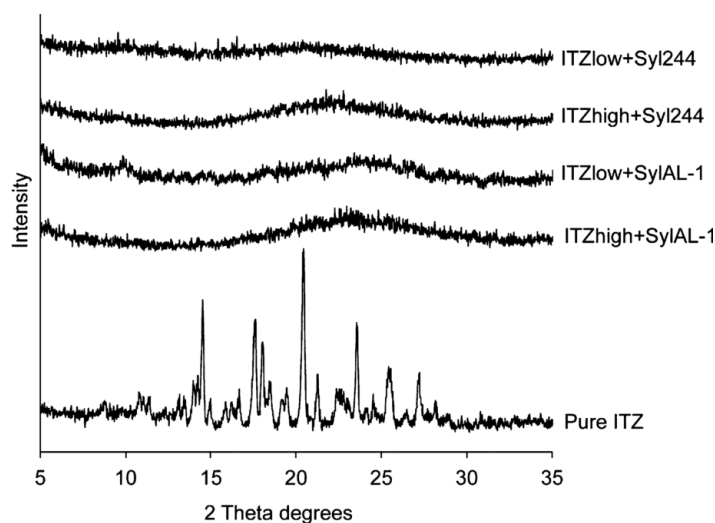


Figure 9 XRPD patterns of itraconazole loaded on mesoporous silica

Table 4 Physical characterization of the S244 silica and SAL-1 silica.

Particles	Particles size (μm)	Surface area (m^2/g)	Pore volume (cm^3/g)	Average pore diameter (nm)
SAL-1 silica	6.5 - 8.1	683 ± 11	0.130 ± 0.005	3.2 ± 0.02
S244 silica	2.5 - 3.7	311 ± 14	1.42 ± 0.04	19.0 ± 1.1

2.7 Polymer

PVP is soluble synthetic polymer which had the chemical structure shown in Figure 10 (7). Different grade with different the number of monomers in polymer chain eventually resulted in different viscosity (Figure 11) (7). The degree of viscosity had been declared as K-value that directly related to the average molecular weight (Table 5) (33). The higher K-value commonly utilize as a binder in tablet formulation due to the higher binding strength. The lower K-value such as K12 typically applied in the suspension for injection as a function of suspending agent. However, the lower K-value has alternatively use as crystallization inhibition. It also provided the amorphous stabilization by reduction of molecular mobility of drug molecule, anti-plasticization, intermolecular interactions and reduction of the chemical potential of drug (60).

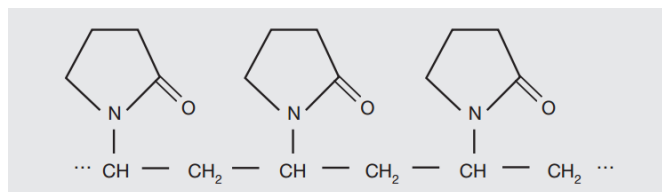


Figure 10 Chemical structure of PVP.

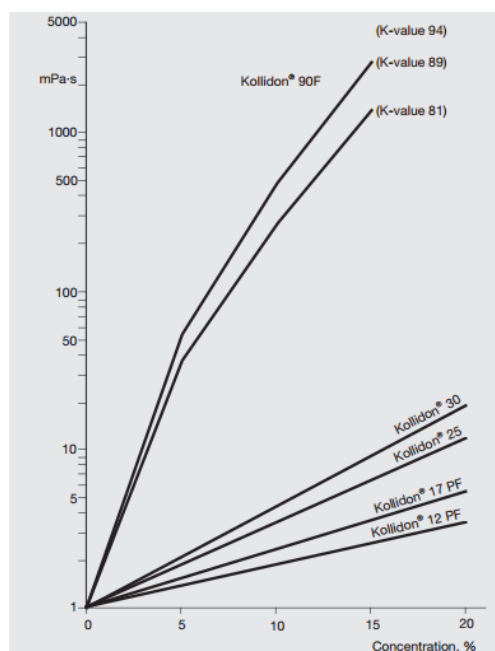


Figure 11 Viscosity curves for the soluble Kollidon[®] grades in water.

Table 5 Average molecular weight of PVP at different K-value.

K-value	Molecular weight (g/mol)
12	2500
25	25,000
30	40,000
90	1,100,000

Mechanism of PVP-stabilized amorphous drug are described herein after. PVP K29/32 could decrease the nucleation rate of felodipine spin-coated films at dry state as seen in Figure 12. Anti-plasticizing agent properties and H-bonding interaction were the main mechanism on stabilization (Figure 13 and 14) (34). Amorphous paracetamol with PVP K17 prepared by co-spray drying showed the mixture between crystalline and

amorphous whereas K29/32 able to provide more purify X-ray amorphous (Figure 15) (72). Amorphous paracetamol with PVP K29/32 showed the stable of non-crystalline arrangement of paracetamol upon storage. Co-milled mixture between SS and different concentration of PVP K30 expressed different ability on amorphous stabilization (5). The effective concentration of PVP K30 of at least 80% w/w was determined (Figure 16). The main mechanism involving the stabilization of amorphous SS with PVP was H-bond interaction (Figure 17).

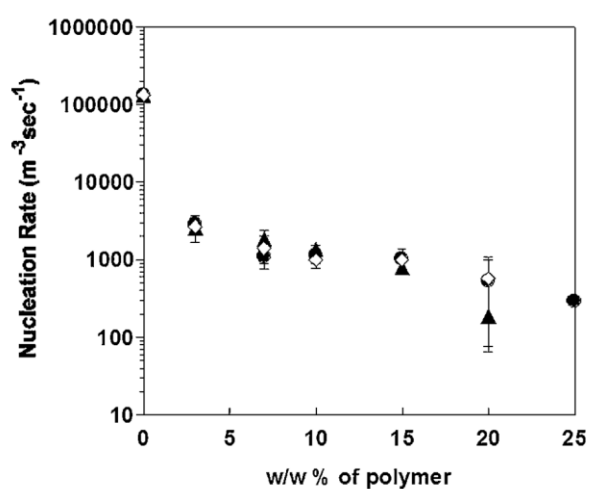


Figure 12 Nucleation rate as a function of PVP K29/32 concentration.

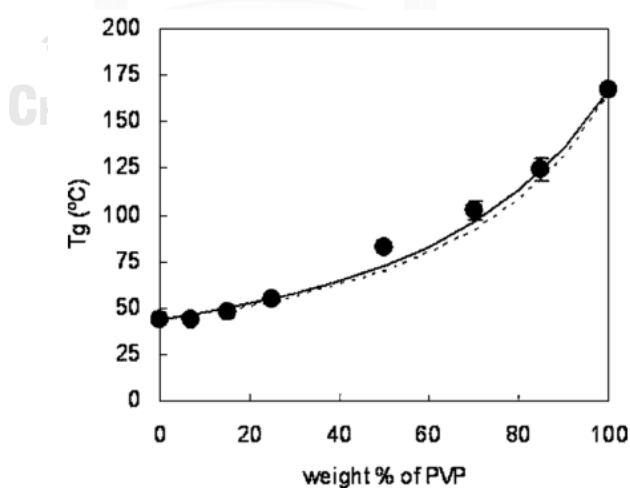


Figure 13 T_g of amorphous felodipine as a function of weight fraction of PVP.

(The broken line represents the fit to the Gordon–Taylor equation, the solid line represents the fit to the Couchman–Karasz equation.)

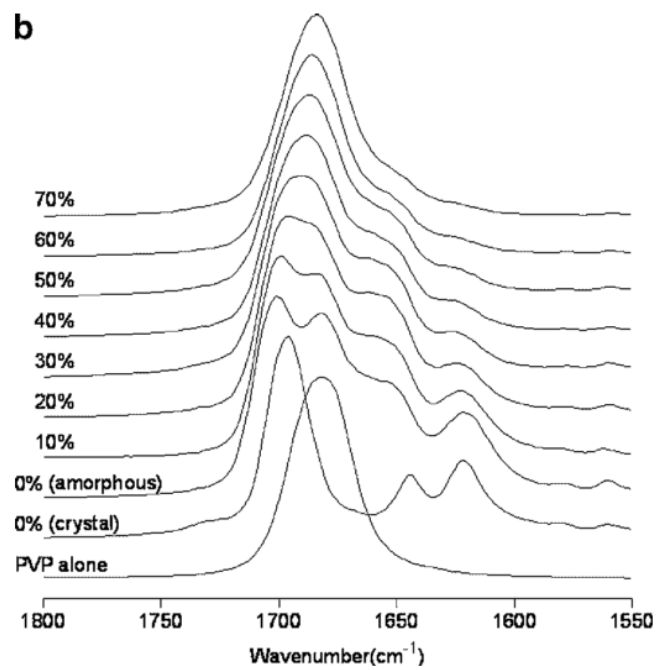


Figure 14 FTIR of felodipine/PVP solid dispersion at different weight ratio.

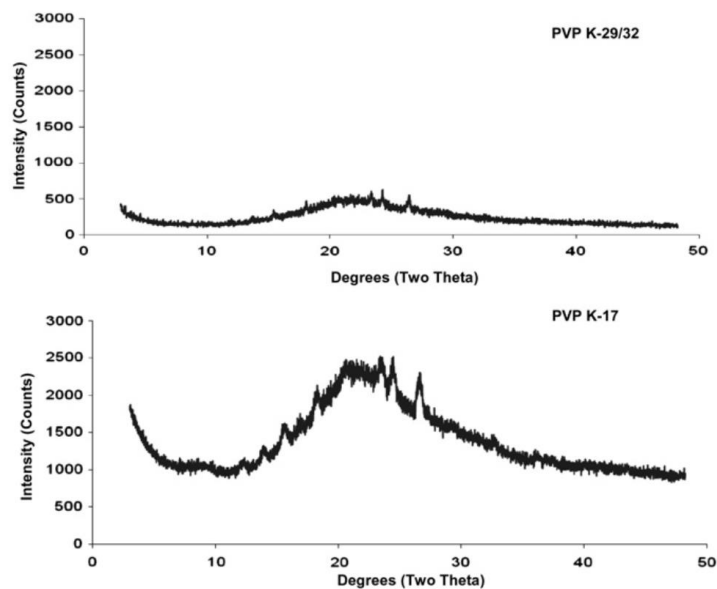


Figure 15 Comparative XRPD of 50% w/w paracetamol dispersions spray dried with various PVP freshly prepared.

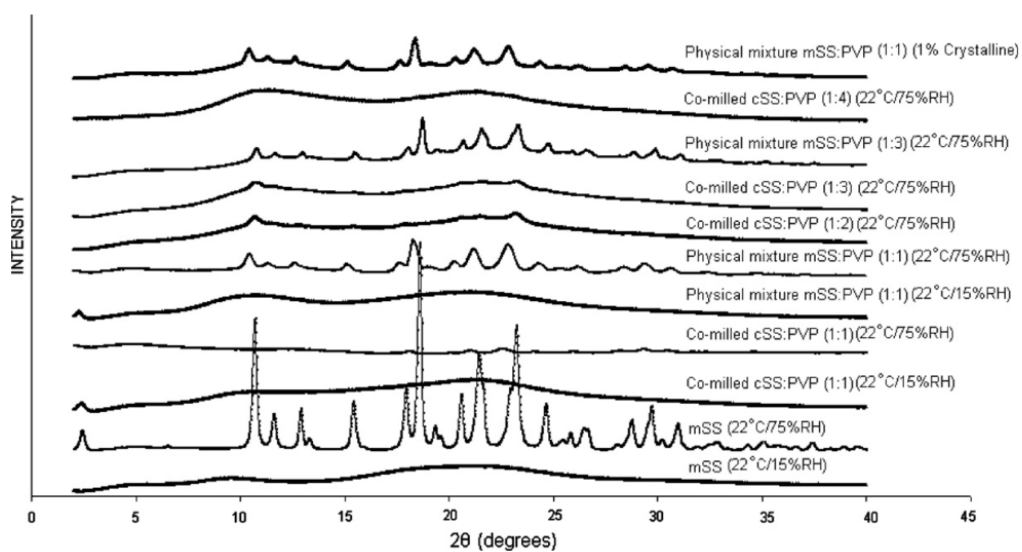


Figure 16 XRPD patterns of co-milled SS: PVP and physical mixture of milled SS: PVP after stored at 22°C and 15/75% RH for 7 days.

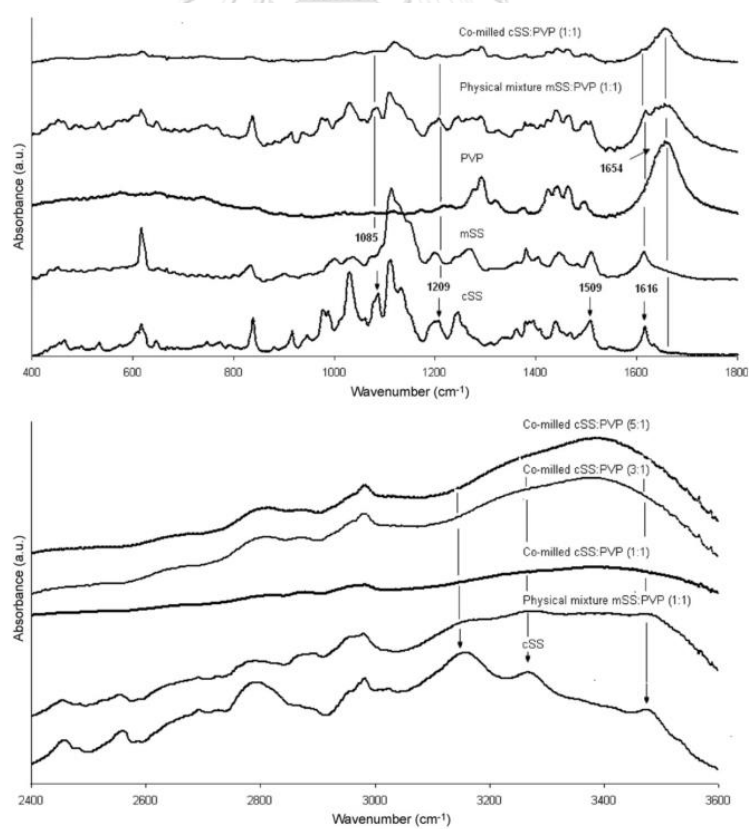


Figure 17 FTIR spectra of SS, milled SS, PVP, physical mixture of milled SS: PVP 1:1, co-milled mixtures of SS: PVP (1:1, 3:1 and 5:1).

Not only PVP but other polymer such as HPMC or HPMCP also had a spectrum on amorphous stabilization (34-36,61,63,72). It was therefore necessary to be consider the type of polymer on the ability of recrystallization inhibition by taking into account of the chemical structure including polymer chain length.



CHAPTER III

MATERIALS AND METHODS

MATERIALS

- Absolute ethanol (American Chemical Society grade, EMSURE[®], Merck KGaA, Darmstadt, Germany)
- Acetonitrile (HPLC Grade, J.T.Baker[®], Avantor Performance Materials, Inc., Pennsylvania, USA)
- Deionized water
- Hydrochloric acid (36%, Analytical reagent, Ajax Finechem Pty Ltd., New South Wales, Australia)
- Poly (vinylpyrrolidone) K12 (Kollidon[®] 12, BASF, Ludwigshafen, Germany) was obtain from VIV group (Bangkok, Thailand)
- Potassium dihydrogen orthophosphate (Analytical reagent, Ajax Finechem Pty Ltd., New South Wales, Australia)
- Salbutamol sulfate crystalline form I (SS) Batch No. SS10112003 (Neuland Laboratories Limited, Telangana, India)
- Sodium chloride (American Chemical Society Reagent, J.T.Baker[®], Avantor Performance Materials, Inc., Pennsylvania, USA)
- SYLOID[®]244 FP Silica Batch No. 1000277196 (Grace GmbH & Co., Worms, Germany) was obtain from Tinnakorn Chemical and supply Co., Ltd. (Bangkok, Thailand)
- Ultrapure water

EQUIPMENT

- Amber glass bottle 20 mL (diameter 2.00 cm, length 5.50 cm) with aluminium cap
- Analytical balance (A200s, Sartorius Goettingen, Germany), (ML303, Mettler Toledo, Schwarzenbach, Switzerland), (XP205, Mettler Toledo, Schwarzenbach, Switzerland)
- Central processor (FP90, Mettler Toledo, Columbus, USA)
- Centrifuge (Centrifuge 5810, Eppendorf AG, Hamberg, Germany)
- Cryomill[®] (Retsch GmbH, Haan, Germany)
- Desiccator
- Differential scanning calorimeter (DSC822^e, Mettler Toledo, Columbus, USA), (DSC 201 F1 Phoenix, NETZSCH, Selb, Germany)
- Fourier transform infrared spectrometer (Nicolet iS10, Thermo Fisher Scientific, Wisconsin, USA), (Perkin Elmer, Spectrum One, Perkin Elmer, Massachusetts, USA)
- High performance liquid chromatography (Shimadzu, Kyoto, Japan) equipped with a model series LC-20AD pump, SIL-20A HT Autosampler and SPD-20A UV-Vis detector
- Hot air oven (Mettler, Schwabach, Germany)
- Hot stage (FP82HT, Mettler Toledo, Columbus, USA)
- High performance liquid chromatography column Capcell PAK C18, 150x4.6 mm (Shiseido Co., Ltd., Japan)
- Hygro-thermometer (Brannan, Leconfield Industrial Estate, Cumbria, England)
- Magnetic stirrer (MSH-300, BIOSAN, Riga, Latvia)
- Membrane filter holder (Whatman, GE Healthcare, Illinois, USA)
- Microscope (Nikon Eclipse E200-LED, Tokyo, Japan)
- Nylon membrane filter 0.45 µm (Membrane solution, Washington, USA)
- Nylon syringe filter 0.45 µm (VertiClean[™], Vertical Chromatography Co., Ltd., Nonthaburi, Thailand)

- pH meter (FiveEasy™ FE20-I, Mettler Toledo, Columbus, USA)
- Polarizing set (Nikon MBB 75310, Tokyo, Japan)
- Shaking incubator (LabTech, New Delhi, India)
- Sonicator (VGT-1730QT, GT Sonic, Guangdong, China)
- Thermogravimetric analyzer (TGA/SDTA851^e, Mettler Toledo, Columbus, USA)
- Vacuum pump (General electric motor, Arthur H. Thomas Co., Philadelphia, USA)
- X-ray powder diffractometer (Miniflex II, Rigaku, Tokyo, Japan)



METHODS

3.1. Preparation of X-ray amorphous SS powder

SS was ground at room temperature by using Cryomill[®] (a planetary ball mill). The milling was equipped with stainless steel jar 25 mL in conjunction with 5 zirconium oxide balls (Diameter 10 mm). The frequency of shaking of 25 Hz was employed. Two governing process conditions of loaded quantity of SS and time of milling were investigated in order to achieve X-ray amorphous SS as shown in Table 6.

Table 6 Loaded quantity of SS and time of milling of the preparation of amorphous SS.

Loaded quantity of SS (gram)	Time of milling (hour)
1.0	2
0.5	2
0.5	2.5
0.5	3

After milled sample powder was fabricated, it was collected and kept in air tight amber glass vial. It was then stored under dry condition by using silica gel as desiccant at room temperature. The sample obtained was characterized by using XRPD as soon as possible due to the fact that amorphous milled SS was rapidly crystallized and eventually interconverted to more stable crystalline form I (11,71).

3.2. Preparation of SS adsorbed on mesoporous silica

SS was loaded on S244 silica by using incipient wetness impregnation method. The hydroalcoholic (50:50 v/v) solution of SS at concentration of 3% w/w was incorporated onto S244 silica powder with gently and thoroughly mixing by using mortar and pestle. The ratio of 1:4 (gram of S244 silica: mL of drug solution) was used for each time of impregnation. The remained solvents of sample prepared were then evaporated by hot air oven at 40°C for 6 hours. The specification of the total residual solvents was not more than 6 %w/w since the weight loss of the sample of SS

adsorbed on S244 silica was found to be lower than 6.0 (appendix A). The S244 silica were impregnated several times with a solution of SS.

3.3. Preparation of SS adsorbed on mesoporous silica with polymer

The hydroalcoholic (50:50 v/v) solution of SS at concentration of 3% w/w combined with PVP K12 at concentration of 0.1, 0.5, 1, 5, 10, 20 and 30% w/w of SS were prepared and incorporated to S244 silica by impregnation at the ratio of 1:4 (gram of S244 silica: mL of drug solution) for each time of impregnation. The impregnation procedure was conducted the same as in the method of 3.2.

Table 7 Master formula of SS with PVP K12 in hydroalcoholic solution.

SS (g)	PVP K12 (g) (% of SS)	hydroalcoholic (50:50 % v/v) qs. to (g)
3	0.003 (0.1%)	100
3	0.015 (0.5%)	100
3	0.03 (1%)	100
3	0.15 (5%)	100
3	0.3 (10%)	100
3	0.6 (20%)	100
3	0.9 (30%)	100

The control group referred to SS adsorbed on S244 silica at 4.5 times of impregnation without the addition of PVP K12.

3.4. Solid state characterization

3.4.1 Crystal morphology

Microscope equipped with hot stage was used to observe the physical appearance of sample. A small amount of sample was placed on glass slide and subjected on the stage of microscope. Heating with the range of 30–300°C at a rate of 10°C/min was performed in case of the investigating of the thermally assisted particle deformation. Polarized setting device comprised of polarizer and analyzer was utilized

in conjunction with microscope when the investigating of birefringence was needed to analyzed.

3.4.2 Solid state molecular arrangement

XRPD was employed to detect the solid state structure. The sample was gently packed and carefully flattened on zero-background silicon holders and analyzed without humidity or temperature controller. The scanning condition was in the 2θ range of $5-35^\circ$ with scan speed of $2^\circ/\text{min}$. The PDXL analytical software was used for analyzing the performed data.

3.4.3 Thermal analysis

3.4.3.1 Differential scanning calorimetry (DSC):

Sample of 3-5 mg was weighed accurately in aluminium pan $40\ \mu\text{l}$ with pin holed lid. It was then hermetically sealed. Temperature scan range was 25 to $300\ ^\circ\text{C}$ with heating rate at $10^\circ\text{C}/\text{min}$. Nitrogen gas purged was set up at 60 ml/min as protective gas. STARe evaluation software was used for data analysis.

3.4.3.2 Thermogravimetric analysis (TGA):

Sample of 5-10 mg was weighted accurately in alumina crucible $70\ \mu\text{l}$ wherein covered with pierce lid. The scanning range of temperature was 25 to $300\ ^\circ\text{C}$ with heating rate of $10^\circ\text{C}/\text{min}$. Purged nitrogen gas at 30 ml/min was applied as protective gas. STARe evaluation software was used for data analysis.

3.4.4 Molecular interaction

Attenuated total reflectance infrared spectroscopy (ATR-IR) was utilized for investigating any possible molecular interaction. Sample powder was placed on the window of ATR sampling accessory. The scanning range was in between $4000-600\text{cm}^{-1}$. Spectral setup data was averaged 32 scan at $4\ \text{cm}^{-1}$ resolution. Spectral subtraction with blank is needed to be routinely done before gaining the final spectra. It was then analyzed by OMNIC software.

3.5. Quantitative determination of the degree of crystallinity of SS

The calibration curve between percent crystallinity of SS versus corresponded to the Bragg's peak height at $10.6^\circ 2\theta$ was constructed. Spike-placebo method was used as a platform for quantitative determination. S244 silica particles represented the placebo since it existed in the product as an inert material including their amorphous nature. Spiking of crystalline SS form I should regularly be prepared at different concentrations in order to provide the responses their characteristic ($10.6^\circ 2\theta$). One of the most important concerning factor of this method is the homogeneous of sample prepared. Spike placebo method of solid state mixture is generally non homogeneous system. Thus, the particle size of each component should have the comparable particle size that would give homogeneous mixture. In this case, SS raw material has been proved to be crystalline form I with the average particle size of $3.79\ \mu\text{m}$. Nevertheless, loose agglomeration of S244 silica particle was found. That was the reason of the disadvantages of non-homogeneous physical mixture (1). The grinding can give the smaller particle size of crystalline SS. Unfortunately, preliminary result showed the grinding induced amorphization of SS. Therefore, there was an alternative way to fabricate comparable size of crystalline SS to S244 silica. Smaller particle with amorphous nature of SS was prepared by milling. It was then kept in high humidity chamber to drive the polymorphic transformation

To achieve the different % concentration of crystalline SS form I, pure amorphous S244 silica was gently mixed with crystalline SS form I at different weight ratio in mortar. The target concentration of crystalline SS form I was in the range of 10-50% w/w. All concentration standard mixture were packed on the quartz sample holder to ensure a constant irradiated throughout the sample volume for XRPD measurements. The peak position at $10.6 \pm 1^\circ 2\theta$ was used for the quantification of crystalline SS (because it was the obvious respond peak after stored interested sample from preliminary stability test). The PDXL software was used to determination the peak height for each sample using hide background procedure. Linearity of above method was considered from the coefficient of determination (r^2). Acceptable procedure should provide r^2 more than 0.95. Limit of detection (LOD) and limit of quantification

(LOQ) were determined according to the criteria of signal to noise (S/N) ratio of 3 and 10, respectively.

3.6. Determination of SS quantity adsorbed on mesoporous silica

Samples of approximately 5 mg were suspended in ultrapure water 50 ml. It was then vigorously shaken at 100 rpm for 12 hours and centrifuged at 1000 rpm for 30 min. The clear supernatant was decanted and filtered through membrane 0.45 μm . The drug content was analyzed by High Performance Liquid Chromatography (HPLC) system which was modified from Maithani and Singh (44). Separation and quantitation was made on a C18 Column 150x4.6 mm. For HPLC condition, mobile phase consisted of acetonitrile and 0.05M phosphate buffer 65:35 (v/v) (pH 4.2 ± 0.02 , adjusted with 0.1N hydrochloric acid (HCl)). Flow rate of mobile phase was 1.0 ml/min. and injection volume was 5 μL . The UV detector was set up at 235 nm.

This method had been validated in accordance with ICH guideline Q2(R1)(26) in terms of linearity, range, specificity, precision and accuracy (appendix C).

3.7. Stability investigation

Stability of amorphous SS powder, SS adsorbed on mesoporous silica and SS with polymer adsorbed on mesoporous silica were investigated.

Samples were stored in humidity chamber at $75 \pm 5\%$ RH and room temperature. The humidity control chamber of $75 \pm 5\%$ RH comprised of saturated sodium chloride solution filled in desiccator. It was equilibrated for a week before using. The level of humidity in chamber was determined by using hygro-thermometer every time before starting of storage. Sample was then monitored in term of the solid state structure by using XRPD. The starting time of changing from amorphous to crystalline was investigated and named as induction time.

CHAPTER IV

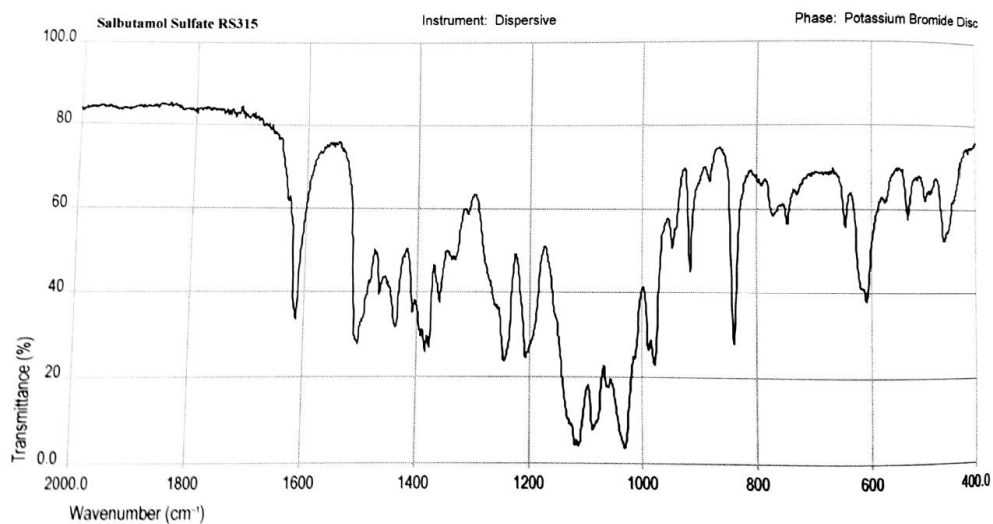
RESULTS AND DISCUSSION

4.1. Characterization of SS raw material and milled SS

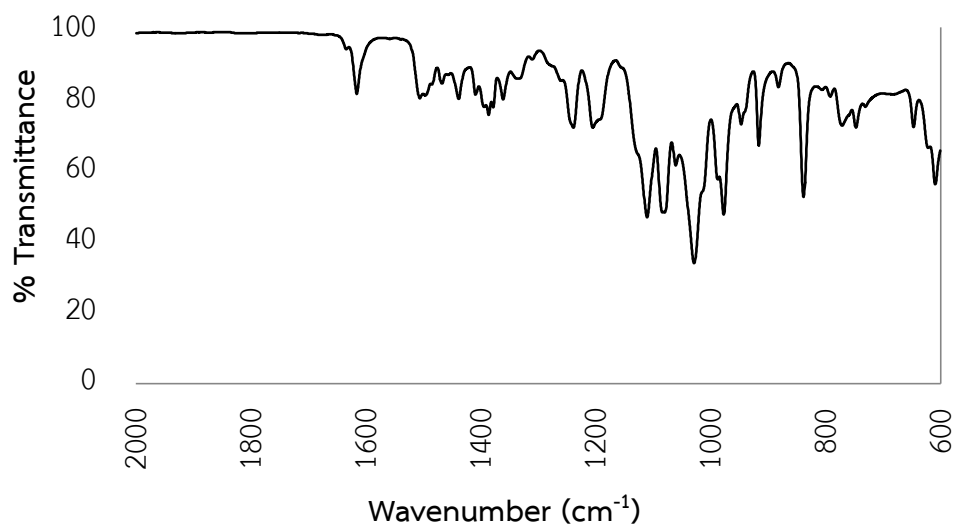
4.1.1 Characterization of SS raw material

SS raw material was received and used without any further treatment for this experiment as reference. Most of starting material used is necessary to be correctly identified and characterized in order to avoid the misinterpretation. Firstly, the identification of SS was performed by using FTIR spectroscopy in accordance with British Pharmacopoeia (BP) 2015. The FTIR spectra of SS raw material is shown in Figure 18B. The result showed that the spectra of SS provided a nearly identical pattern including several peak responses well agreed with FTIR spectra of SS in BP 2015 (Figure 18A). Therefore, raw material used in this studies was identified as SS.

Generally SS showed a few crystalline forms. At least three crystalline forms had already been characterized and published by Rao et al. (50). However, our studies need to use only specified crystalline form I as a starting material due to the most stable crystalline form (53). Thus, SS used is needed to be further characterized precisely in term of polymorphic form. IR spectra of different polymorphic forms of SS were previously reported (47,50) but they were not clearly distinguished amidst them. More precise method of polymorphic determination, XRPD, was then selected for characterization. XRPD pattern of SS raw material exhibited main characteristic peak responses at 10.6, 18.4, 21.3 and 23.0 °2 θ . It was well corresponded to the diffraction pattern of crystalline form I (Figure 19) (50,53).

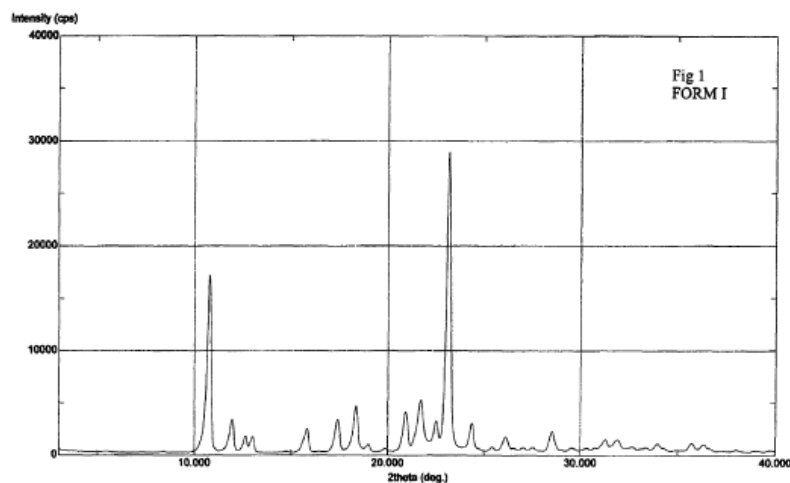


(A)

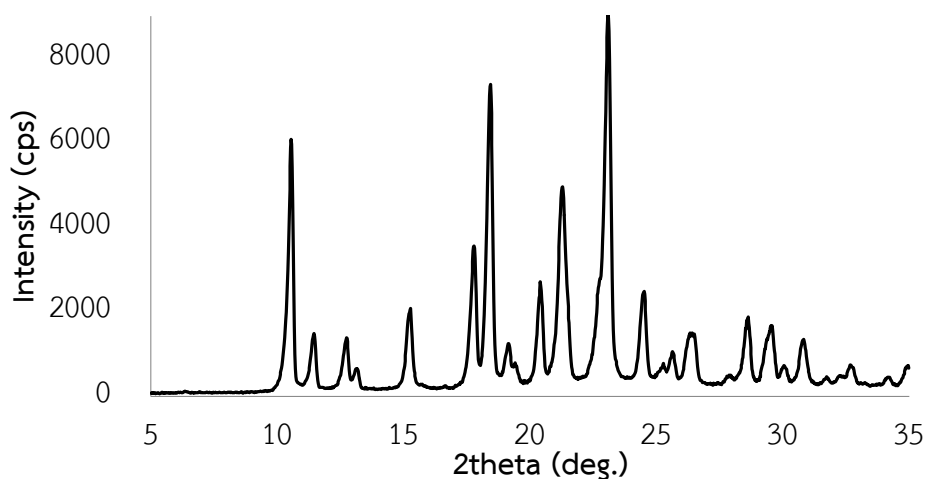


(B)

Figure 18 Comparative FTIR spectra of SS reference standard referred to BP 2015 (A) and SS raw material used (B).



(A)



(B)

Figure 19 Comparative XRPD of SS crystalline form I (A) and SS raw material used (B).

In order to confirm the existence of the crystallinity of SS raw material, the investigation of birefringence was performed with PLM. SS showed an elongate shape crystal habit with an illumination under polarized light (Figure 20) which was a good evidence of crystalline state. It was hence confirmed that SS was in the crystalline state.

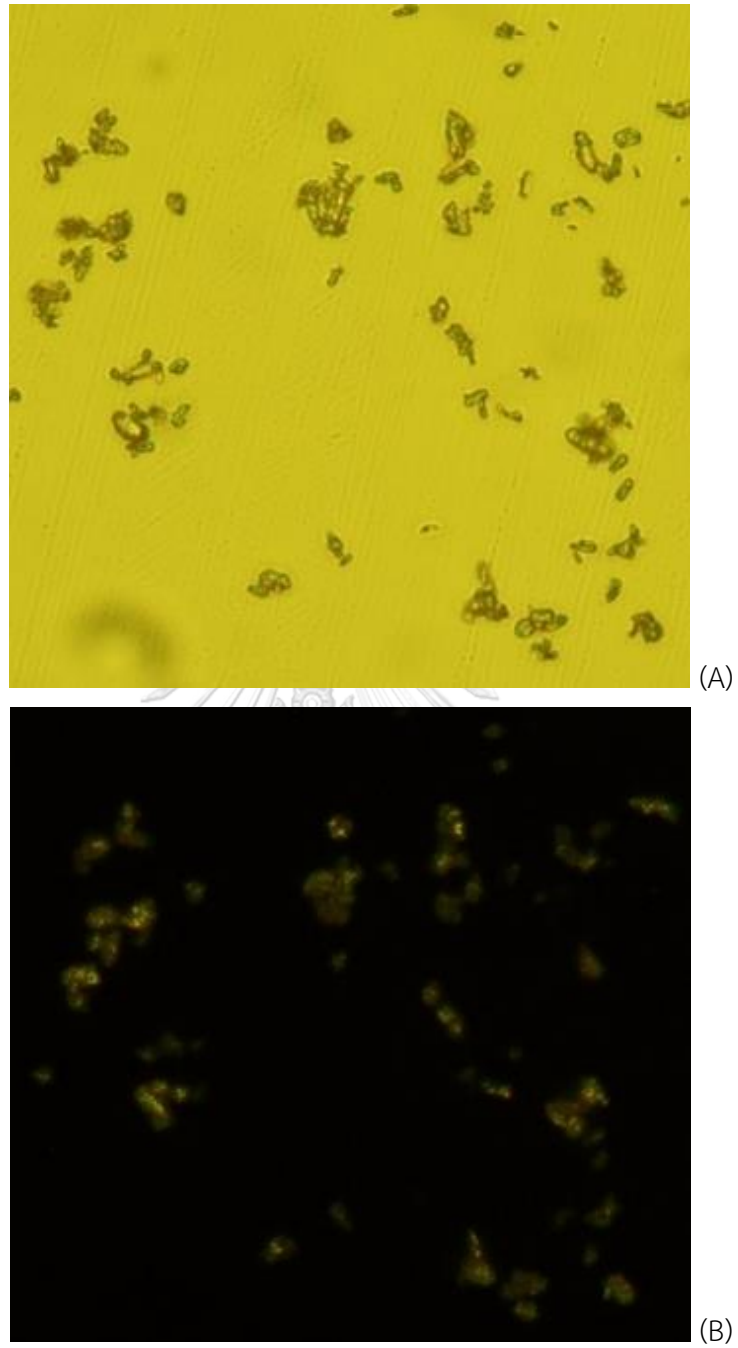


Figure 20 Photomicrograph of SS under bright field (A) and polarized light (B) (at magnification of 400).

Thermal analysis of SS were additionally investigated in order to know about thermal history and properties of SS. DSC thermogram of SS raw material (Figure 21) comprised of the first broad endothermic at initial condition (25 °C) until 165 °C, the second sharp endothermic peak (170-220 °C) and followed with the third endotherm in between 220 and 290 °C. To clearly identify the thermal event of SS, TGA was operated simultaneously. During the first endothermic peak, weight loss of less than 0.5% w/w was observed. It was negligible and should be therefore related to the dehydration of adsorbed water on SS particles. The second thermal event showed the sharp endothermic peak in conjunction with two consecutive steps of weight change. Less than 1 % of weight loss was recorded at the initial condition temperature range of 170 till 195 °C and followed with the weight loss of around 11% afterward (195-230 °C). This result suggested that the second thermal event was found to be the melting with decomposition synchronously (39,47,56). The third endotherm obviously involving the thermal decomposition due to huge weight loss. Further study of the thermal history of SS was carried out by using hot stage microscopy (Figure 22). The SS sample was heated on hot stage from 30 to 165 °C (comparable to the first endotherm). The crystal habit remained intact while it became more brownish at the higher temperature (230 °C). Discoloration of SS crystal under high temperature might be the effect of the instability or degradation. All of above DSC and TGA results indicated the crystalline form I of SS. It was due to the fact that the melting endotherm of SS appeared at approximately 205 °C was related with melting point of SS crystalline form I from previous reported (56) whereas crystalline form II had the higher melting endotherm (around 7 °C) than that of form I (47). In conclusion, SS raw material used in this studies was found to be crystalline form I.

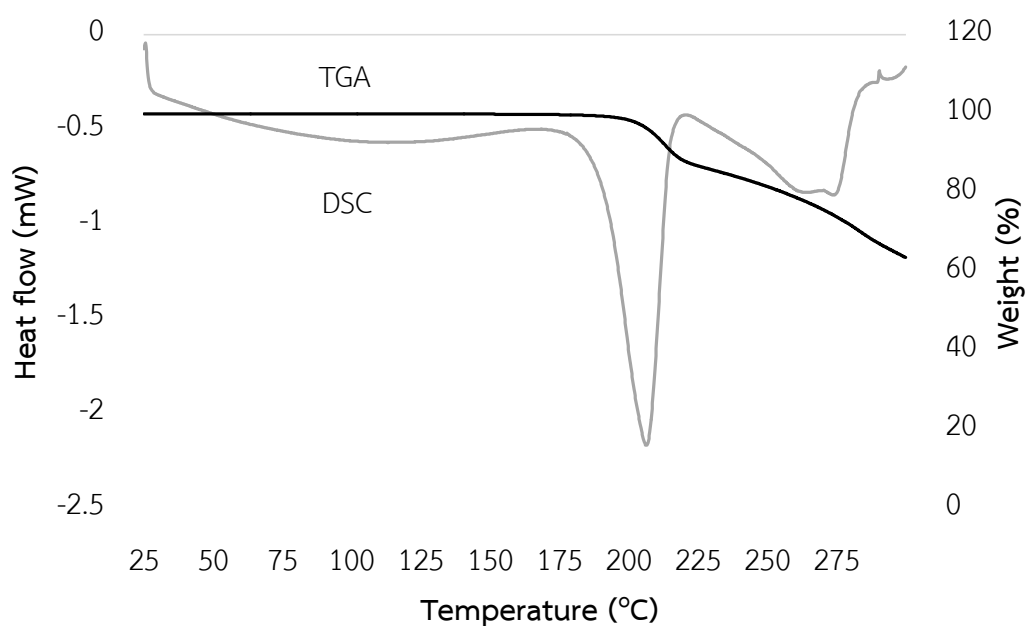


Figure 21 DSC and TGA thermograms of SS raw material.

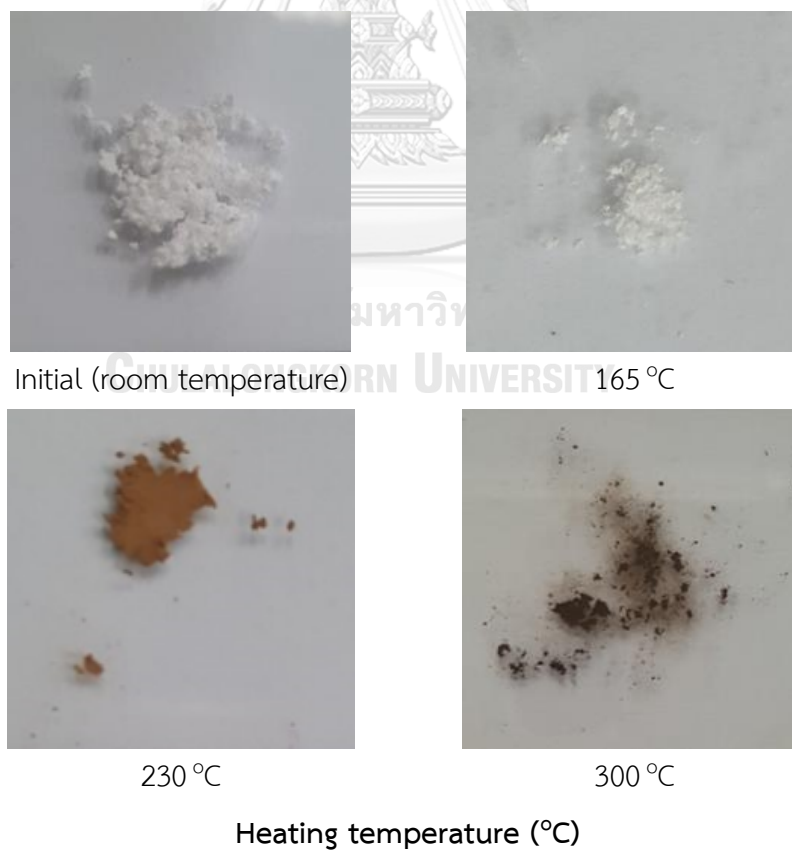


Figure 22 Physical appearance of the SS raw material under different heating temperatures.

4.1.2 Characterization of milled SS produced

Amorphization of SS was prepared via milling method. SS was previously reported on the ability of amorphization after grinding (5,6,13,19,20). Generally, the critical process parameters (CPP) of milling were the type and process condition of milling. In this study, ball milling was selected as milling equipment because of ease and convenience. The CPP of ball milling were loaded quantity of material and time of milling. (31,42) Initially, the CPP of loaded quantity was studied by controlling the milling time at 2 hours constantly. It was due to the fact that 2 hours of milling for SS would not provide any degradation which was observed by HPLC (data not shown). Two levels of loading 0.5 and 1.0 g of SS were loaded into ball mill. After milling was operated with the predetermined time, the samples were collected and further solid state characterized. XRPD results revealed that milled sample of loaded quantity of 1.0 g exhibited the peak responses at 10.6, 18.4, 21.3 and 23.0 °2θ with less crystallinity comparing to that of starting material. It was shown that the degree of amorphization was remarkably increased after milling process. However, it was found to be the mixture between crystalline form I and amorphous. Therefore, this condition was not appropriate to generate pure X-ray amorphous SS. When loaded quantity was reduced about 50% (0.5 g), XRPD result indicated that the higher degree of X-ray amorphous SS was produced which was seen from halo pattern with the disappearance of most of the characteristic Bragg's peak of crystalline form I. Nevertheless, some peak responses at 18.4, 21.3 °2θ which corresponded to crystalline form I still existed (Figure 23). Thus the obtained sample was incomplete X-ray amorphous which containing the trace of crystalline form I. In order to produced pure X-ray amorphous SS, the CPP of milling time was varied. Three levels of milling time were studied (Figure 24). At the moderate level of milling time (2.5 hours), XRPD showed the absence of peak at 18.4 °2θ but the peak at 21.3 °2θ was presented. It would be said that the longer milling time provided the more X-ray amorphous SS with the remained of small amount of crystalline form I. At the longest time period of milling in this studies (3 hours), the disappearance of both peaks at 18.4 °2θ and 21.3 °2θ was investigated. Therefore, complete X-ray amorphous SS was generated with no degradation (data not shown). The longer the milling time the more the X-ray amorphous production. In conclusion, X-ray

amorphous SS was prepared by ball milling with the process condition of 0.5 g loaded quantity and 3 hours of milling.

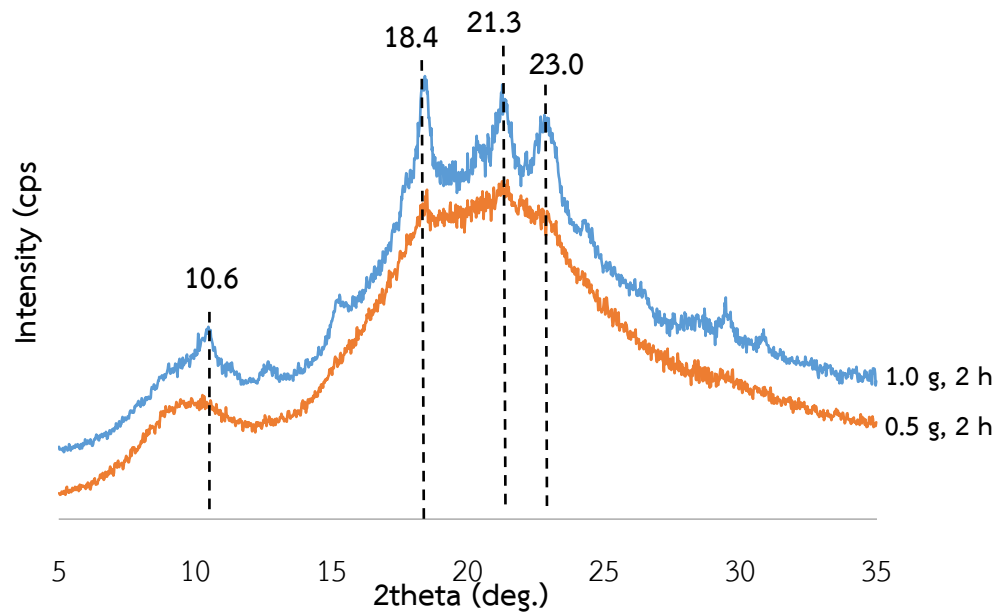


Figure 23 Comparative XRPD of milled SS at time of milling of 2 hours with different of loaded quantities.

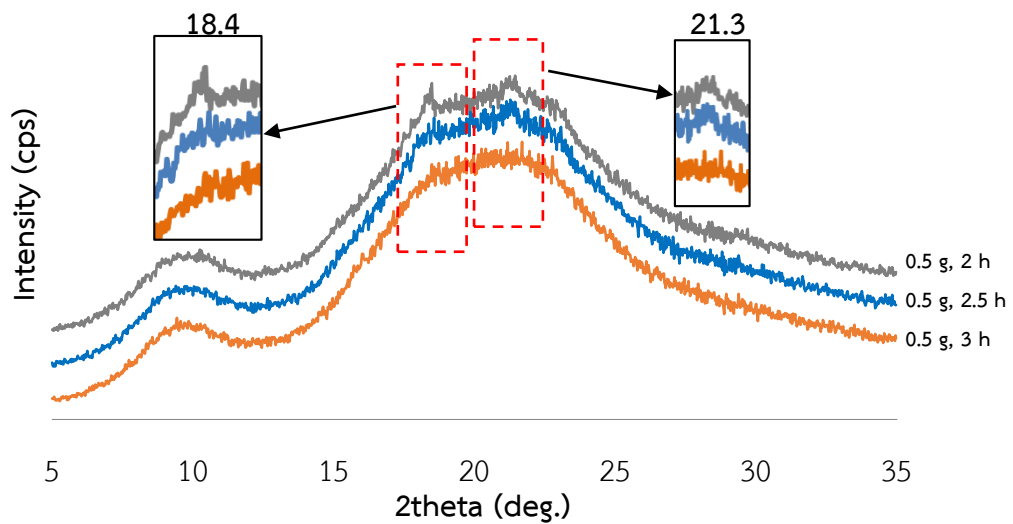


Figure 24 Comparative XRPD of milled SS at loaded quantity of 0.5 g with different times of milling.

X-ray amorphous milled SS showed irregular crystal habit with no birefringence under polarized light (Figure 25B). It agreed with XRPD that X-ray amorphous milled SS was non-crystalline state.

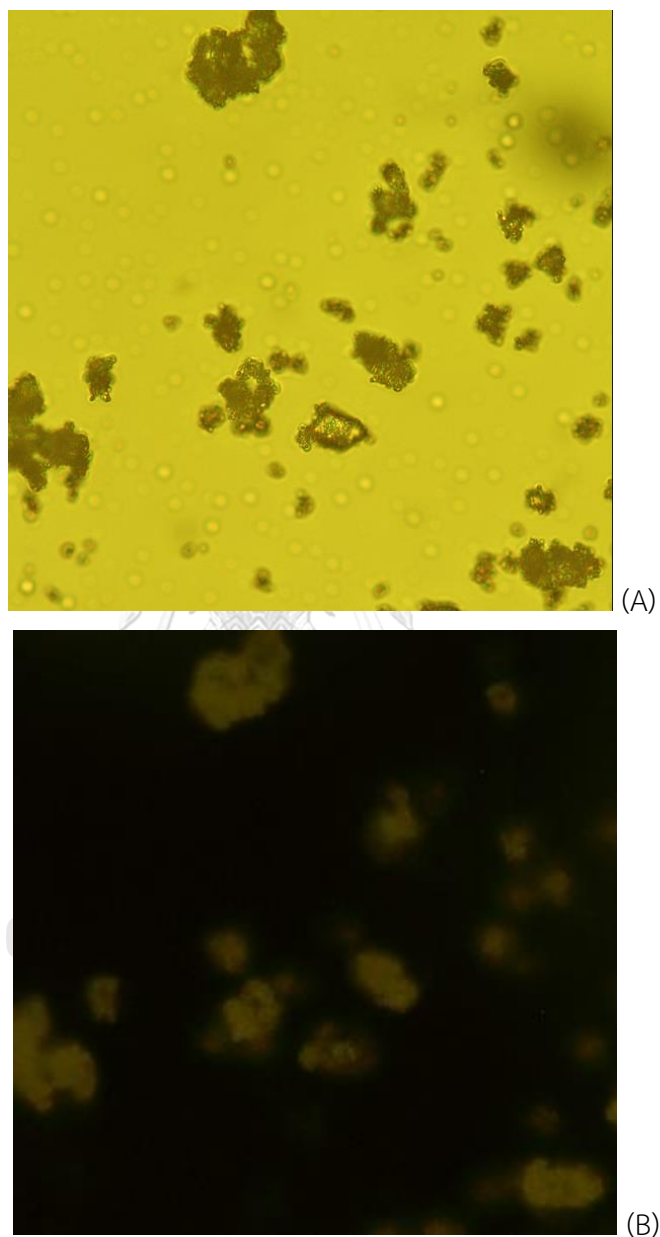


Figure 25 Photomicrograph of X-ray amorphous milled SS under bright field (A) and polarized light (B) (at magnification of 400).

To confirm the state of X-ray amorphous SS produced by milling, thermal analysis was carried out. Amorphous material commonly shows T_g while crystalline counterpart is absent. DSC results of milled SS consisted of four consecutive responses. The first response was the endothermic peak from 25 °C to 130 °C with the transition of baseline at around 60 °C. The second response was exothermic peak in between 140 to 155 °C. The third endothermic peak (160-205 °C) followed with the last fourth endothermic peak (230-300 °C) were later found. The investigation of weight loss of milled SS sample was synchronously performed. Comparative TGA and DSC thermograms were constructed (Figure 26). The result demonstrated that the first broad endothermic peak has the weight loss around 4% w/w that might be due to the adsorbed water. However, the larger amount of such water content should be related to the more adsorbed water on huge surface area of milled sample (small particles). Unfortunately, the transition of baseline was found in that temperature range. It directly correlated and was inferred to the glass transition state. Above results agreed well with previous studies (5,16). Negligible change of weight (less than 1%) was found and supported the glass transition state. Next exothermic peak related to the recrystallization of amorphous SS which eventually resulted in the crystalline state. During above temperature range, there was no weight loss that supporting the recrystallization without any degradation. The second endothermic peak was the most important characteristic of amorphous SS produced by milling which had been found by Curtin, et al. (13). It concerned with the melting of amorphous SS. In addition, significant weight loss of 8% w/w was investigated in that temperature range. It also indicated the decomposition with melting which was clearly supported from the discoloration of sample (Figure 27). The last endothermic peak had the greatest weight loss (more than 12% w/w) that indicated the major decomposition.

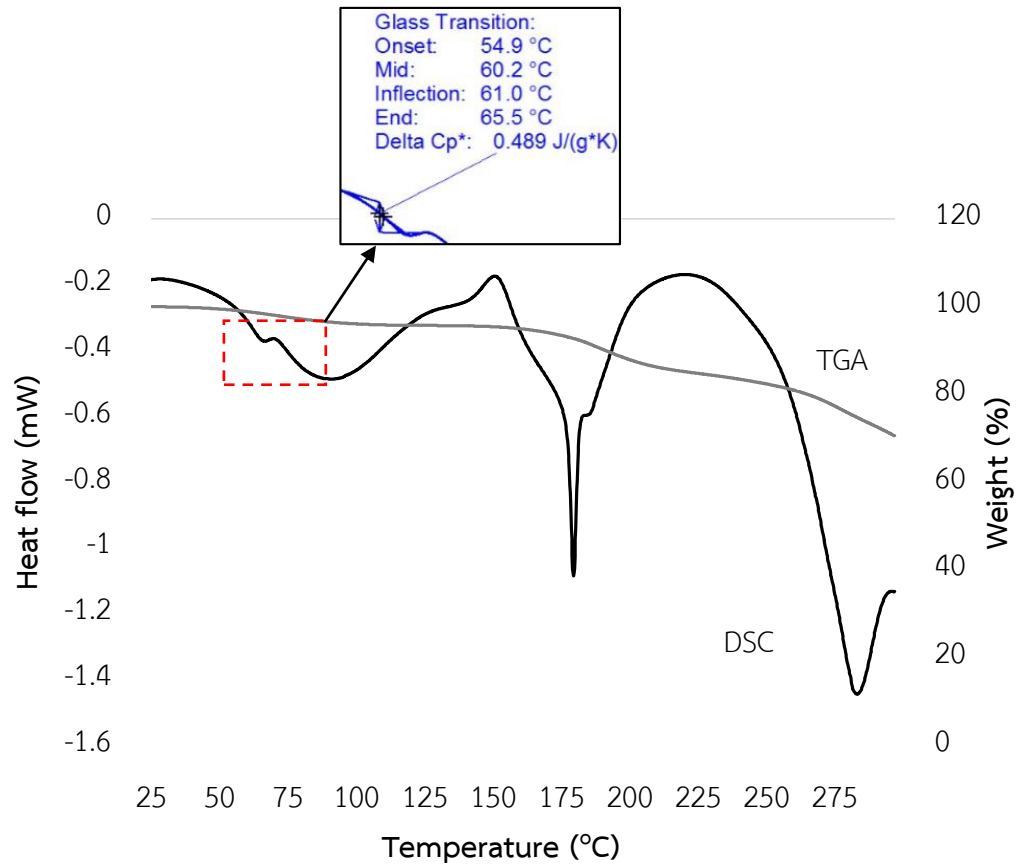


Figure 26 DSC and TGA thermograms of X-ray amorphous milled SS.

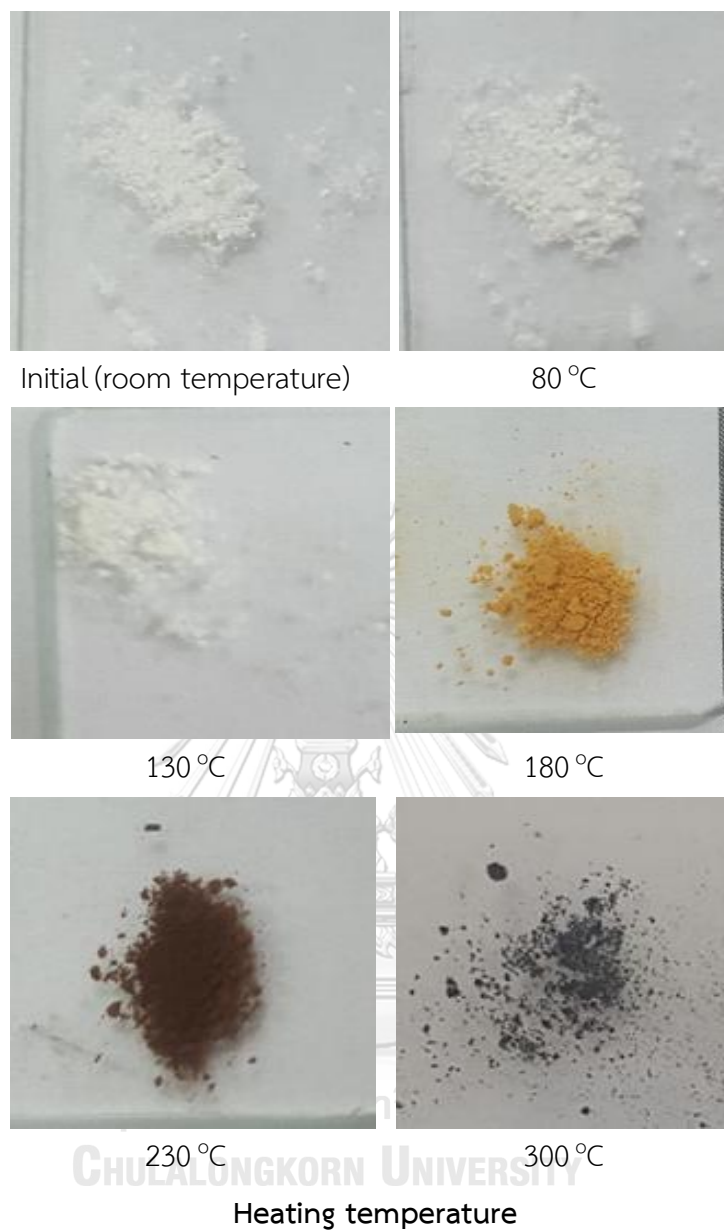


Figure 27 Physical appearance of X-ray amorphous milled SS under different heating temperature.

Molecular disorder of amorphous might be resulted in difference of hydrogen-bonding pattern between its molecules. Thus, FTIR spectra of amorphous might pose the broadening and/or diffusion of bands attributed to the differences of hydrogen-bonding patterns of two solid-state forms (30). The FTIR spectra of X-ray amorphous milled SS and crystalline SS are remarkable difference that shown in previous studies (5,19,20)

When considering the SS chemical structure (Figure 28), there were ten possible hydrogen atoms playing a function of hydrogen bond donor. They were found in hydroxyl group (eight atoms) including two atoms in secondary amine group. Meanwhile, the proton acceptors available for hydrogen bonding are (i) four oxygen atoms of sulfate ion, (ii) six oxygen atoms of C-O-H bond and (iii) two nitrogen atoms of secondary amine. FTIR spectra of X-ray amorphous SS produced showed the distinguished pattern with crystalline counterpart (Figure 29). The changing of hydrogen bonding due to the peak shift including peak broadening and intensity decreasing at several wavenumbers were observed as described herein in Table 8. In addition, the non-hydrogen bonding site of CH₃ bending, C-H bending and CH₂/CH₃ rocking also changed. It might be due to the greater flexible of conformational in the amorphous state, thus allowing increased interaction with other functionalities in molecule (30).

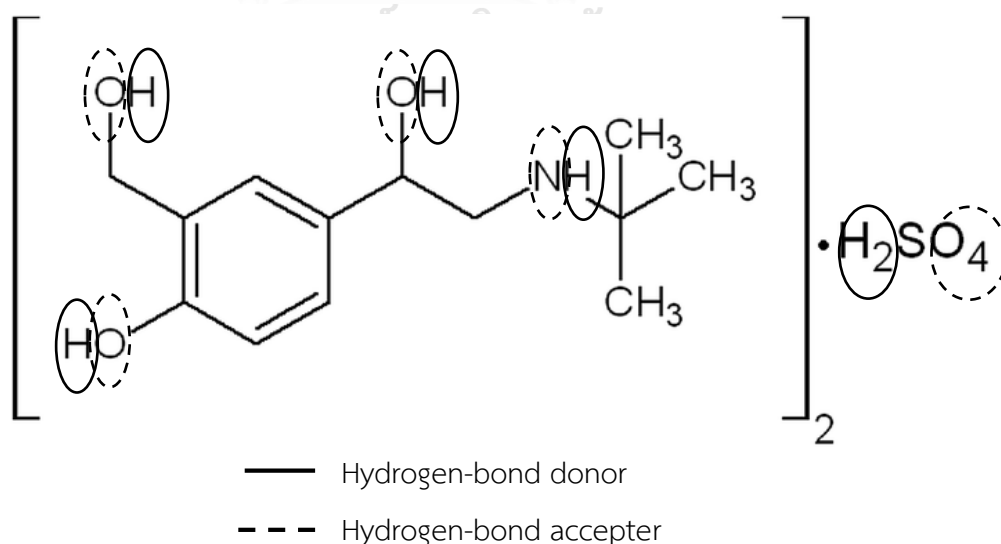


Figure 28 Chemical structure of SS.

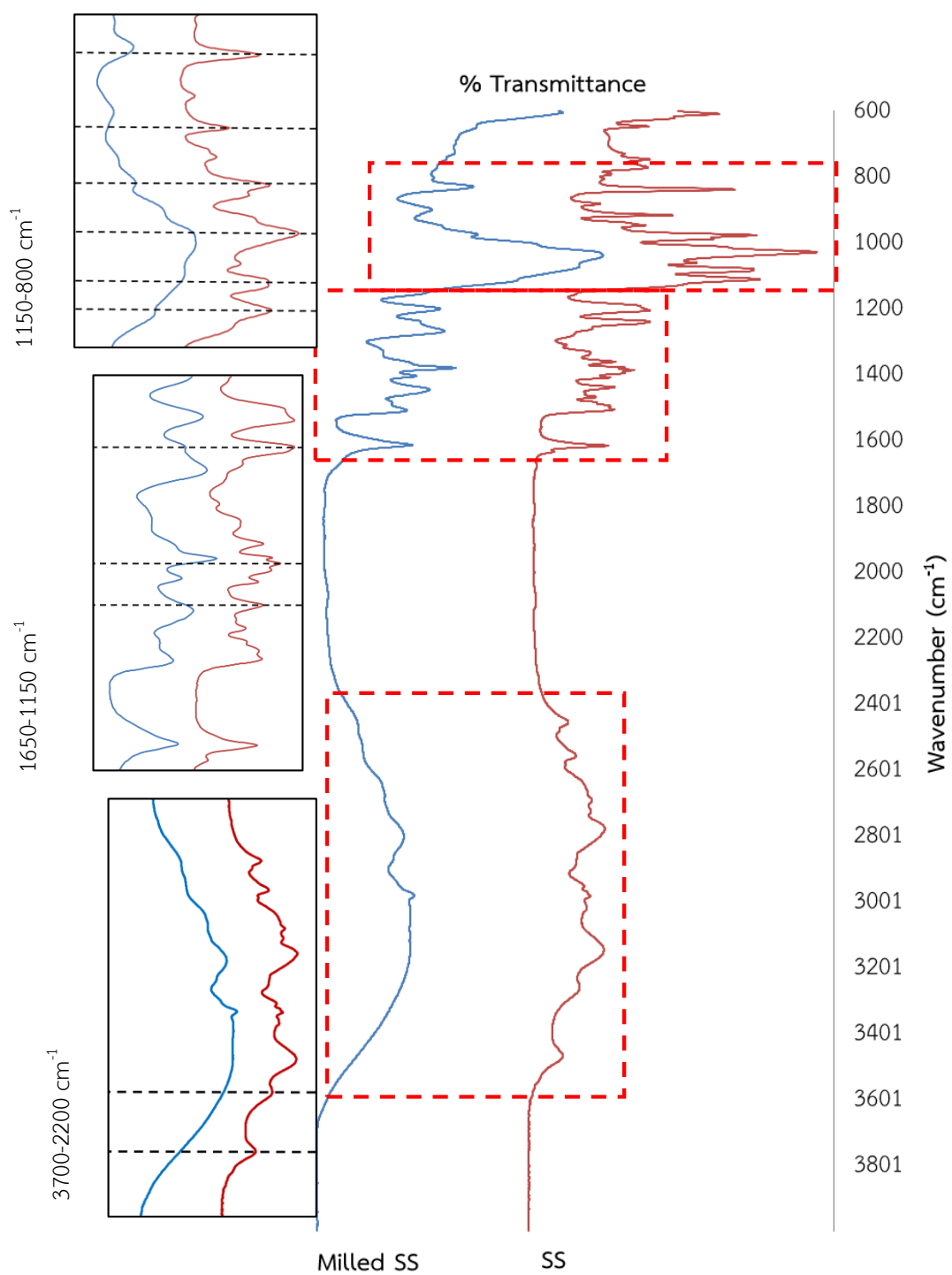


Figure 29 Comparative FTIR spectra of X-ray amorphous milled SS and SS raw material.

Table 8 FTIR band assignments, positions, and intensities of SS and X-ray amorphous milled SS.

No	Vibration	SS		Milled SS		Reference
		Position (cm^{-1})	Intensity (%T)	Position (cm^{-1})	Intensity (%T)	
1	OH stretching/ NH stretching	3472	92.8	broad	90.6	(19,25)
2	NH stretching	3262	88.8	broad	80.3	(19)
3	Secondary amine salt (C-N-C)	1616	82.2	1614	77.6	(25)
4	C=C-C stretching/ Secondary amine salt (C-N-C)	1506	80.8	1508	78.8	(25,67)
5	CH ₂ N bending	1438	80.7	1445	73.6	(29)
6	CH ₃ bending	1386	76.2	1379	67.6	(29)
7	C-H bending	1239	72.5	1268	70.1	(67)
8	Phenolic CO stretching	1205	72.6	1200	71.1	(5,67)
9	Sulphate ion/ CH bending/OH bending	1110	47.2	broad	53.1	(29,67)
10	C-O stretching/ C-H bending	1084	48.6	broad	42.6	(29)
11	S=O stretching/ CH ₃ rocking/ CC ₃ stretching	1028	34.1	1038	33.5	(29,67)
12	C-O stretching	977	47.9	broad	62.7	(29)
13	CH ₂ rocking/ CH ₃ rocking	916	67.4	broad	75.9	(29)
14	C-H bending	838	52.9	829	63.5	(29)

4.2. Stability of X-ray amorphous milled SS

Amorphous SS which were prepared from different methods showed the solid state instability under moderate to severe storage condition (humidity and temperature) (11,71). The rate of interconversion of amorphous SS to the stable crystalline form occurred within 5 hours when storage at 25 °C and 70% RH that had previously been reported (71). In our studies, milled SS powder was necessary to investigate the solid state stability in order to determine the optimum storage condition including the time of interconversion or induction time for using as a reference in the next studies.

XRPD pattern of X-ray amorphous milled SS after storage at $75 \pm 5\%$ RH, room temperature within 2 hours exhibited the same responses comparable to the freshly prepared (Figure 30). However, the signal responses of crystalline form appeared after 2.25 hours of storage and would be then remarkably seen after 2.5 hours. In this study, the criteria of the solid state interconversion was employing the use of S/N ratio at $10.6 \text{ }^\circ 2\theta$ as shown in chapter 2 title 3.5 . The r^2 of calibration curve was found to be 0.9829 which has been accepted according to the criteria (>0.95). The value of LOQ of this method (appendix B) was quite high (more than 24.14% of crystalline form I) whereas LOD was around 6% of crystalline form I. All response in this study was found to be lower than LOQ. Thus, it was not appropriate to report the level of crystallinity as % of crystalline form I but it should only be observed on the transformation by using the LOD (S/N ratio of 3). At 2 hours, the S/N ratio was less than 3. It was revealed that no acceptable solid state transformation was occurred. Nevertheless, the sample kept for longer time period (2.25 hours) provided the S/N ratio above 3 that would be inferred to the more transformation. Therefore, the transition period of solid state interconversion of X-ray amorphous milled SS to crystalline SS form I would be occurred within 2 to 2.25 hours. In this experiment, the time of interconversion or induction time was found in the range of 2 to 2.25 hours for X-ray amorphous milled SS.

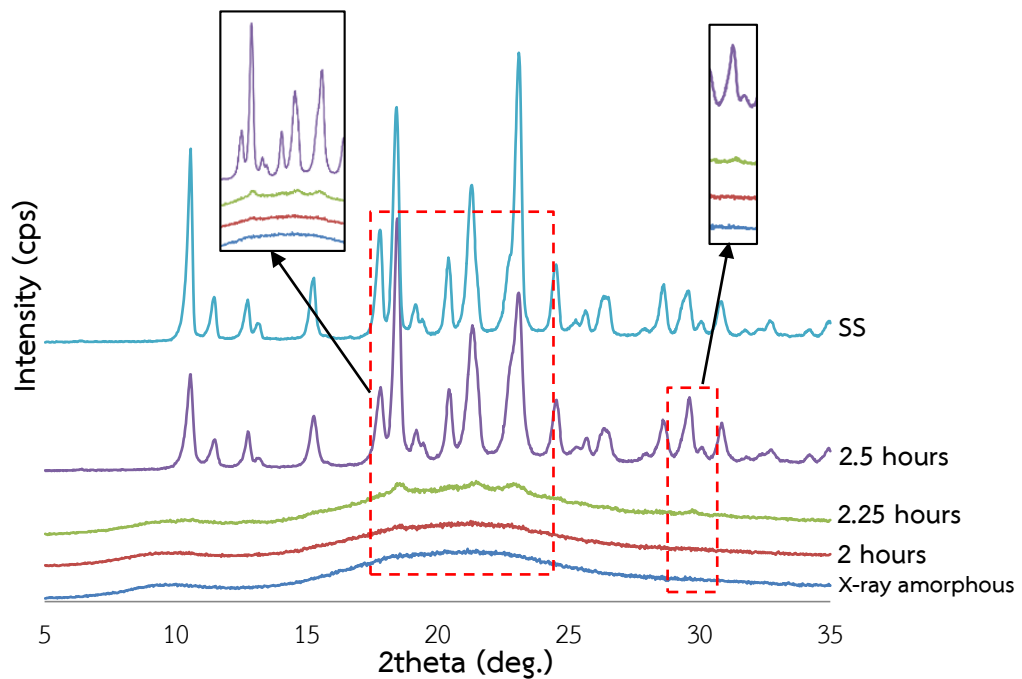


Figure 30 Comparative XRPD of X-ray amorphous SS powder stored for $75 \pm 5\%$ RH, room temperature for 2, 2.25 and 2.5 hours, respectively.

Photomicrograph of X-amorphous SS powder stored at $75 + 5\%$ RH, room temperature for 1 day showed the unclear bright appearance under dark field (Figure 31B). It might due to the crystal size and aggregation state. The smaller the particle size the more complicated the reflection of light. Above result primarily indicated the crystalline state of SS that well agreed with XRPD result.

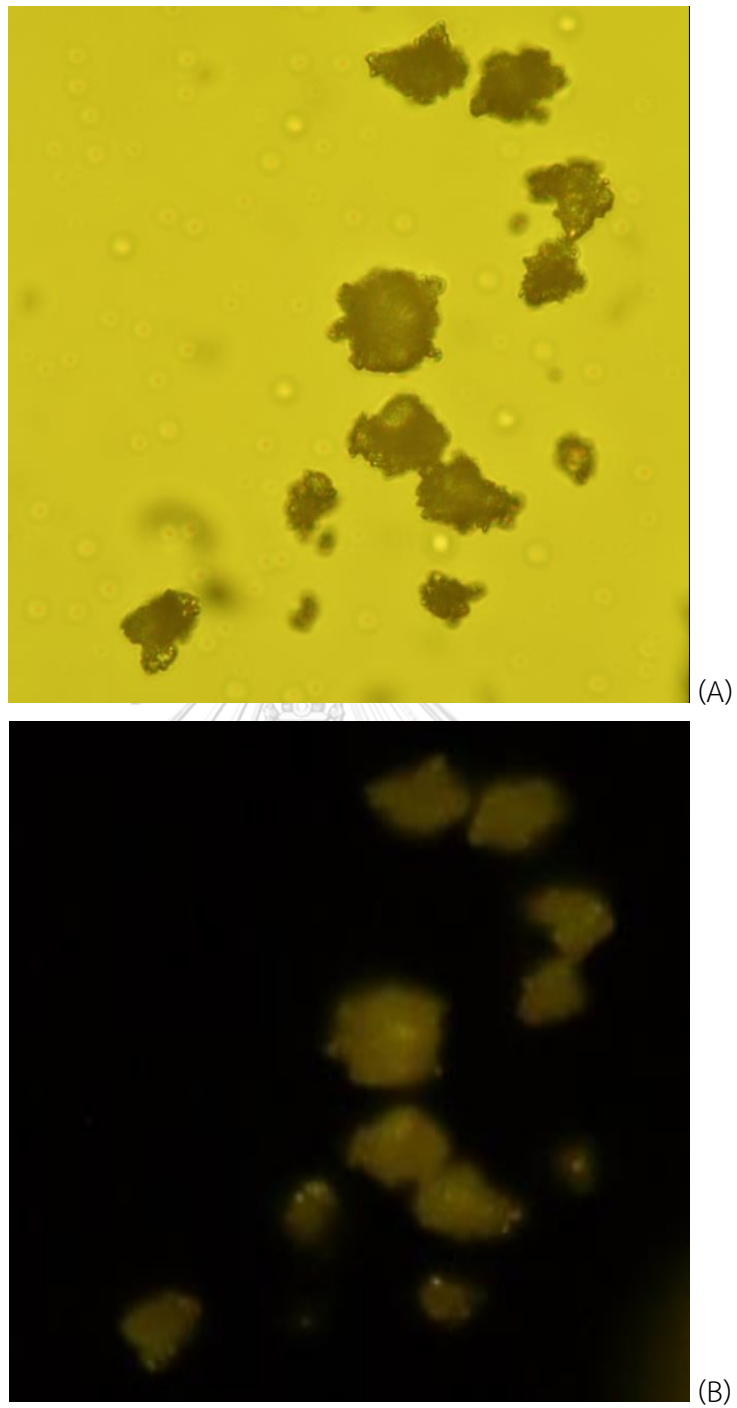


Figure 31 Photomicrograph of X-ray amorphous SS powder stored at $75 \pm 5\%$ RH, room temperature for 1 day under bright field (A) and polarized light (B) (at magnification of 400).

4.3. Preparation and solid state characterization of SS adsorbed on mesoporous silica

In this study, amorphous SS was intentionally prepared based on the molecular adsorption on solid substrate approach. S244 silica was selected and utilized as solid substrate. It was due to the fact that silica material provides more possibility on molecular adsorption according to its reactive silanol group. Hydrogen bonding is a key role on such molecular interaction (49). In addition, silica material has a wide varieties of physical structure particularly with the porosity. Macroporous, mesoporous and microporous silica are now available in the market. Currently, mesoporous silica is one of the most solid substrate which was studied on solubility improvement via amorphization of several drugs (3,8,65). Therefore, it was appropriate for employing in drug amorphization.

The S244 silica were impregnated several times with an aqueous solution of SS. Initially, three, six and nine times of impregnation were proposed and roughly investigated the state of SS adsorbed on S244 silica surface in term of crystallinity with XRPD. XRPD was interpreted by observing the presence of distinct peak responses of crystalline form I. The results showed that the sample after three times of impregnation provided no any signs of crystallization of SS. It could be seen from the absence of any peak responses of crystalline form (Figure 32). For the sixth impregnation time, the presence of small Bragg's peaks at 10.6, 18.4, 21.3 and 23.0 °2θ was detected which revealed the formation of crystalline SS form I (Figure 33). It was further clearly demonstrated that the impregnation of nine times showed the remarkable peak responses with higher intensity that determined the existence of crystalline form I.

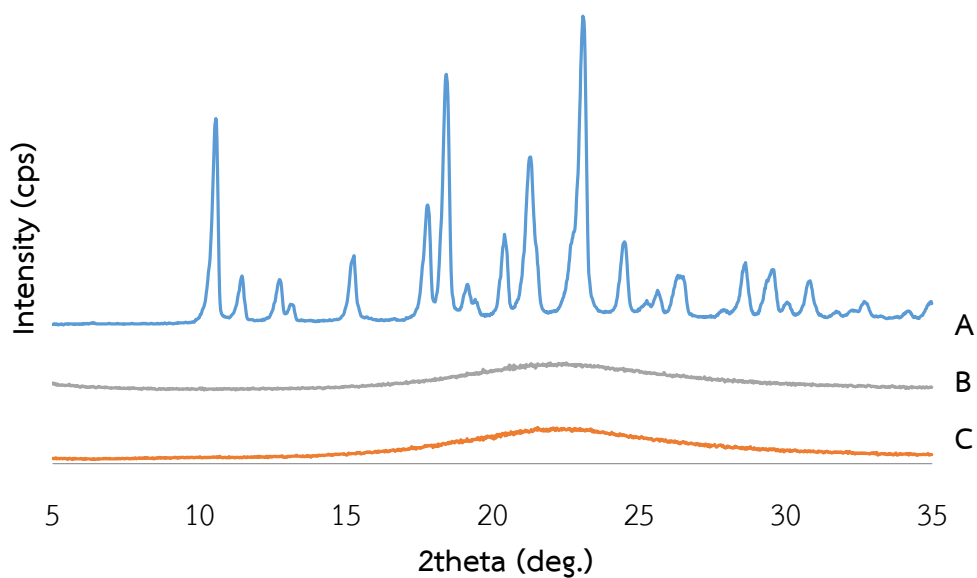


Figure 32 Comparative XRPD of crystalline SS form I (A), S244 silica (B) and SS adsorbed on S244 silica three times (C).

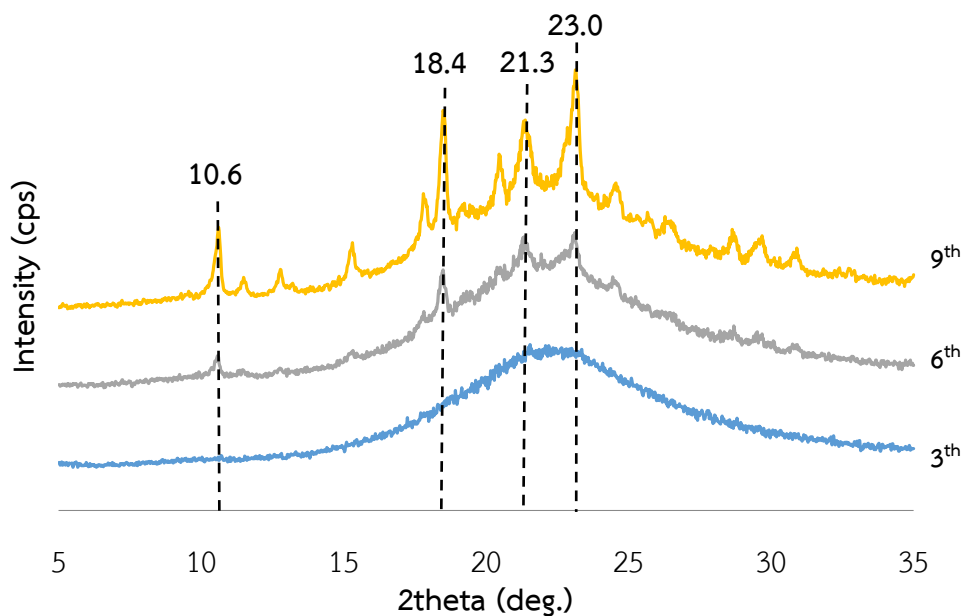


Figure 33 Comparative XRPD of SS adsorbed on S244 silica at three, six and nine times of impregnation, respectively.

There are an argument of amorphous phase formation on the surface of porous solid substrate. It was explained that the formation of amorphous state was the result of the deposition of fewer adsorbed molecules onto the larger surface of adsorbent that resulted in the longer distance between each adsorbed molecule. Thus, each molecule is more difficult to come close together due to the longer distance on mobile. To get rid of above limitation, maximum number of adsorbed molecule on the silica adsorbent surface was determined. Therefore, the maximum loading of SS in which still obtained X-ray amorphous state should be within three to five times of impregnation. In Figure 34, the impregnation time of four and five were additionally prepared. They provided the identical XRPD pattern comparing with that of three times of impregnation. Amorphous halo pattern with no any significant peak responses of crystalline form were investigated. It should be concluded that the impregnation of SS on S244 silica with up to five times yielded the X-ray amorphous SS. Hence, the incipient wetness impregnation with optimal loading successfully generated the X-ray amorphous SS on S244 silica. Loaded quantity of SS on S244 silica of five times impregnation was determined by HPLC and found to be 36.64 % w/w.

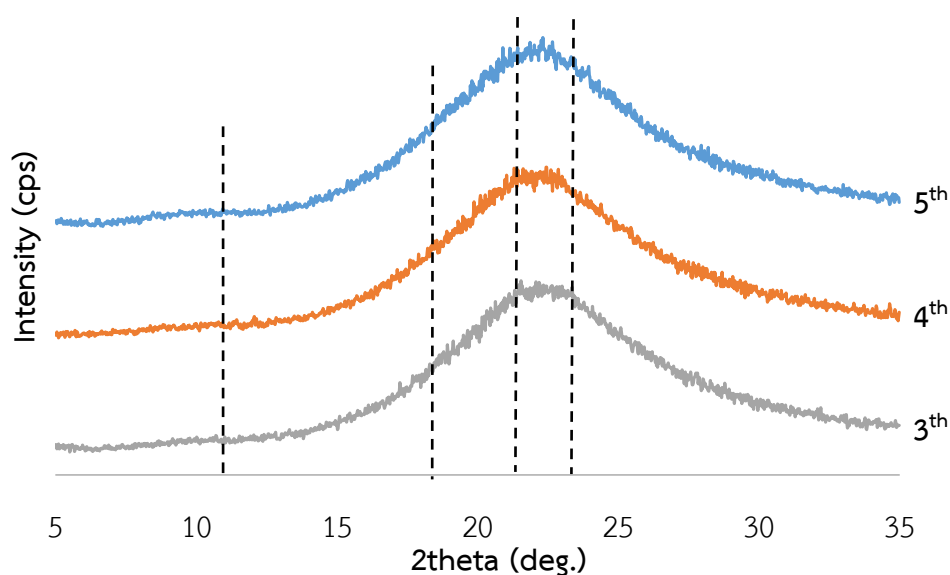


Figure 34 Comparative XRPD of SS adsorbed on S244 silica at three, four and five times of impregnation, respectively.

Further characterization of the sample with five time impregnation was performed. The detection of birefringence of the surface of SS adsorbed on S244 silica sample was done. S244 silica commonly showed the nature of amorphous which should not provide any sign of birefringence under polarized light (Figure 35B). The loaded S244 silica sample particles showed irregular crystal habit with also no birefringence of the surface under polarized light (Figure 36B). It was the good supporting evidence that SS adsorbed on surface of S244 silica was presented in the form of non-crystalline state.

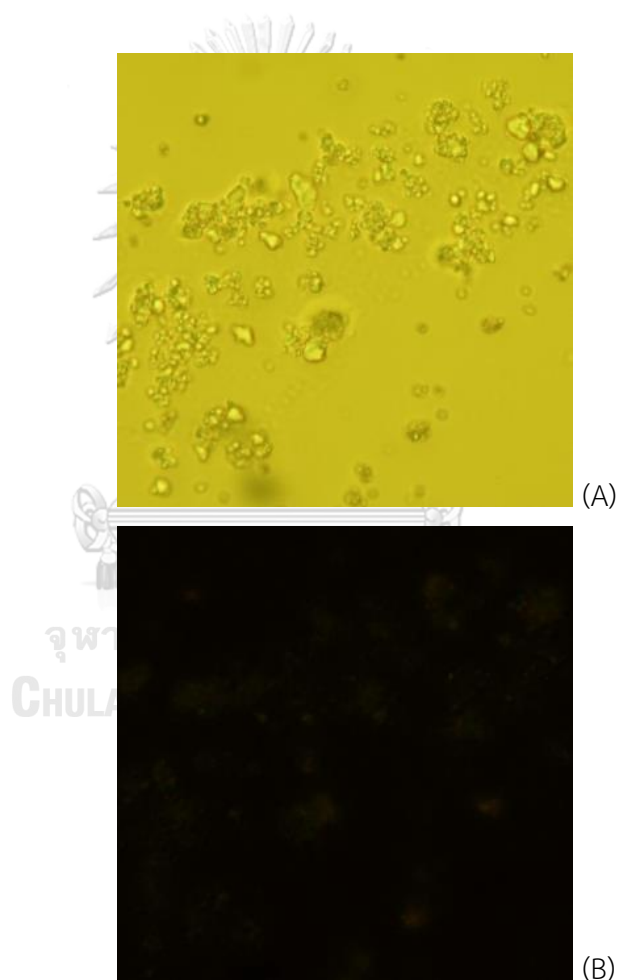


Figure 35 Photomicrograph of S244 silica under bright field (A) polarized light (B) (at magnification of 400).

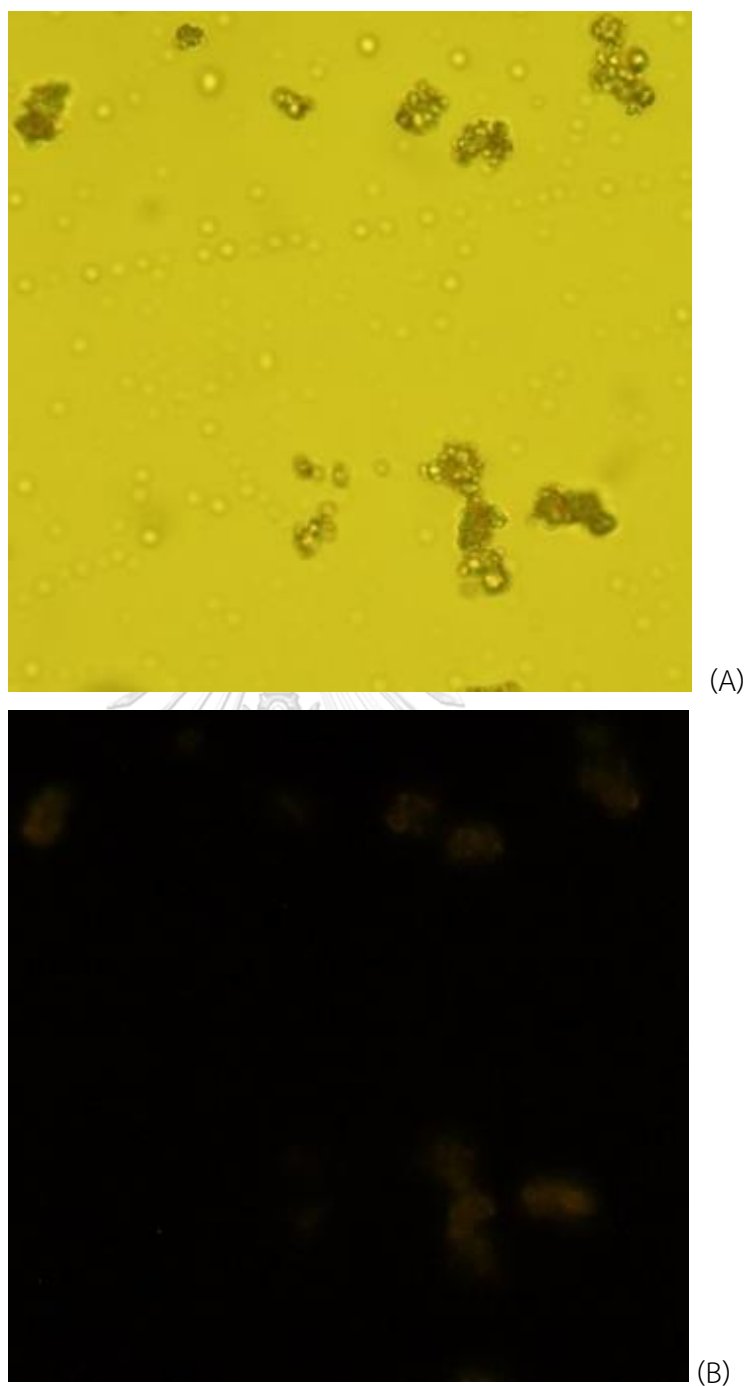


Figure 36 Photomicrograph of SS adsorbed on S244 silica under bright field (A) polarized light (B) (at magnification of 400).

Thermal analysis of X-ray amorphous SS adsorbed on S244 silica, S244 silica, the physical mixture of SS raw material and S244 silica of 40% w/w and the physical mixture of X-ray amorphous milled SS and S244 silica of 40% w/w samples were performed and compared.

In Figure 37, DSC thermogram of SS adsorbed on S244 silica sample showed the first broad endothermic peak (30 to 115 °C), the second endothermic peak in between 150-210 °C followed with third endothermic peak from 215-300 °C. The first broad endothermic peak has the weight loss around 3% w/w that might be related to the desolvation of adsorbed water and/or ethanol. The second and third endothermic peak has weight loss around 4 and 10%, respectively. It was suggested that they were the decomposition with melting of surface adsorbed SS which could be physically seen from the discoloration from brownish and later became darker homogeneously (Figure 38). The TGA result had also confirmed the decomposition of SS in such above temperature range by obvious weight loss.

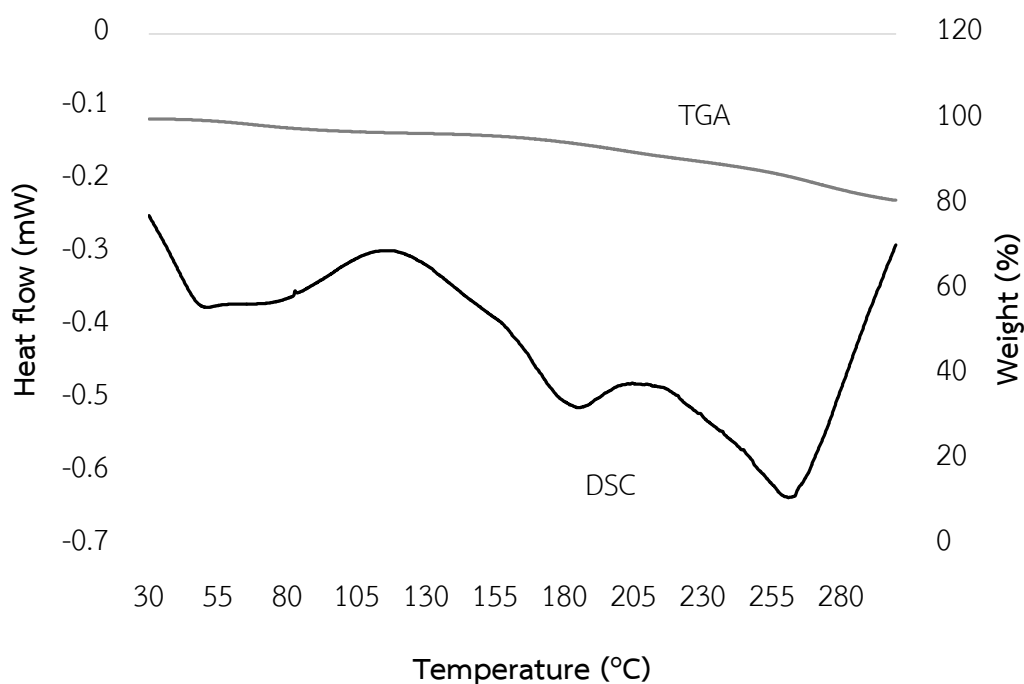


Figure 37 DSC and TGA thermograms of SS adsorbed on S244 silica.

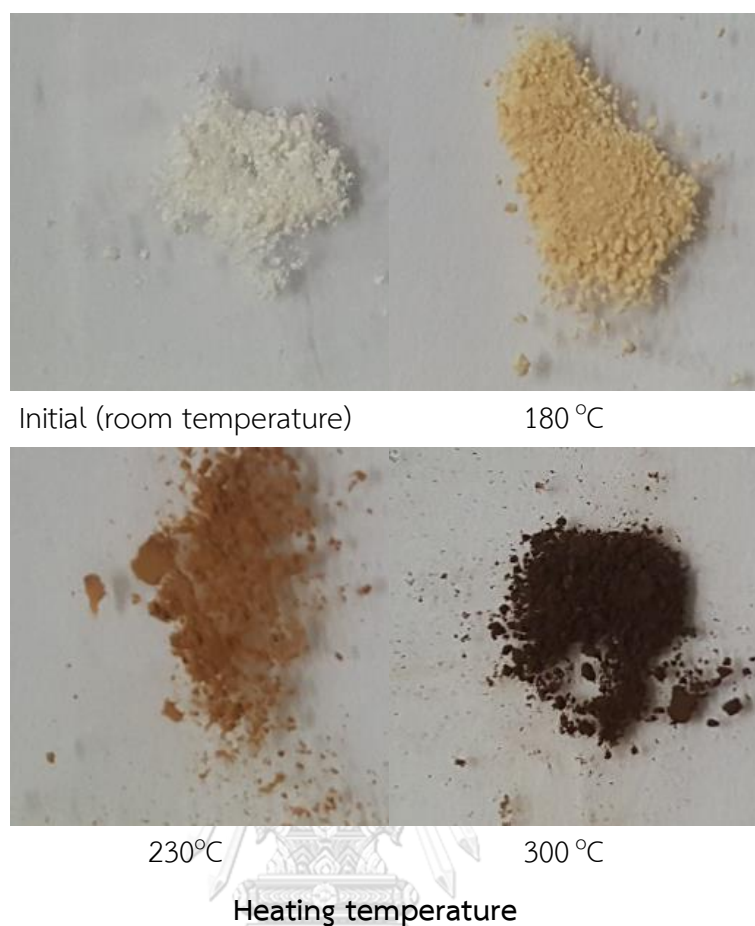


Figure 38 Physical appearance of the SS adsorbed on S244 silica under difference heating temperature.

Comparative DSC thermogram of SS adsorbed on S244 silica sample and the physical mixture between SS with S244 silica at the same concentration (40% w/w) exhibited the different pattern. The endothermic peaks of physical mixture were found to be comparable to that of SS raw material (endothermic peak at 205 and 275 °C). Meanwhile the SS adsorbed on S244 silica sample showed two different endothermic peaks (Figure 39). It might indicate that the SS adsorbed on silica surface was different from SS crystalline form I (37). Once, when comparing the DSC thermogram between X-ray amorphous SS adsorbed on S244 silica sample and the physical mixture between X-ray amorphous milled SS with S244 silica at the same concentration (40% w/w), it was found that endothermic peak responses of both sample were well agreed in term of the peak temperature (Figure 40). However, there was a significant difference at

endothermic sharp peak at 180 °C. It was possibly due to the difference in the state of X-ray amorphous. X-ray amorphous produced by milling was composed of only SS molecule itself with non-ordered arrangement in its crystal lattice whereas the X-ray amorphous produced by impregnation was the non-ordered molecular arrangement by the adsorption between each SS molecule and surface of silica material. It might hence be concluded that the state of SS which has been adsorbed on S244 silica with five times of impregnation was X-ray amorphous.

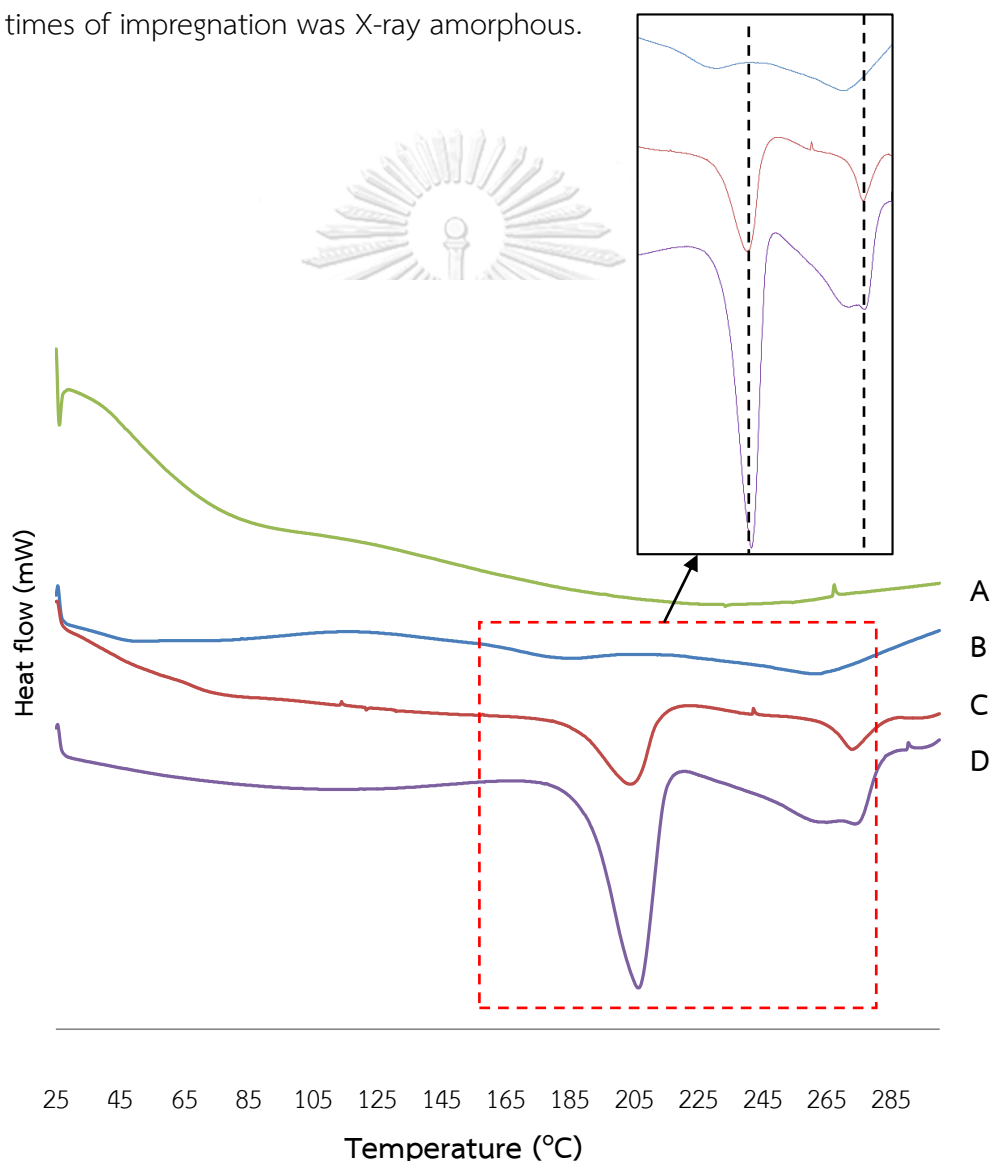


Figure 39 Comparative DSC thermograms of S244 silica (A), SS adsorbed on S244 silica (B) the physical mixture of SS with S244 at 40% w/w (C) and SS (D).

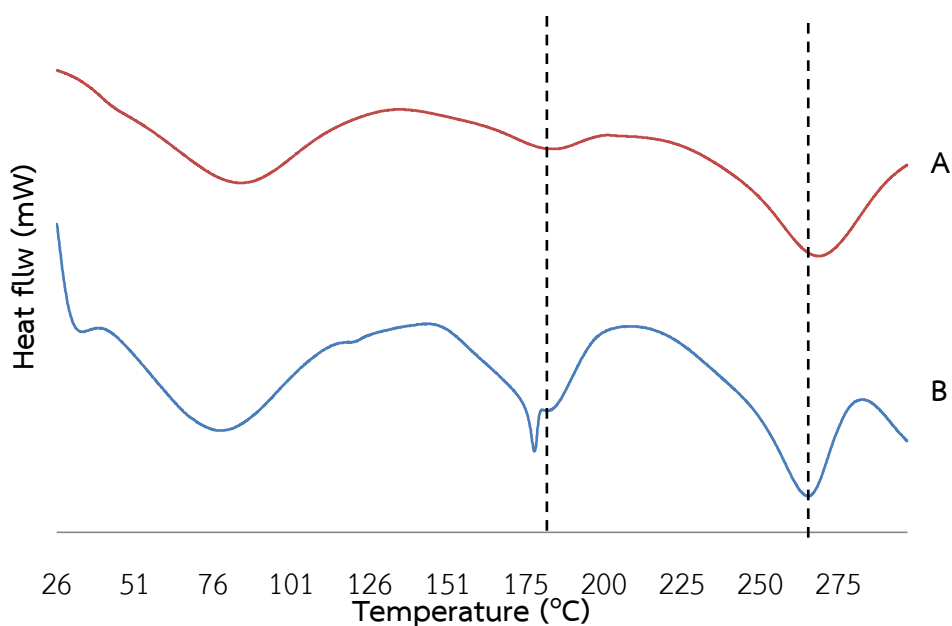


Figure 40 Comparative DSC thermograms of SS adsorbed on S244 silica (A) and the physical mixture of X-ray amorphous milled SS with S244 silica at 40% w/w (B).

In term of the investigation of molecular interaction between adsorbed SS molecule and S244 silica, FTIR was employed as a tool. FTIR spectra of the physical mixture between SS with S244 silica at the concentration of 40% w/w exhibited the combination of peaks from both SS and S244 silica without any more responses (Figure 41). It should be concluded that no interaction between SS and S244 was occurred. Meanwhile, the interaction of SS adsorbed on S244 silica sample was detected which could be seen by the shift of peaks when comparing with pure SS and S244 silica (Table 9). The promising peaks shift were at 1447 and 1386 cm^{-1} , respectively. The first peak shift at 1447 cm^{-1} was related to CH_2N group that might be governed a hydrogen bond formation. The second peak shift was at 1386 cm^{-1} which was assigned to CH_3 vibration. It might have the possibility to interact with S244 silica via weak interaction force. Other broad peak responses at 976, 916 and 838 cm^{-1} were not clearly interpreted the interaction due to the dilution effect of adsorbed SS and S244 silica.

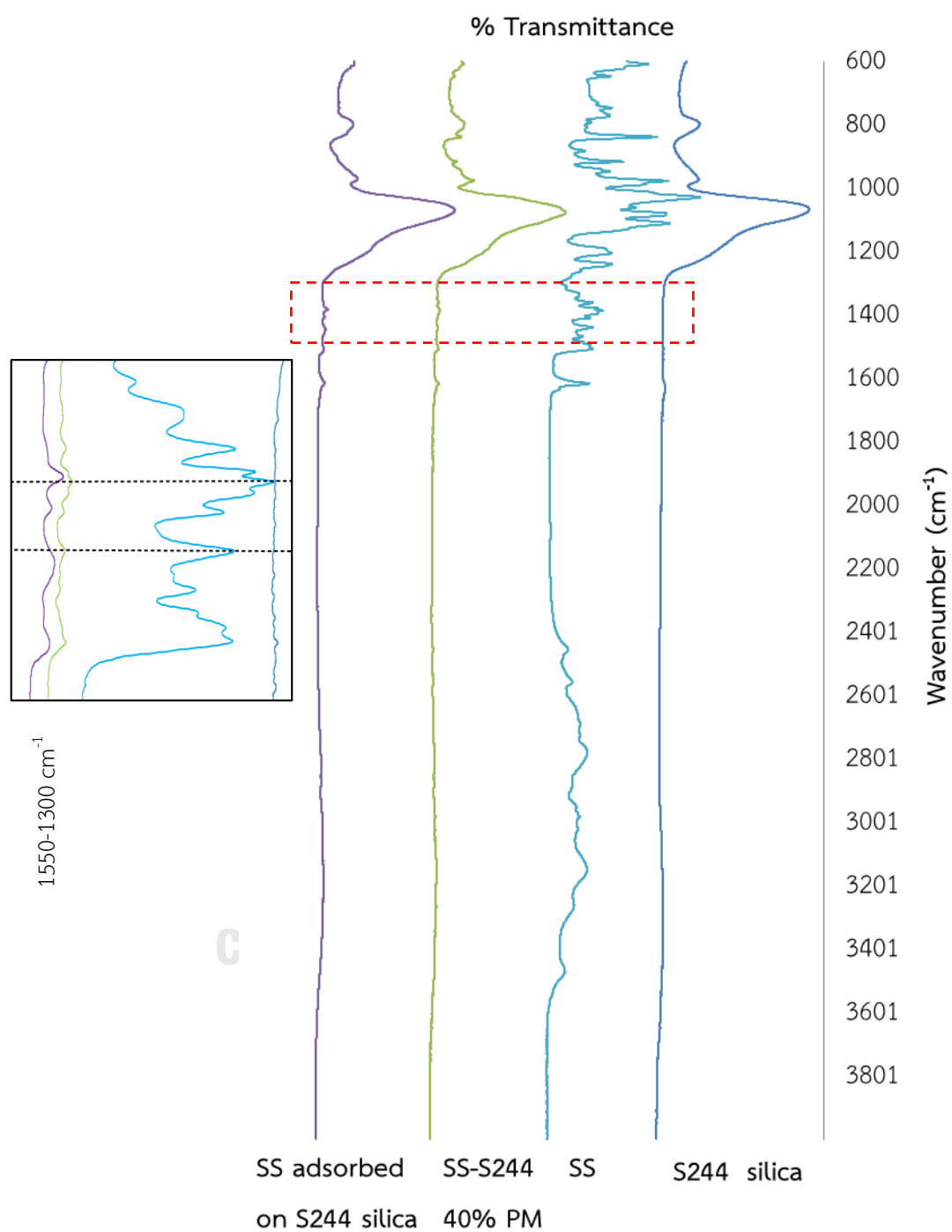


Figure 41 Comparative FTIR spectra of SS adsorbed on S244 silica, the physical mixture of SS with S244 silica at 40% w/w, SS and S244 silica.

Table 9 FTIR band assignments, positions, and intensities of SS adsorbed on S244 silica, the physical mixture of SS with S244 silica at 40% w/w.

No	Vibration	SS adsorbed on S244 silica		SS-S244 40% PM		Reference
		Position (cm ⁻¹)	Intensity (%T)	Position (cm ⁻¹)	Intensity (%T)	
1	CH ₂ N bending	1447	97.04	1438	97.90	(19,29)
2	CH ₃ bending	1382	96.08	1386	97.07	(29)
3	C-O stretching	969	82.91	976	82.29	(29)
4	CH ₂ rocking/ CH ₃ rocking	broad	91.15	916	89.89	(29)
5	C-H bending	broad	90.54	838	87.94	(29)

4.4. Stability of SS adsorbed on mesoporous silica

For the solid state stability of SS adsorbed on S244 silica which was produced by five times of impregnation. The 24 hours of storage at $75 \pm 5\%$ RH, room temperature provided the X-ray amorphous SS on S244 silica due to the X-ray halo pattern without any distinct Bragg's peaks of crystalline form. Nevertheless, the characteristic peak at $10.6^\circ 2\theta$ appeared at 44 hours and 64 hours, respectively. The criteria of the solid state interconversion rate was mentioned earlier (section 4.2). The S/N ratio of $10.6^\circ 2\theta$ at 44 hours of storage was found to be lower than 3 while the S/N ratio above 3 was obtained at 64 hours (Figure 42) (crystallinity around 9%). It might be concluded that the induction time of SS adsorbed on S244 silica was found in the range of 44 to 64 hours. The solid state stability was further observed in the longer period of storage. The result revealed the higher of crystalline form I formation that reflected directly on the peak response at $10.6^\circ 2\theta$. In addition, some of minor peaks were gained. In conclusion, the longer the storage time the higher the degree of crystallinity (Figure 43) (% crystallinity more than 10).

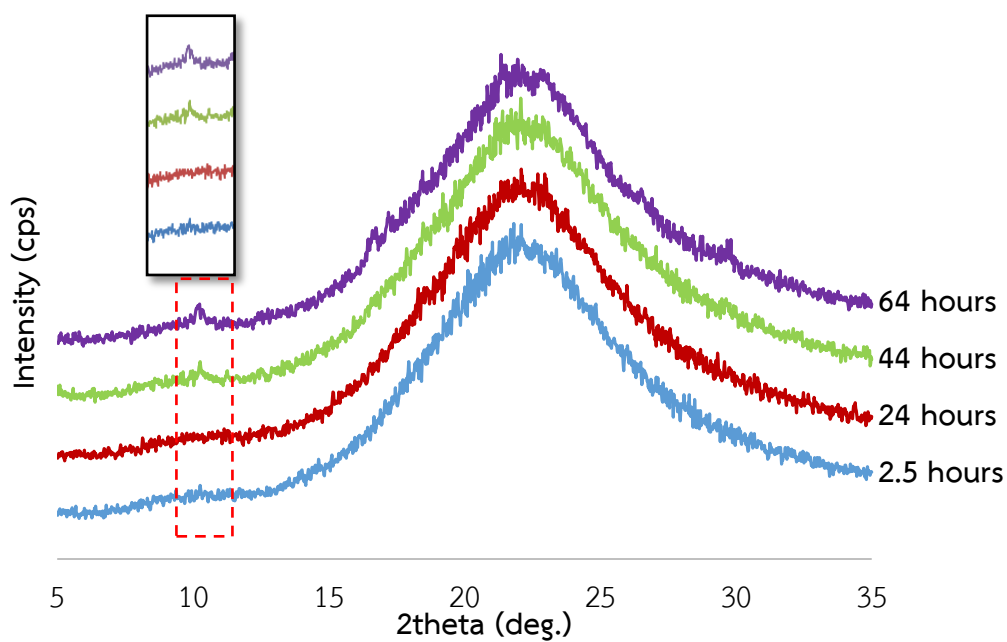


Figure 42 Comparative XRPD of SS adsorbed on S244 stored at $75 \pm 5\%$ RH, room temperature at different storage times of 2.5, 24, 44 and 64 hours, respectively.

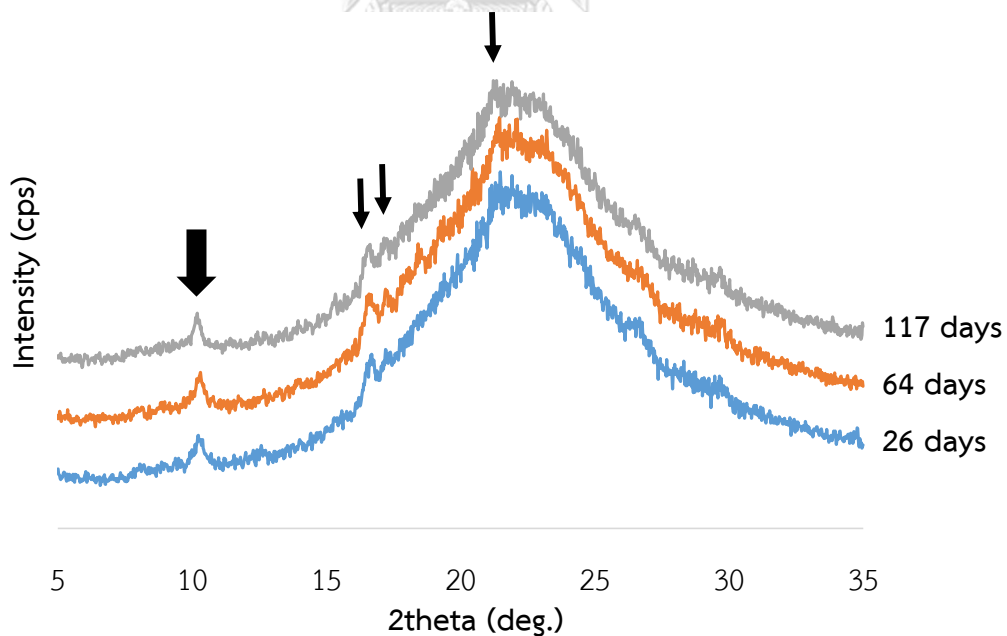


Figure 43 Comparative XRPD of SS adsorbed on S244 stored at $75 \pm 5\%$ RH, room temperature at different storage times of 26, 64 and 117 days, respectively.

The incipient wetness impregnation of SS on S244 silica showed the better solid state stability of X-ray amorphous SS produced comparing to that of milling which could be proved from the longer induction time. However, the better stability of X-ray amorphous SS adsorbed on S244 silica was quite short and could not effectively preserved their non-ordered structure when it will be used in the formulation that might have humidity involved such as wet granulation. Stabilization of amorphous SS nature with polymer should be proposed and studied in the next section. Conclusively, the method of adsorption of interested compound on the porous material could retard the solid state interconversion rate of amorphous to crystalline.

4.5. Preparation and solid state characterization of SS adsorbed on mesoporous silica with polymer.

Nowadays, amorphous stabilization by means of the aid of polymer was extensively studied (5,34,35,55). It was due to the fact that polymer with different functional group or molecular structure can be applied with the amorphous in order to gain steric stabilization and eventually resulted in stable molecular non-ordered arrangement. Typical polymer used for amorphous solid dispersion was short chain polymer because of low viscosity, less occupy space and less competitive surface adsorption. In this study, short chain PVP K12 was employed as a model polymer on stabilization of X-ray amorphous SS adsorbed on S244 silica. The effect of polymer concentration used was investigated. PVP K12 at maximum estimated concentration of 30% w/w of SS was preliminary loaded on S244 silica by adding in the hydroalcoholic solution of SS with five times of impregnation. Unfortunately, the XRPD results of above freshly prepared sample showed the appearing of response peaks of crystalline state (Figure 44). Meanwhile the control sample (without PVP K12) provided the amorphous halo pattern without any Bragg's peaks of crystalline. It might be due to the occupying of free space of silica surface by PVP K12 (2,21,52,59). The competitive interaction between drug and polymer with silica surface affected the available free surface area of silica. The less of free space from the occupying of PVP K12 directly impacted on the closeness of SS molecules resulted in high tendency of SS recrystallization.

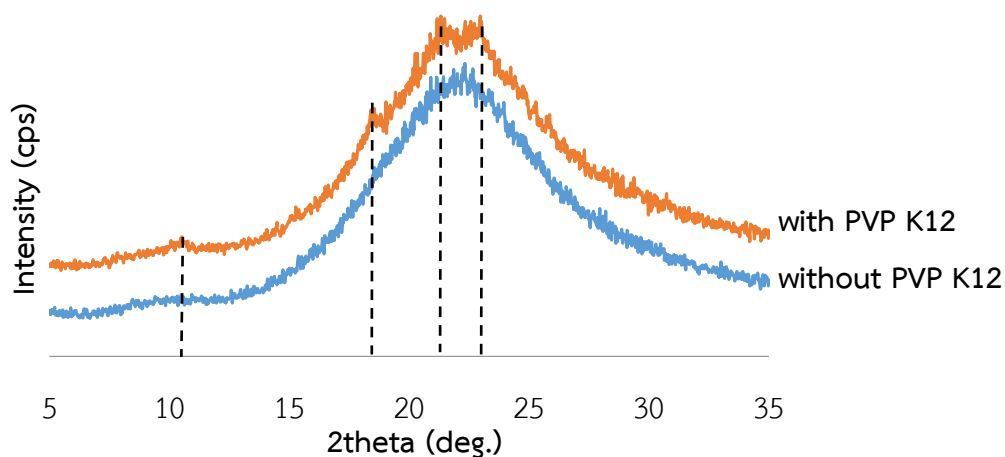


Figure 44 Comparative XRPD of SS adsorbed on S244 silica with and without PVP K12 30% w/w of SS at five times of impregnation.

To overcome mentioned problem, an adjustment of loaded quantity of SS by minimizing the impregnation time was performed. Four and a half time of impregnation was proposed and studied. The result showed that no any Bragg's peak were occurred (Figure 45). On the molecular interaction point of view, the interaction between three components by FTIR showed unclear peak responses due to dilution effect (Figure 46) but the presence of C=O at 1652 cm^{-1} still existed that showed the characteristic of PVP. Further investigation of chemical interaction amidst PVP K12, SS and/or S244 silica with more sensitive analytical instrument are required in order to precise clarification.

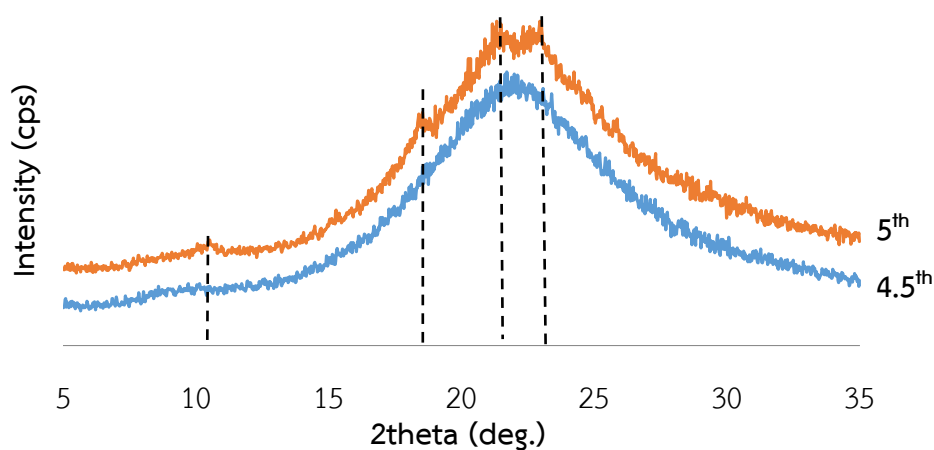


Figure 45 Comparative XRPD of SS adsorbed on S244 silica with PVP K12 30% w/w of SS between four and haft times and five times of impregnation.

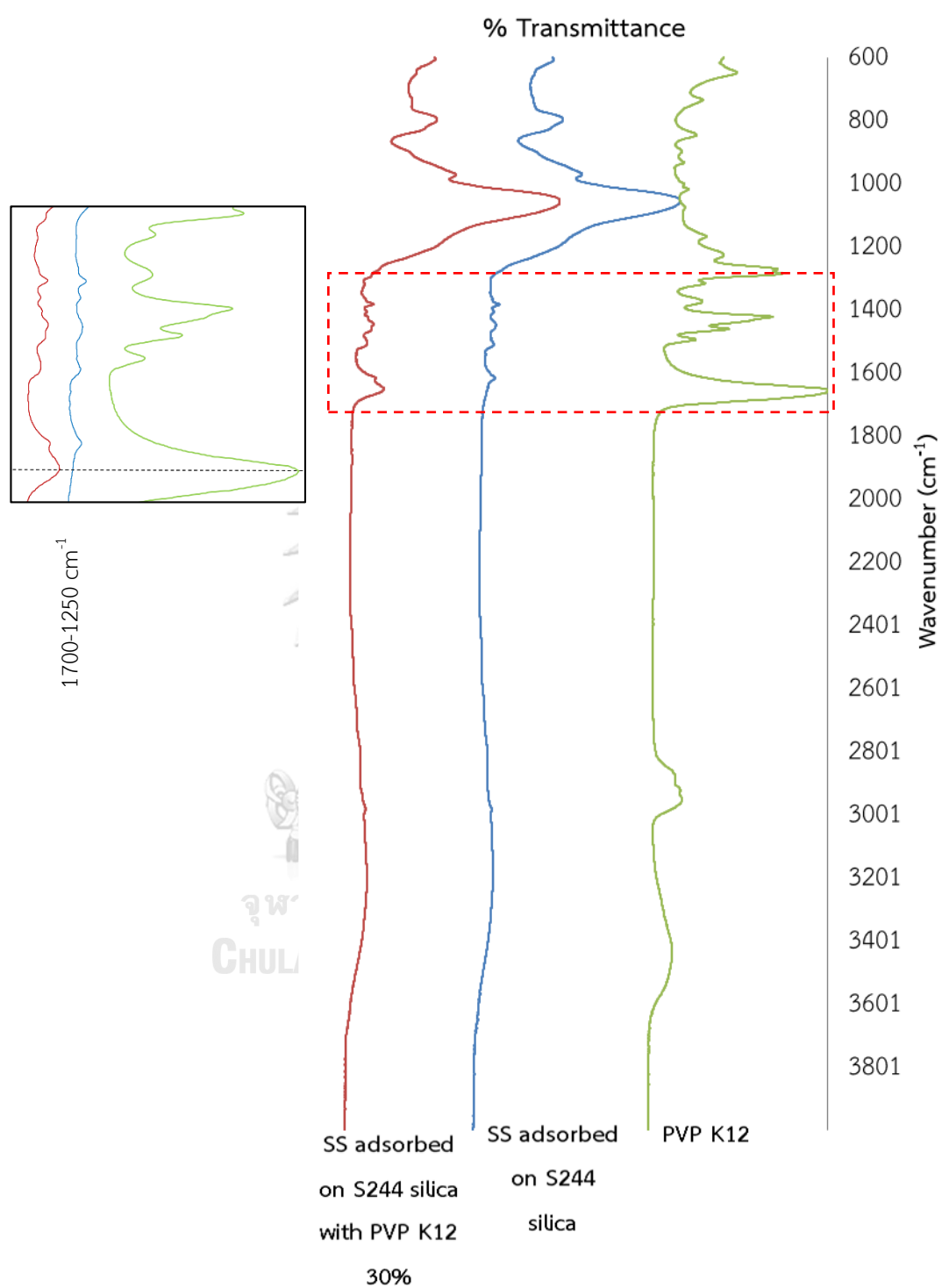


Figure 46 Comparative FTIR spectra of SS adsorbed on S244 silica with PVP K12 at 30% w/w of SS, SS adsorbed on S244 silica and PVP K12.

However, the less of impregnation times absolutely provided lower drug loading. The quantitative determination of SS with HPLC indicated that SS could be loaded at 33.42 ± 0.51 % w/w (without PVP K12) whereas 29.80 ± 1.18 % w/w of loaded quantity was found when PVP K12 (30% w/w of SS) was added. There was a significant difference ($p < 0.05$). Therefore, the prototype of sample in the experiment governing the effect of polymer concentration on solid state interconversion of SS was set up at four and half time of impregnation. XRPD patterns of freshly prepared SS adsorbed on S244 silica with different concentrations of PVP K12 showed X-ray amorphous halo comparable to the control sample (without PVP K12) (Figure 47). It could not clearly explain about the effect of PVP K12 on the formation of X-ray amorphous SS on S244 silica since X-ray amorphous could be formed even PVP K12 was not added.

However, the assumption of the utilization of short chain polymer on amorphous stabilization is still directly governed with the time of retardation of solid state interconversion.

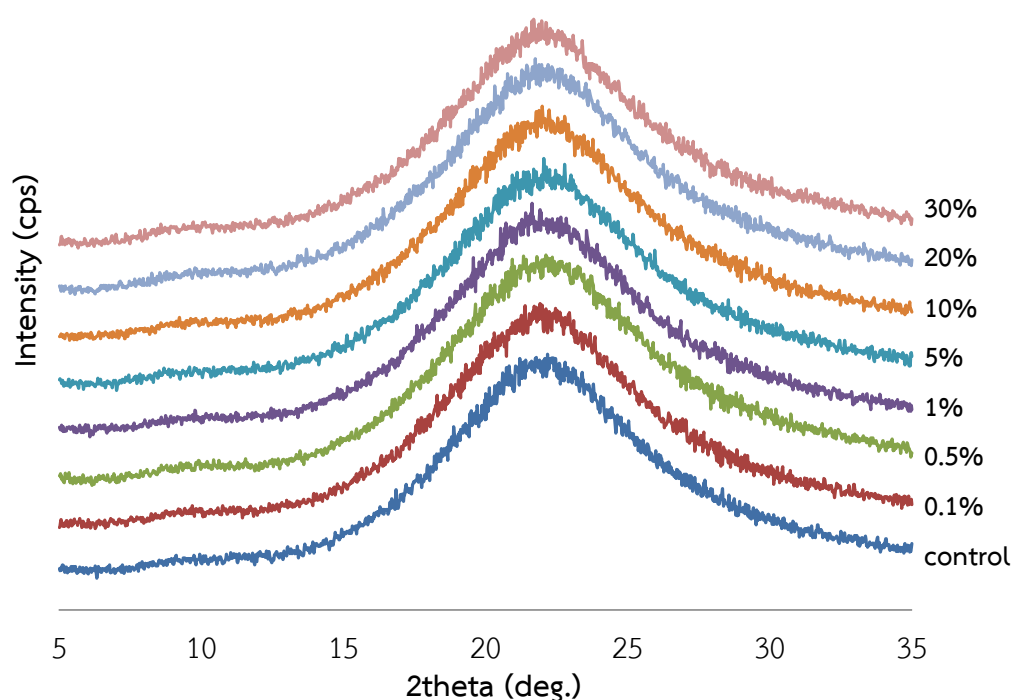


Figure 47 Comparative XRPD of SS adsorbed on S244 silica with PVP K12 at different concentration freshly prepared.

4.6. Stability of SS adsorbed on mesoporous silica with polymer

As seen in several publications, amorphous SS possibly transformed to crystalline state under ambient condition that depended on the humidity and time of exposure (11,71). The higher the humidity the faster the rate of interconversion (71). Thus, the storage condition in this experiment was chosen at $75 \pm 5\%$ RH and room temperature. Above storage condition was alike accelerated condition in order to investigate the induction time. The solid state stability of samples prepared with PVP K12 at 10, 20 and 30% w/w of drug were investigated under specified condition as mention earlier for 6 days. XRPD results showed the presence of some Bragg's peaks of samples with PVP K12 at 20 and 30% w/w with the S/N ratio higher than 3 (% crystallinity around 8 and 9, respectively) (Figure 48). These demonstrated that SS tended to crystallize. Meanwhile, the sample with PVP K12 at 10% w/w of SS remained unchanged due to no sign of crystalline formation. Thus, the higher concentration of PVP K12 at 20 and 30% w/w of SS could not effectively retard the crystallization of X-ray amorphous SS.

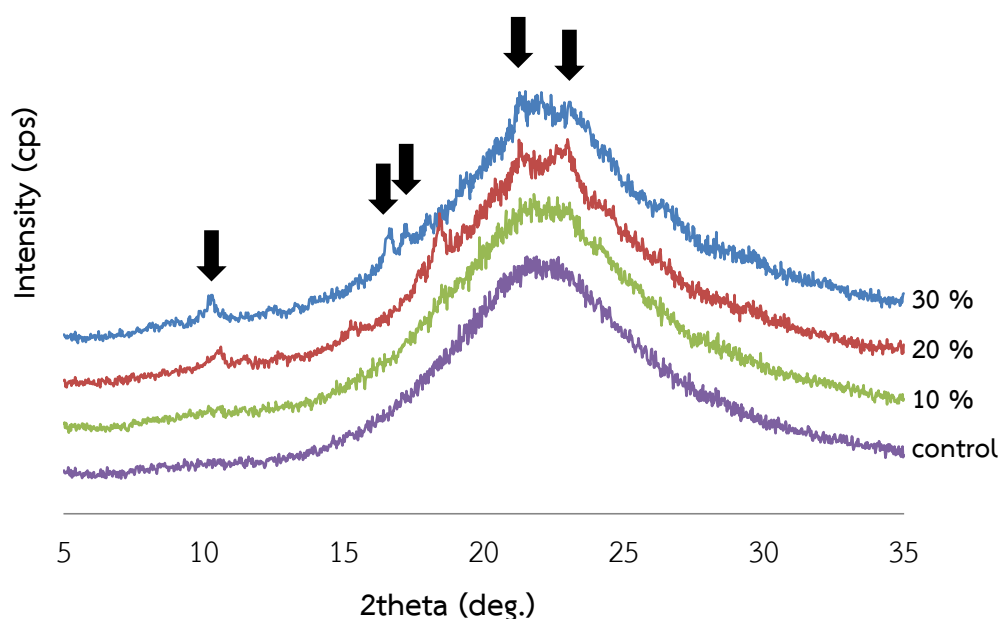


Figure 48 Comparative XRPD of SS adsorbed on S244 silica with PVP K12 at 10, 20 and 30% w/w of SS stored at $75 \pm 5\%$ RH, room temperature for 6 days.

Besides, the lower concentrations of PVP K12 might provide the better crystallization inhibition due to the less of silica surface area occupying. The preparation of SS adsorbed on S244 silica with lower PVP K12 concentrations at 1 and 5% w/w of SS were additionally done. Freshly prepared samples were then stored at $75 \pm 5\%$ RH, room temperature for the longer time (12 days) than that of previous studies. The result showed that Bragg's peak of samples with PVP K12 at 5 and 10% w/w of SS with the S/N ratio above 3 were investigated (crystallinity around 9%) (Figure 49). It was indicated that SS starting to crystallize and would turn to be the crystalline form. On the other hand, the XRPD of sample with PVP K12 at 1% w/w of SS seem to be changed but the S/N ratio of all Bragg's peaks were lower than 3. Thus, the lower concentration of PVP K12 at 1% w/w seem to be more effective on the deceleration of the recrystallization of X-ray amorphous SS.

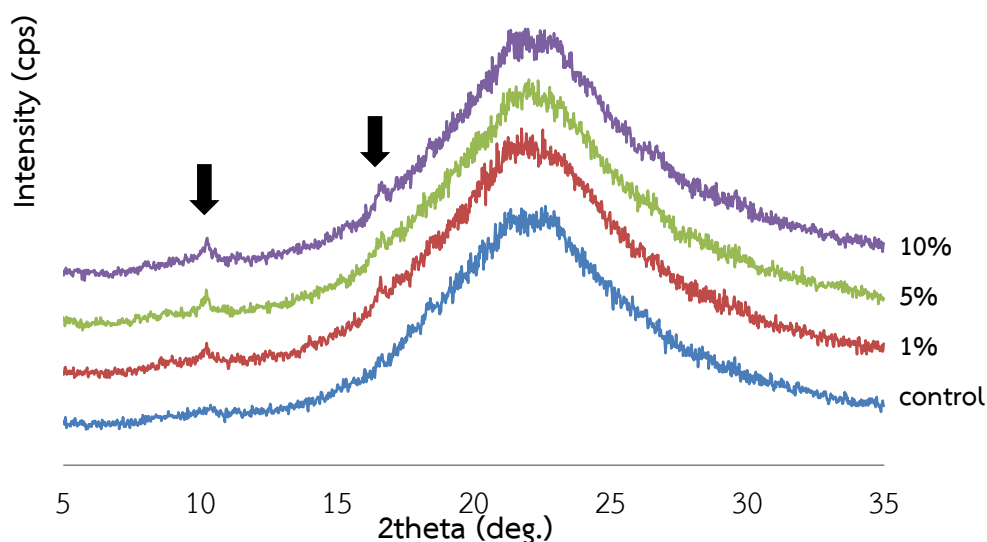


Figure 49 Comparative XRPD of SS adsorbed on S244 silica with PVP K12 at 1, 5 and 10% w/w stored at $75 \pm 5\%$ RH, room temperature for 12 days.

To find tune the most appropriated concentration of PVP K12 on the retardation of recrystallization, the samples with PVP K12 at 0.1 and 0.5% w/w of SS were fabricated and then characterized after kept in the predetermined condition with the longer time (20 days). The results showed that all of sample exhibited some of Bragg's peaks with lower S/N ratio (less than 3). Therefore, the interconversion time of sample with above concentration ranges of PVP K12 were the same as control (without PVP K12) (Figure 50).

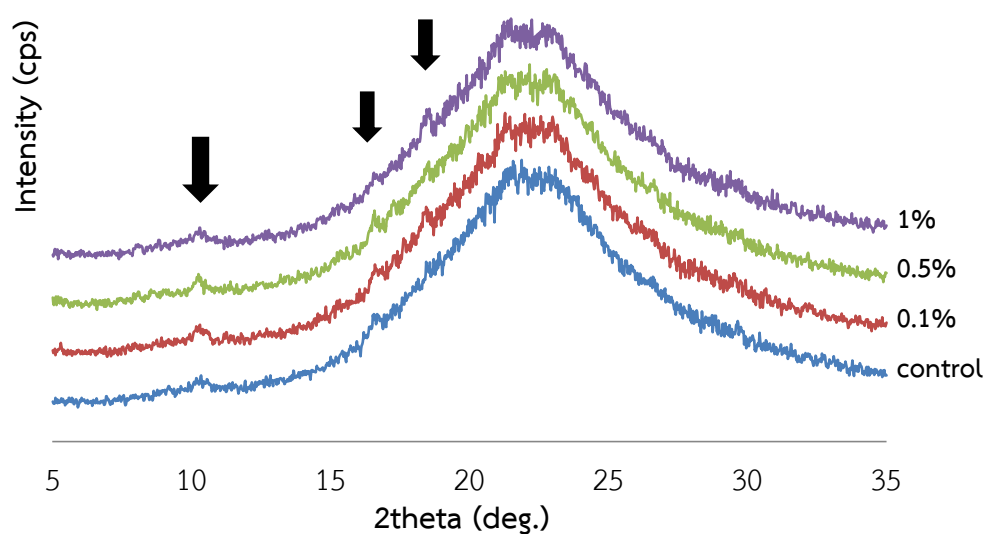


Figure 50 Comparative XRPD of SS adsorbed on S244 silica with PVP K12 at 0.1, 0.5 and 1% w/w of SS stored at $75 \pm 5\%$ RH, room temperature for 20 days.

Our result was not agree according to the previous findings. Konno and Taylor found that amorphous solid dispersion of homogeneous felodipine molecularly dispersed in polymer of PVP K29/32 which was created as a thin film showed the relatively slower nucleation rate when higher amount of polymer was applied (35). They proposed that larger amount of polymer could have ability on retarding the nucleation rate of felodipine through the interaction between drug and polymer. If the nucleation rate of drug was slower, the crystallization tendency was also lower. The physical or chemical interaction between drug and polymer chain played a pivotal role on the recrystallization inhibition. However, the molecular mechanism of the transformation X-ray amorphous SS produced by surface adsorption to crystalline might be result from the competitive interaction between drug-silica and polymer-silica including drug-polymer. The main mechanism was proposed to polymer-silica surface interaction. PVP could be adsorbed over the surface of silica via hydrogen bond as a function of molar mass of the polymer (2,21,52,59). It affected on the availability of free silica surface space and later impacted on the adsorption of SS molecule. It was therefore led to the faster recrystallization of free SS. Hence, it was not surprising that our results is controversial with Konno and Taylor findings.

CHAPTER V

CONCLUSIONS

X-ray amorphous SS particles could be prepared by grinding which was confirmed by amorphous halo pattern. It also showed non birefringence under polarized light and supported the non-ordered structure. The rapid interconversion of X-ray amorphous SS to crystalline form I was observed within 2.25 hours after storage under high humidity condition ($75 \pm 5\%$ RH). On the other hand, X-ray amorphous SS could be fabricated via incipient wetness impregnation with S244 silica. The maximum SS loading of 36.64 % w/w was found. It was clearly demonstrated that the quantity of SS loaded on S24 silica affected to its solid state form. The higher the quantity of loaded on S244 silica the more possible the formation of crystalline form. The time of interconversion to crystalline of X-ray amorphous SS adsorbed on S244 silica was longer than milled amorphous SS produced. It was proposed that SS molecules was directly adsorbed on the surface of silica via hydrogen bond and other attractive forces. Meanwhile, X-ray amorphous milled SS converted to the former crystalline structure due to their own molecular interaction.

In order to extend the interconversion time or stability improvement of x-ray amorphous SS adsorbed on S244 silica, short chain polymer of PVP was introduced and investigated. In general, polymer could stabilize the non-ordered state of drug from their stearic hindrance. Unfortunately, this study showed that higher concentration of PVP K12 did not provide positive effect on amorphous solid state stabilization. The higher range of PVP K12 concentration (20 and 30% w/w of SS) gave the faster rate of interconversion than that of control (SS adsorbed on S244 silica without PVP K12). In addition, the lower level of concentration (5 and 10% w/w of SS) still also showed the faster interconversion rate. Nevertheless, the concentration of 0.1 to 1 % w/w of SS apparently interconverted the X-ray amorphous SS as same as the control (without PVP K12). It might be explained with the concept of competitive surface adsorption of SS molecules and PVP K12 polymer chain on the silica free surface area. PVP K12 was more favorable to be adsorbed and located on the surface

of S244 silica than SS molecule itself (2,21,52,59). The free space on silica surface for SS molecules was then reduced according to the readily occupy space of PVP K12. Consequently, SS molecule were closely located together on the surface and prone to be recrystallize at the end.

However, not only the effect of polymer concentration but chemical structure of polymer might also an important role on the deceleration of X-ray amorphous SS adsorbed on S244 silica that would be planned in future study.



REFERENCES

1. CHEMICALS. Chemical & Engineering News Archive. 1954;32(21):2146.
2. Al-Harbi LM, Kosa SA, Baloch MK, Bhatti QA, El-Mossalamy E-SE-BH. Adsorption of polyvinylpyrrolidone over the silica surface: as affected by pretreatment of adsorbent and molar mass of polymer adsorbate. International Journal of Polymer Science. 2016;2016:1-9.
3. Ambrogi V, Marmottini F, Pagano C. Amorphous carbamazepine stabilization by the mesoporous silicate SBA-15. Microporous and Mesoporous Materials. 2013;177:1-7.
4. Baghel S, Cathcart H, O'Reilly NJ. Polymeric amorphous solid dispersions: a review of amorphization, crystallization, stabilization, solid-state characterization, and aqueous solubilization of biopharmaceutical classification system class II drugs. Journal of Pharmaceutical Sciences 2016:1-18.
5. Balani PN, Wong SY, Ng WK, Widjaja E, Tan RB, Chan SY. Influence of polymer content on stabilizing milled amorphous salbutamol sulphate. International Journal of Pharmaceutics. 2010;391(1-2):125-36.
6. Brodka-Pfeiffer K, Langguth P, Graß P, Häusler H. Influence of mechanical activation on the physical stability of salbutamol sulphate. European Journal of Pharmaceutics and Biopharmaceutics. 2003;56(3):393-400.
7. Kollidon® [Internet]. BASF SE. 2008 [cited 7 JUNE 2017]. Available from: <https://products.basf.com/documents/pim;view/en/8800483977685.Kollidon%C2%AE%20Polyvinylpyrrolidone%20excipients%20for%20the%20pharmaceutical%20industry.pdf>.
8. Charnay C, Bégu S, Tourné-Péteilh C, Nicole L, Lerner DA, Devoisselle JM. Inclusion of ibuprofen in mesoporous templated silica: drug loading and release property. European Journal of Pharmaceutics and Biopharmaceutics. 2004;57(3):533-40.
9. Chaudhari S, Gupte A. Mesoporous silica as a carrier for amorphous solid dispersion. British Journal of Pharmaceutical Research. 2017;16(6):1-19.

10. Chieng N, Rades T, Aaltonen J. An overview of recent studies on the analysis of pharmaceutical polymorphs. *Journal of Pharmaceutical and Biomedical Analysis*. 2011;55(4):618-44.
11. Columbano A, Buckton G, Wikeley P. A study of the crystallisation of amorphous salbutamol sulphate using water vapour sorption and near infrared spectroscopy. *International Journal of Pharmaceutics*. 2002;237(1-2):171-8.
12. Crowley KJ, Zografi G. Cryogenic grinding of indomethacin polymorphs and solvates: assesement of amorphous phase foemation and amorphous phase physical stability. *Journal of Pharmaceutical Sciences*. 2002;91(2).
13. Curtin V, Amharar Y, Gallagher KH, Corcoran S, Tajber L, Corrigan OI, et al. Reducing mechanical activation-induced amorphisation of salbutamol sulphate by co-processing with selected carboxylic acids. *International Journal of Pharmaceutics*. 2013;456(2):508-16.
14. De Gusseme A, Neves C, Willart JF, Rameau A, Descamps M. Ordering and disordering of molecular solids upon mechanical milling: The case of fananserine. *Journal of Pharmaceutical Sciences*. 2008;97(11):5000-12.
15. Descamps M. Amorphous pharmaceutical solids. *Advanced Drug Delivery Reviews*. 2016;100:1-2.
16. Dhumal RS, Biradar SV, Paradkar AR, York P. Particle engineering using sonocrystallization: salbutamol sulphate for pulmonary delivery. *International Journal of Pharmaceutics*. 2009;368(1-2):129-37.
17. Di Pasqua AJ, Sharma KK, Shi YL, Toms BB, Ouellette W, Dabrowiak JC, et al. Cytotoxicity of mesoporous silica nanomaterials. *Journal of Inorganic Biochemistry*. 2008;102(7):1416-23.
18. Syloid FP silica [Internet]. Alltech associates. 2012 [cited 13 January 2015]. Available from: http://www.tinnakorn.com/2013/wp-content/uploads/2013/02/SyloidFP-Customer-Presentation-2012-Q3-notes_JP.pdf.
19. Grisedale LC, Jamieson MJ, Belton PS, Barker SA, Craig DQ. Characterization and quantification of amorphous material in milled and spray-dried salbutamol sulfate: a comparison of thermal, spectroscopic, and water vapor sorption approaches. *Journal of Pharmaceutical Sciences* 2011;100(8):3114-29.

20. Grisedale LC, Belton PS, Jamieson MJ, Barker SA, Craig DQ. An investigation into water interactions with amorphous and milled salbutamol sulphate: the development of predictive models for uptake and recrystallization. *International Journal of Pharmaceutics* 2012;422(1-2):220-8.
21. Guzenko NV, Pakhlov EM, Lipkovskaya NA, Voronin EF. Sorption modification of fine silica with polyvinylpyrrolidone. *Russian Journal of Applied Chemistry*. 2001;74(12):2017-20.
22. Hancock BC, Zografi G. Characteristics and significance of the amorphous state in pharmaceutical systems. *Journal of Pharmaceutical Sciences*. 1997;86(1):1-12.
23. Heikkilä T, Santos HA, Kumar N, Murzin DY, Salonen J, Laaksonen T, et al. Cytotoxicity study of ordered mesoporous silica MCM-41 and SBA-15 microparticles on Caco-2 cells. *European Journal of Pharmaceutics and Biopharmaceutics*. 2010;74(3):483-94.
24. Huang X, Teng X, Chen D, Tang F, He J. The effect of the shape of mesoporous silica nanoparticles on cellular uptake and cell function. *Biomaterials*. 2010;31(3):438-48.
25. Hyvönen S, Peltonen L, Karjalainen M, Hirvonen J. Effect of nanoprecipitation on the physicochemical properties of low molecular weight poly(L-lactic acid) nanoparticles loaded with salbutamol sulphate and beclomethasone dipropionate. *International Journal of Pharmaceutics*. 2005;295(1-2):269-81.
26. Validation of analytical procedure: text and methodology Q2(R1) [Internet]. 2005 [cited 4 April 2016]. Available from: http://www.ich.org/fileadmin/Public_Web_Site/ICH_Products/Guidelines/Quality/Q2_R1/Step4/Q2_R1__Guideline.pdf.
27. IUPAC. Reporting physisorption data for gas/solid systems with special reference to the determination of surface area and porosity. *Pure and Applied Chemistry*. 1985;57(4):603-19.
28. IUPAC. Recommendation for the characterization of porous solids. *Pure and Applied Chemistry*. 1994;66(8):1739-58.
29. Izquierdo-Lorenzo I, Sanchez-Cortes S, Garcia-Ramos JV. Adsorption of beta-adrenergic agonist used in sport doping Drugs on metal nanoparticles : a detection study based on surface-enhanced raman scattering. *Langmuir*. 2010;26(18):14663-70.

30. Kaushal AM, Chakraborti AK, Bansal AK. FTIR studies on differential intermolecular association in crystalline and amorphous states of structurally related non-steroidal anti-inflammatory drugs. *Molecular Pharmaceutics*. 2008;5(6):937-45.
31. Khadka P, Ro J, Kim H, Kim I, Kim JT, Kim H, et al. Pharmaceutical particle technologies: an approach to improve drug solubility, dissolution and bioavailability. *Asian Journal of Pharmaceutical Sciences*. 2014;9(6):304-16.
32. Kinnari P, Makila E, Heikkila T, Salonen J, Hirvonen J, Santos HA. Comparison of mesoporous silicon and non-ordered mesoporous silica materials as drug carriers for itraconazole. *International Journal of Pharmaceutics* 2011;414(1-2):148-56.
33. Knopp MM, Olesen NE, Holm P, Langguth P, Holm R, Rades T. Influence of polymer molecular weight on drug-polymer solubility: a comparison between experimentally determined solubility in PVP and prediction derived from solubility in monomer. *Journal of Pharmaceutical Sciences*. 2015;104(9):2905-12.
34. Konno H, Taylor LS. Influence of different polymers on the crystallization tendency of molecularly dispersed amorphous felodipine. *Journal of Pharmaceutical Sciences*. 2006;95(12):2692-705.
35. Konno H, Taylor LS. Ability of different polymers to inhibit the crystallization of amorphous felodipine in the presence of moisture. *Pharmaceutical Research*. 2008;25(4):969-78.
36. LaFontaine JS, Prasad LK, Brough C, Miller DA, McGinity JW, Williams RO, III. Thermal processing of PVP- and HPMC-based amorphous solid dispersions. *An Official Journal of the American Association of Pharmaceutical Scientists*. 2016;17(1):120-32.
37. Lai J, Lin W, Scholes P, Li M. Investigating the effects of loading factors on the In vitro pharmaceutical performance of mesoporous materials as drug carriers for ibuprofen. *Materials (Basel)*. 2017;10(2).
38. Laitinen R, Lobmann K, Strachan CJ, Grohganz H, Rades T. Emerging trends in the stabilization of amorphous drugs. *International Journal of Pharmaceutics* 2013;453(1):65-79.
39. Larhrib H, Martin GP, Marriott C, Prime D. The influence of carrier and drug morphology on drug delivery from dry powder formulations. *International Journal of Pharmaceutics*. 2003;257(1-2):283-96.

40. Li Y, Han J, Zhang GG, Grant DJ, Suryanarayanan R. In situ dehydration of carbamazepine dihydrate: a novel technique to prepare amorphous anhydrous carbamazepine. *Pharmaceutical Development and Technology* 2000;5(2):257-66.
41. Limnell T, Santos HA, Makila E, Heikkila T, Salonen J, Murzin DY, et al. Drug delivery formulations of ordered and nonordered mesoporous silica: comparison of three drug loading methods. *Journal of Pharmaceutical Sciences* 2011;100(8):3294-306.
42. Loh ZH, Samanta AK, Heng PWS. Overview of milling techniques for improving the solubility of poorly water-soluble drugs. *Asian Journal of Pharmaceutical Sciences*. 2015;10(4):255-74.
43. Lowell S, Shields JE, Thomas M, Thommes M. *Characterization of porous solids and powders: surface area, pore size and density*. Kluwer Academic Publishers. 2004.
44. Maithani M, Singh R. Development and validation of a stability-indicating HPLC method for the simultaneous determination of salbutamol sulphate and theophylline in pharmaceutical dosage forms. *Journal of Analytical & Bioanalytical Techniques*. 2011;02(01).
45. Mistry P, Suryanarayanan R. Strength of drug-polymer interactions: implications for crystallization in dispersions. *Crystal Growth & Design*. 2016;16(9):5141-9.
46. Nejem RaM, Issa MM, Al-Kholy MH, Saleh AA, Shanab AA, Stefan van Staden RI, et al. Development and validation of kinetic and atomic absorption spectrophotometric methods for the determination of salbutamol sulfate. *Royal Society of Chemistry*. 2015;5(70):57164-70.
47. Palacio MA, Cuffini S, Badini R, Karlsson A, Palacios SM. Solid-state characterization of two polymorphic forms of R-albuterol sulfate. *Journal of Pharmaceutical and Biomedical Analysis* 2007;43(4):1531-4.
48. Patel VI, Dave RH. Evaluation of colloidal solid dispersions: physiochemical considerations and in vitro release profile. *American Association of Pharmaceutical Scientists*. 2013;14(2):620-8.
49. Qian KK, Bogner RH. Application of mesoporous silicon dioxide and silicate in oral amorphous drug delivery systems. *Journal of Pharmaceutical Sciences* 2012;101(2):444-63.

50. Rao DR, Kankan RN, Chaudhary A, inventors; CIPLA Limited, assignee. Crystalline levosulbutamol sulphate and polymorphic forms thereof patent.US Patent 7,579,505 B2. 2009 Aug 2.
51. Rengarajan GT, Enke D, Steinhart M, Beiner M. Stabilization of the amorphous state of pharmaceuticals in nanopores. *Journal of Materials Chemistry*. 2008;18(22):2537.
52. Robinson S, Williams PA. Inhibition of protein adsorption onto silica by polyvinylpyrrolidone. *Langmuir*. 2002;18(23):8743-8.
53. Santos OMM, Reis MED, Jacon JT, Lino MEdS, Simões JS, Doriguetto AC. Polymorphism: an evaluation of the potential risk to the quality of drug products from the Farmácia Popular Rede Própria. *Brazilian Journal of Pharmaceutical Sciences*. 2014;50(1):1-24.
54. Sawicki E, Schellens JH, Beijnen JH, Nuijen B. Inventory of oral anticancer agents: Pharmaceutical formulation aspects with focus on the solid dispersion technique. *Cancer Treatment Reviews*. 2016;50:247-63.
55. Schram CJ, Taylor LS, Beaudoin SP. Influence of polymers on the crystal growth rate of felodipine: correlating adsorbed polymer surface coverage to solution crystal growth inhibition. *Langmuir*. 2015;31(41):11279-87.
56. Shariare MH, de Matas M, York P. Effect of crystallisation conditions and feedstock morphology on the aerosolization performance of micronised salbutamol sulphate. *International Journal of Pharmaceutics*. 2011;415(1-2):62-72.
57. Shi Y, Miller ML, Di Pasqua AJ. Biocompatibility of mesoporous silica nanoparticles. *Comments on Inorganic Chemistry*. 2015;36(2):61-80.
58. Sing KSW. The use of gas adsorption for the characterization of porous solids. *Colloids and Surfaces*. 1989;38(1):113-24.
59. Stuart MAC, Fler GJ, Bijsterbosch BH. The adsorption of poly(vinyl pyrrolidone) onto silica I. adsorbed amount. *Journal of Colloid and Interface Science*. 1982;90(2):310-20.
60. Surikutchi BT, Patil SP, Shete G, Patel S, Bansal AK. Drug-exipient behavior in polymeric amorphous solid dispersions. *Journal of Excipients and Food Chemicals*. 2013;4(3):70-94.

61. Surwase SA, Itkonen L, Aaltonen J, Saville D, Rades T, Peltonen L, et al. Polymer incorporation method affects the physical stability of amorphous indomethacin in aqueous suspension. *European Journal of Pharmaceutics and Biopharmaceutics*. 2015;96:32-43.
62. Thakral S, Terban MW, Thakral NK, Suryanarayanan R. Recent advances in the characterization of amorphous pharmaceuticals by X-ray diffractometry. *Advanced Drug Delivery Reviews*. 2016;100:183-93.
63. Tian Y, Jones DS, Andrews GP. An investigation into the role of polymeric carriers on crystal growth within amorphous solid dispersion systems. *Molecular Pharmaceutics* 2015;12(4):1180-92.
64. Vallhov H, Gabrielsson S, Stromme M, Scheynius A, Garcia-Bennett AE. Mesoporous silica particles induce size dependent effects on human dendritic cells. *Nano Letters*. 2007;7(12):3576-82.
65. Vogt FG, Roberts-Skilton K, Kennedy-Gabb SA. A solid-state NMR study of amorphous ezetimibe dispersions in mesoporous silica. *Pharmaceutical Research* 2013;30(9):2315-31.
66. Wang B, Wang D, Zhao S, Huang X, Zhang J, Lv Y, et al. Evaluate the ability of PVP to inhibit crystallization of amorphous solid dispersions by density functional theory and experimental verify. *European Journal of Pharmaceutical Sciences*. 2017;96:45-52.
67. Wasimul Hasan MD, Someshwar K, Chaitanya P, Mohd AB, Pratyusha A, Rao VU. Formulation and evaluation of press coated tablets of salbutamol sulphate for time controlled release. *Asian Journal of Pharmaceutics*. 2014;8(3):161.
68. Willart JF, Caron V, Lefort R, Danède F, Prévost D, Descamps M. Athermal character of the solid state amorphization of lactose induced by ball milling. *Solid State Communications*. 2004;132(10):693-6.
69. Xu W, Riikonen J, Lehto VP. Mesoporous systems for poorly soluble drugs. *International Journal of Pharmaceutics* 2013;453(1):181-97.
70. Yu L. Amorphous pharmaceutical solids: preparation, characterization and stabilization. *Advanced Drug Delivery Reviews*. 2001;48(1):27-42.

71. Zellnitz S, Narygina O, Resch C, Schroettner H, Urbanetz NA. Crystallization speed of salbutamol as a function of relative humidity and temperature. *International Journal of Pharmaceutics*. 2015;489(1–2):170-6.
72. Zhao M, Barker SA, Belton PS, McGregor C, Craig DQM. Development of fully amorphous dispersions of a low T_g drug via co-spray drying with hydrophilic polymers. *European Journal of Pharmaceutics and Biopharmaceutics*. 2012;82(3):572-9.
73. Zidan AS, Rahman Z, Sayeed V, Raw A, Yu L, Khan MA. Crystallinity evaluation of tacrolimus solid dispersions by chemometric analysis. *International Journal of Pharmaceutics*. 2012;423(2):341-50.





APPENDIX

จุฬาลงกรณ์มหาวิทยาลัย
CHULALONGKORN UNIVERSITY

Appendix A

The total residual solvents

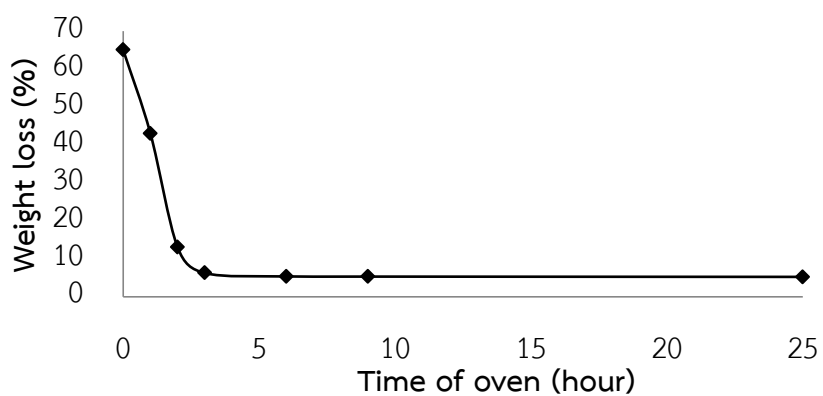


Figure 51 % Weight loss of freshly prepared SS adsorbed on S244 silica after subjected into hot air oven at 40°C for different drying time.



Incipient wetness impregnation process

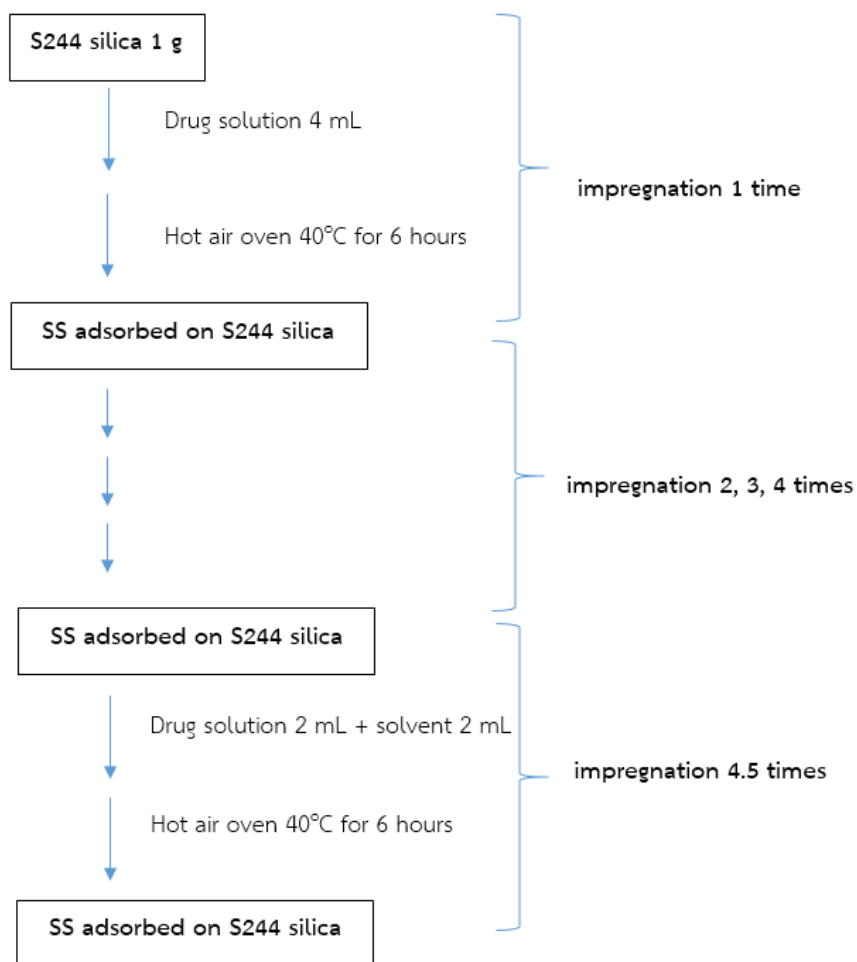


Figure 52 the flow chart of incipient wetness impregnation process with different impregnation times.

** Remark: In case of 4.5 times, it meant to the process of 4 times of impregnation with the additional load of the mixture of two milliliters of drug solution and equal volume of solvent that eventually resulted in the constant volume of loading solution.

Appendix B

Quantitation of crystalline SS form I

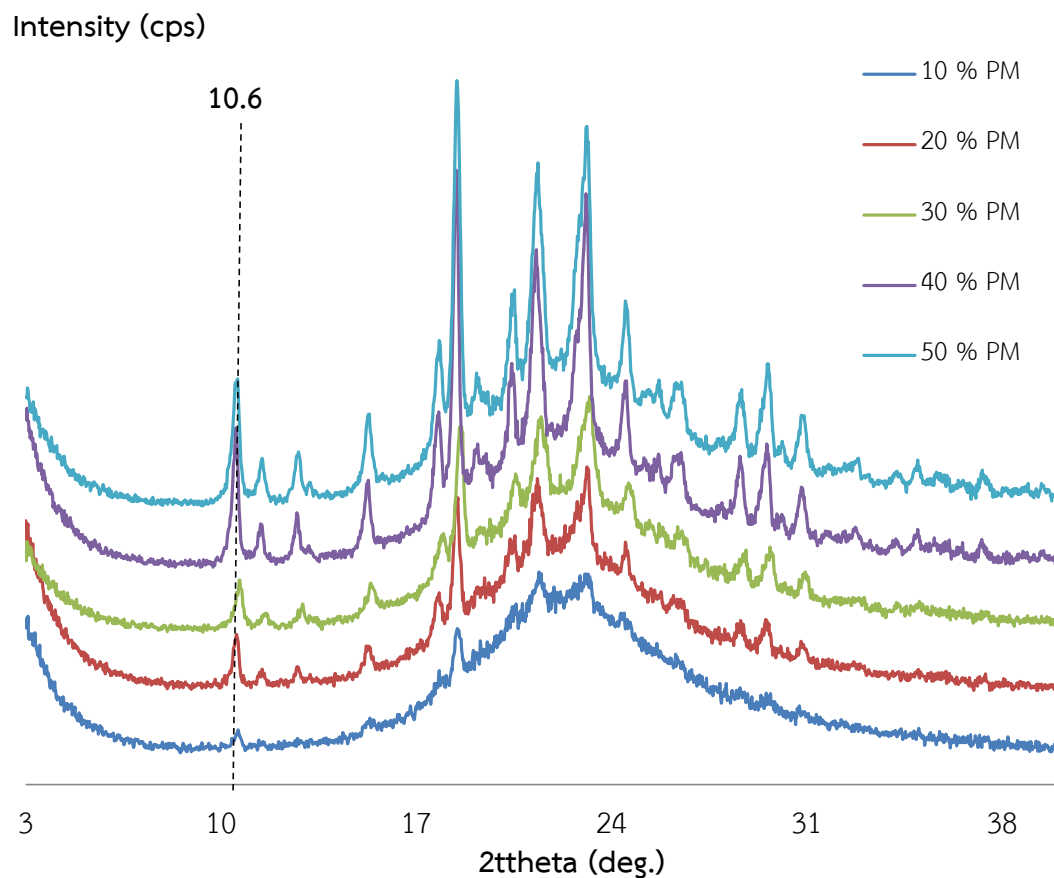


Figure 53 XRPD of the physical mixture between moisture equilibrated milled SS (crystalline form I small particle size) and S244 silica (as the placebo) at different spike concentrations.

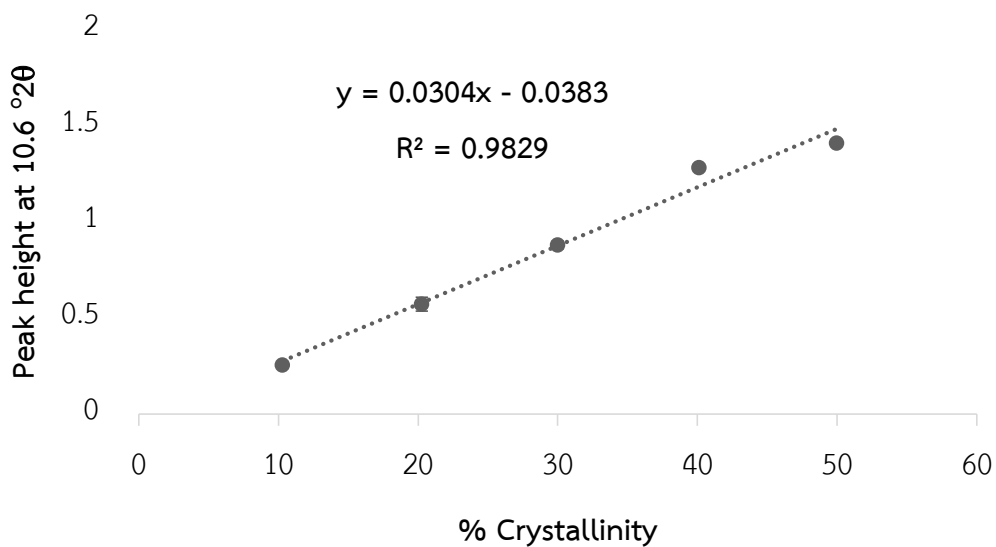


Figure 54 XRPD calibration curve of peak height at 10.6 °2θ and % crystallinity of SS form I.

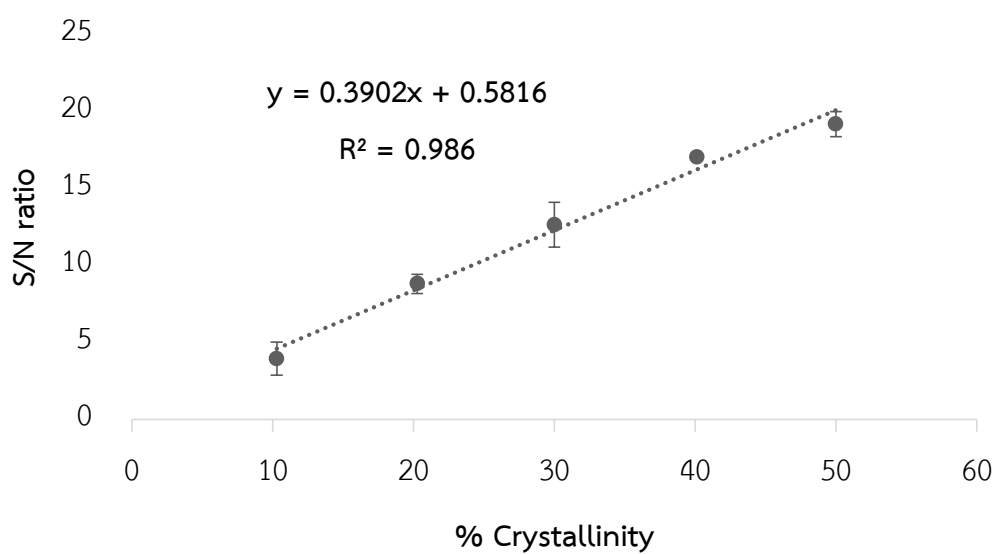


Figure 55 XRPD calibration curve of signal to noise ratio and % crystallinity of SS form I.

Signal to noise = 3, concentration = 6.20%

Signal to noise = 10, concentration = 24.14%

Appendix C

Quantification of SS by using HPLC

- Milled SS

100.86 ± 0.61

- SS adsorbed on S244 silica

Table 10 Quantity of SS in sample of SS adsorbed on S244 silica at different time of impregnation

Time of impregnation	Quantity of SS
1	10.75 ± 0.27
2	17.48 ± 0.88
3	22.61 ± 1.96
4	30.95 ± 0.75
4.5	33.42 ± 0.51
5	36.64 ± 0.93

- SS adsorbed on S244 silica with PVP K12 (four and half time of impregnation)

Table 11 Quantity of SS in sample of SS adsorbed on S244 silica with PVP K12 at different concentration of PVP K12.

Concentration of PVP K12 (% w/w of SS)	Quantity of SS
0.1%	33.87 ± 0.88
0.5%	33.59 ± 0.63
1 %	33.06 ± 1.36
5%	32.64 ± 0.65
10%	29.46 ± 1.13
20%	30.75 ± 1.02
30%	29.80 ± 1.18

Method validation of HPLC

Linearity and range

Table 12 HPLC; linearity and range of SS.

concentration	Replicate	Peak area	Average Peak area	% RSD
10.040	1	34081	34047	0.53
	2	34209		
	3	33851		
20.125	1	80731	80798.67	0.08
	2	80866		
	3	80799		
30.250	1	120413	120597.7	0.18
	2	120846		
	3	120534		
40.250	1	158601	158929	0.18
	2	159152		
	3	159034		
50.200	1	204295	203905.7	0.16
	2	203791		
	3	203631		
60.500	1	247625	248444	0.31
	2	248527		
	3	249180		
70.400	1	288480	288792.3	0.29
	2	289732		
	3	288165		

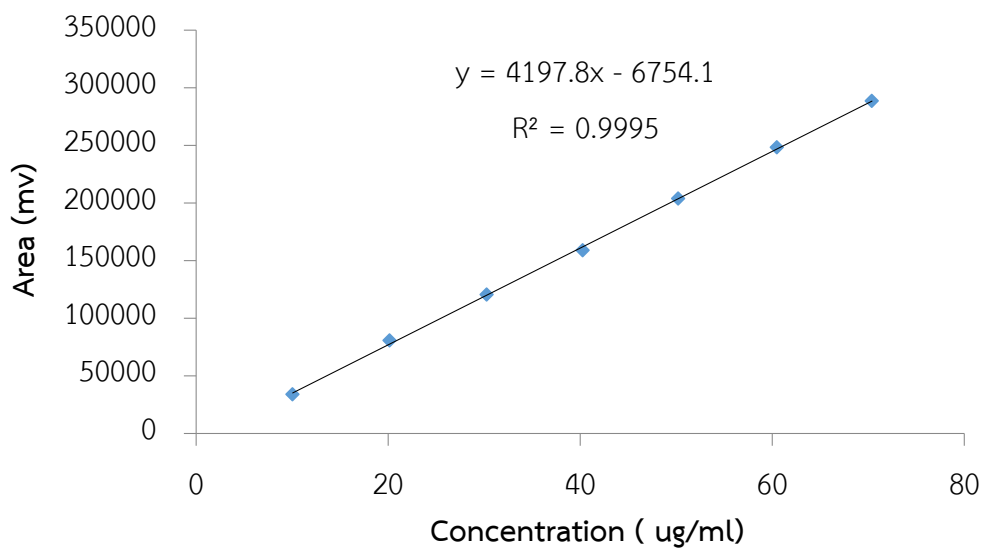


Figure 56 HPLC; calibration curve of SS.

Specificity

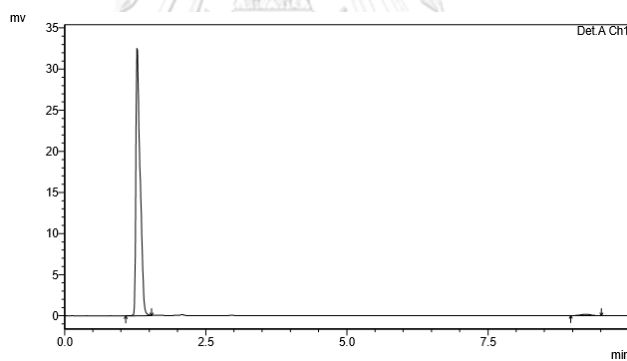


Figure 57 HPLC chromatogram of SS.

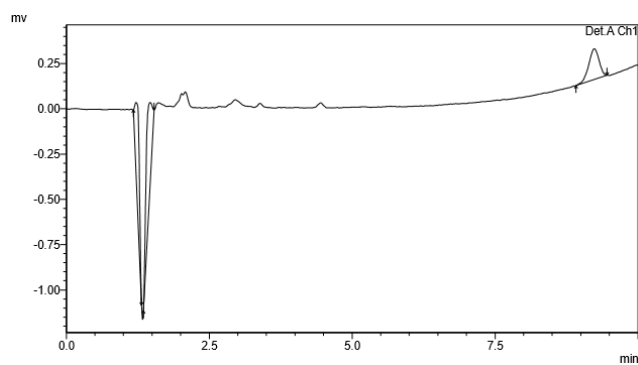


Figure 58 HPLC chromatogram of S244 silica.

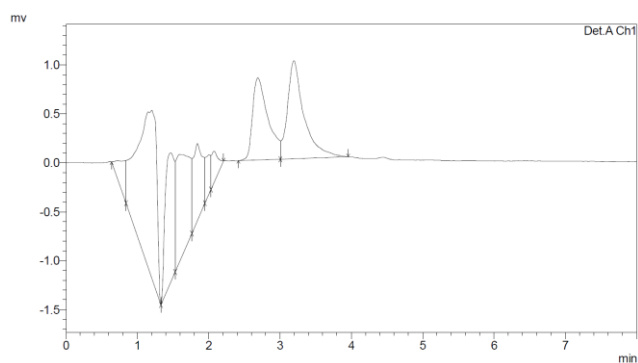


Figure 59 HPLC chromatogram of PVP K12.

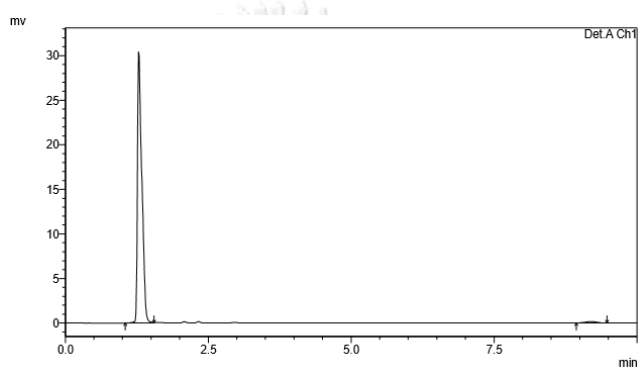


Figure 60 HPLC chromatogram of SS adsorbed on S244 silica.

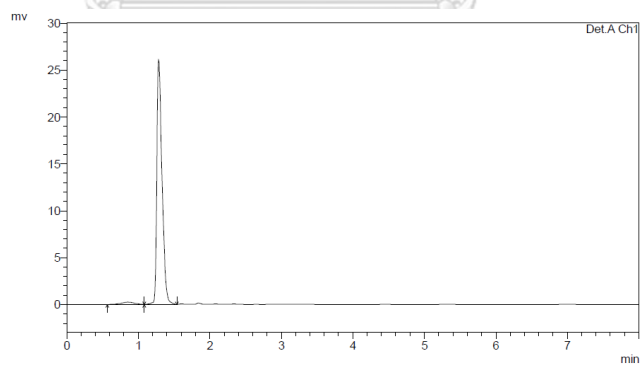


Figure 61 HPLC chromatogram of SS adsorbed on S244 silica with PVP K12 30% w/w of SS.

Precision

Table 13 HPLC; repeatability and intermediate precision.

Conc.	Rep.	Day 1			Day 2			% RSD of 2 days
		Peak area	Average peak area	% RSD	Peak area	Average peak area	% RSD	
30.250	1	120413	120597.7	0.19	119540	119670	0.12	0.55
	2	120846			119827			
	3	120534			119643			
40.250	1	158601	158929	0.18	157603	157691.3	0.13	0.55
	2	159152			157920			
	3	159034			157551			
50.200	1	204295	203905.7	0.17	203095	202459	0.27	0.50
	2	203791			202062			
	3	203631			202220			

Accuracy

Table 14 HPLC; percent recovery of SS.

Concentration	Replicate	Assay	% recovery	Average % recovery	% RSD
30.25	1	30.29	100.14	100.29	0.17
	2	30.40	100.49		
	3	30.32	100.24		
40.25	1	39.39	97.87	98.06	0.17
	2	39.52	98.19		
	3	39.49	98.12		
50.20	1	50.28	100.15	99.97	0.16
	2	50.16	99.91		
	3	50.12	99.84		

Forced degradation studies

Thermal stress

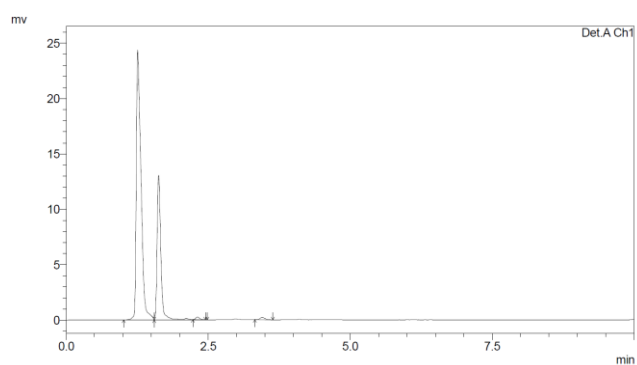


Figure 62 HPLC chromatogram of SS solution incubated at 80°C for 42 hours.



VITA

Miss Treeruk Prasertsri was born in Chaiyaphum, Thailand, on May 14th, 1990. She received her Bachelor in Pharmaceutical degree in 2013 from Faculty of Pharmacy, Rangsit University, Thailand. She presented a proceeding poster of title "PREPARATION AND STABILITY EVALUATION OF X-RAY AMORPHOUS SALBUTAMOL SULFATE ADSORBED ON MESOPOROUS SILICA" in the The JSPS-NRCT Follow-Up Seminar 2017 and 33rd International Annual Meeting in Pharmaceutical Sciences (JSPS-NRCT 2017 and IAMP533) on March 2-3, 2017 at Bangkok, Thailand.

